Title
The Role of Autophagy in Tumor Immunology and Vasculature

Author
Starobinets, Hanna Sonia

Publication Date
2016

Peer reviewed|Thesis/dissertation

The Role of Autophagy in Tumor Immunology and Vasculature

by

Hanna Sonia Starobinets

DISSERTATION

Submitted in partial satisfaction of the requirements for the degree of

DOCTOR OF PHILOSOPHY

in

Biomedical Sciences

in the

GRADUATE DIVISION

of the

UNIVERSITY OF CALIFORNIA, SAN FRANCISCO

[redacted]

Dedication

To Galina: for teaching me to think

To Mark: for teaching me attentiveness

To Timur: for lifting me up

To Aurora: my next great experiment

Acknowledgements

To earn a Ph.D., a student must expand the boundaries of human knowledge. This process is largely independent, but it cannot be accomplished without “standing on the shoulders of giants” (Sir Isaac Newton, 1676). I have a deep and eternal gratitude for all the giants who helped me in small and big ways along the long and winding road to becoming a scientist. Some have laid the groundwork upon which I based my research studies; others have taught, mentored, and collaborated with me in my scientific life; and others have supported me in my personal life. I would like to thank the following people in particular.

First, I would like to thank my mentor, Jay Debnath. Those who know me well know that I generally don’t like being told what to do. In this way, Jay was the perfect mentor for me. He gave me complete freedom to explore whatever topics interested me, allowing me to be an independent scientist from day one in his laboratory. When I came to him with new ideas that pivoted my research into a new direction, he showed a versatility and breadth of knowledge, supporting me and providing whatever guidance he could, even when we moved outside his area of expertise. Jay was also an incredible mentor in scientific writing and grantsmanship. His ability to edit and rearrange his mentees’ scientific writing is masterful, and helped me secure multiple fellowships during my graduate career. Jay also supported me in connecting with other scientists, whether it was consulting other experts, finding collaborators, or sharing my research at scientific meetings. I’m not the only student who has noticed Jay’s wonderful mentoring style. It becomes especially obvious when looking at his graduate student retention rate: 100%

of students who have rotated in this lab have joined, which to date is a total of 9 students in just 10 years. I feel extremely fortunate to have crossed career paths with Jay and am deeply grateful for his quiet, hands-off support. Thank you so much for everything, Jay.

I would also like to thank my stellar thesis committee members Zena Werb, Dean Sheppard, and Gabriele Bergers for their time, advice, and support. Their enthusiasm during my committee meetings gave me front row seats to some exciting academic arguments between highly respected experts in the field – particularly on the occasion when I proposed pivoting my work from studying tumor vasculature to tumor immunology, and they began arguing amongst themselves as to which was a more exciting topic. Spoilers: immunology won. I am honored and privileged to have had the opportunity to work closely with these scientists, to spend hours with their attention focused on me and my research, and to have their guidance for my future career.

Thank you also to all members of the Debnath Lab, past and present, with whom I've shared a workplace over the years, who have answered my technical questions, shared reagents, and provided feedback on my work. Thank you especially to Jordan Ye, who as lab manager kept the lab running smoothly, but also stepped in to perform mouse experiments for my paper revisions while I was on maternity leave. Thank you to Fanya Rostker, who as our mouse specialist took care of breeding and genotyping hundreds of my mice, and performed many mouse procedures while I was on leave. Thank you to Juliet Goldsmith and Tim Marsh, who also helped with experiments for paper revisions while I was on leave, finding time to help out even though they had their own thesis projects to work on. I'm grateful to all members of the Debnath lab for being great colleagues and friends.

I must thank all members of the UCSF Biomedical Sciences program. First, I must personally thank Lisa Magargal, the most competent administrator I have ever met. She helped create what I believe must be the most smoothly-run and nurturing Ph.D. program in the country. If anyone in the program ever had a problem, Lisa made it magically disappear. She created a system where student could focus on being students, and she and her team took care of the rest, allowing us BMS students to be the happiest Ph.D. students anywhere. When I interviewed here, I was surprised to hear several current students say that they chose to come to UCSF because of Lisa, but now I am strongly in that same category. I was looking for a cutting-edge but nurturing environment, and thanks to Lisa, it actually exists. Thank you as well to all the BMS students, who were wonderful friends during my five years in San Francisco and great people to consult whenever I had a question outside my area of expertise. The close-knit student community allowed me to reach out and find consultants and collaborators when my research shifted into immunology. Without them, I would never have gotten into this exciting field, which I want to keep exploring in my future career.

I was incredibly lucky to be born into a family of scientists and engineers. As early as I can remember, I always knew I was going to be a biologist when I grew up. My mom took me to her biology lab with her all throughout my childhood, and brought home lab equipment for me to play with in the bathtub. She taught me how to think about the world, and that was the foundation of my inquisitive and organized scientific mind. My dad, although an engineer, also helped me explore the world as a scientist, from learning the names of different trees to taking apart telephones. He also taught me to be attentive and avoid careless mistakes, which has helped me throughout my life as a student. Thank

you, mama and papa, for holding my hand, yet trusting me to do a good job on my own. Thanks to you I've always had a lot of self-confidence in my academic life, and I've never shied away from challenges, however impossible they seemed. I can see now that these qualities were valuable commodities for earning a Ph.D. I'm so proud to have finally reached the same level of higher education as both of you!

Finally, from the depth of my heart, I want to thank my husband, Timur Starobinets. You are my beloved and my friend. Thank you for being my equal. Thank you for always lifting me up. Thank you for sharing my dreams. Thank you for moving to San Francisco with me. Thank you for coming to lab with me on weekends. Thank you for climbing mountains with me. Thank you for collaborating with me on our thesis baby, Aurora. For this and much, much more, I am truly blessed.

The Role of Autophagy in Tumor Immunology and Vasculature

by

Hanna Sonia Starobinets

Abstract

Cancer therapy of the last hundred years has mainly aimed to quell cancer cells' intrinsic abnormalities. Although chemotherapies and targeted therapies have been successful at controlling the disease in the short term, even the best outcomes have largely been long-term remissions. Cancer therapy of the 21st century has turned much of its attention to manipulating the processes that occur in the tumor microenvironment. This approach aims to undermine cancer's ability to hijack its local and distant host environments to support its own growth and progression.

Therapies targeting immune and vascular components of the tumor microenvironment have met with immense success in improving the prognosis of the most devastating forms of cancer such as metastatic melanoma and glioblastoma. Immune therapies unleashing the full potential of the body's anti-cancer immune response are beginning to achieve what clinicians are tentatively labeling as complete cures: a subset of patients with metastatic melanoma have exhibited a survival curve plateau that has already surpassed 10 years in duration (1). Vascular therapies aiming to destroy tumor blood vessels and cut off supply of critical nutrients hit a roadblock until they pivoted their focus toward altering the vasculature in a way to improve drug delivery to tumors, an approach that is showing early signs of promise (2). These and other therapies designed to combat the tumor as a whole and transforming the landscape of preclinical and

translational cancer research. Much effort is now devoted to defining and disrupting the many poorly understood cell interactions with the tumor microenvironment with the aim to develop single and combination therapies with durable responses across all patients and all tumor types.

Here, I investigate the effects of autophagy inhibition on the immune and vascular systems in preclinical immune competent models of cancer. Autophagy, or “self-eating,” is a cellular process involved in homeostatic health and stress survival that has been implicated in tumorigenesis, and thus has gained considerable interest as a target in various ongoing cancer clinical trials. I find that inhibiting autophagy does not impact the anti-cancer T cell response in melanoma or breast cancer models, but alters tumor vascular function within a triple-negative breast tumor microenvironment. My work raises the enticing possibility of combining autophagy inhibition with chemotherapy and/or immune therapy to improve drug delivery and clinical outcomes. This combination approach would weaken cancer cells dependent on autophagy to survive the numerous stresses of the tumor microenvironment, while delivering a second hit of a chemical or immune attack. Many of my findings are in direct contradiction to existing published literature, suggesting that these dynamic and context-specific processes require deeper mechanistic understanding to determine appropriate clinical uses.

Table of Contents

Chapter 1 **1**

Introduction

Chapter 2 **10**

Anti-cancer T cell response remains intact following autophagy inhibition in tumors

Chapter 3 **62**

Abnormal vascular leaking is normalized following autophagy inhibition in tumors

Chapter 4 **101**

Discussion

Appendix A **107**

Additional analysis of immune response following autophagy inhibition in tumors

Appendix B **119**

Generation of transgenic mice for studies of autophagy gene knockout in vascular endothelial cells

References **123**

List of Figures

Chapter 2

Figure 1. Genetic models of autophagy deficiency in mouse melanoma and mammary cancer. 38
Figure 2. T cell infiltration is unchanged in autophagy-deficient mouse tumors. 40
Figure 3. T cell functional status is unchanged in autophagy-deficient mouse tumors. 42
Figure 4. Transgenic OT-I cell activation is unchanged in autophagy-deficient OVA-expressing tumors. 44
Figure 5. Doxorubicin-treated autophagy-deficient tumors elicit equivalent T cell responses despite altered secretion of immunomodulatory factors. 47
Figure 6. Antimalarial-treated tumors elicit equivalent T cell responses. 50
Supplementary Figure 1. Validation of autophagy deficiency in B16 melanoma and 4T1 mammary cancer cells. 52
Supplementary Figure 2. Representative dot plots of T cell functional markers. 54
Supplementary Figure 3. T cell suppression and activation potential are unchanged in autophagy-deficient mouse tumors. 56
Supplementary Figure 4. Validation of autophagy deficiency in B78-OVA mouse melanoma cells. 58
Supplementary Figure 5. Autophagy-deficient cells are more sensitive to Doxorubicin treatment. 60

Chapter 3

Figure 1. Autophagy deficiency decreases necrosis but increases lung metastasis in 4T1 mammary cancer. 89
Figure 2. Infiltration of stromal cell types is equivalent between autophagy-competent and deficient 4T1 mammary tumors. 91
Figure 3. Autophagy deficiency leads to decreased vascular leaking in 4T1 mammary tumors but not B16 melanomas. 93
Figure 4. Autophagy-deficient 4T1 mammary cancer cells exhibit an attenuated

angiogenic secretome. 95
Figure 5. Adaptive immune deficiency leads to decreased vascular leaking in 4T1 mammary tumors. 97
Figure 6. P62/SQTSM1 accumulation, but not inhibition of unconventional secretion, decreases vascular leaking in 4T1 mammary tumors. 99

Appendix A

Figure 1. Myeloid quantity and function are equivalent between autophagy-competent
and deficient melanomas. 113
Figure 2. Quantity and function of splenic T cell populations are equivalent between autophagy-competent and deficient tumors. 115
Figure 3. Autophagy-competent and deficient tumors form with similar growth kinetics in immune-deficiency. 117

Chapter 1

Introduction

Cancer therapy of the last hundred years has witnessed a variety of radiation, chemical, hormonal, antibody, and small molecule treatments utilized as the standard of care. The vast majority of these have aimed to quell the major hallmarks of cancer ([3]), uncontrolled growth and escape of death, by targeting genetic alterations in the cancer genome. Most therapies targeting a rational biomarker identified in preclinical studies have struggled with translation to the clinic ([4]). Even the most successful treatments, controlling the disease in the short term and achieving long-term remissions, have ultimately failed to prevent recurrent and resistant disease ([5]). Furthermore, with the wide variety of subclasses of a wide variety of tissues of origin, cancer's "cure" has remained elusive and highly improbable. Thus, in an effort to expand focus from the behavior of cancer cells themselves and explore the behavior of tumors as organs and cancer as a systemic disease, cancer therapy of the 21st century has turned much of its attention to manipulating the processes that occur in the tumor microenvironment ([6]). This approach aims to undermine cancer's ability to hijack its local and distant host environments to support its own growth and progression.

Overview of the tumor microenvironment

The role of the local host environment in cancer cells' hallmark ([3]) abilities to sustain unchecked growth, avoid intrinsic and extrinsic death signals, invade and spread throughout the host organism, was first proposed by Stephen Paget's "seed and soil" hypothesis over a hundred years ago (reviewed in [7]). More recently, a critical observation was made 30 years ago by Harold Dvorak that "tumors [are] wounds that do not heal" ([8]), a paradigm-shifting parallel between the microenvironments within tumors and healing

wounds that re-defined the abnormal behavior of tumors in the context of tissue and organ biology, rather than a collection of individual abnormal cells. Dvorak realized that the combined behavior of blood vessels ([9]), inflammatory cells ([10]), and the extracellular matrix ([11]) in the tumor microenvironment bear striking similarities to wounded tissues, in which inflammatory and growth signals stimulate rapid epithelial cell growth ([12]).

Turning on the wound healing program is one of the remarkable abilities of cancer cells to repurpose existing programs out of context to support their own unchecked growth. Cancer cells upregulate the expression and secretion of pro-inflammatory and pro-angiogenic signals, disrupting the delicate balance of stimulatory and inhibitory signals in normal tissues ([13],[14]) to recruit blood vessels into expanding areas of tumors to keep them nourished and oxygenated, and inflammatory cells (e.g. macrophages, fibroblasts) to generate positive feedback loops of growth signals ([15]). Considerable work in the last decade has focused on developing targeted therapies inhibiting cells and signals within the microenvironment ([16]). The most recent and successful of these have been cancer immunotherapies that de-repress the adaptive immune system via immune checkpoint blockade have achieved stunning durable responses ([17]).

While chemotherapies and targeted therapies against cancer cell intrinsic and microenvironmental biomarkers have met some success as single and combination agents ([18]), much work still needs to be done in order to achieve acute and durable responses across all patients and all tumor types. Thus far, even the most successful therapies are not successful in 100% of patients. To this end, studies of the dynamics of microenvironments of different tumor types and subtypes, stages and therapeutic contexts, need to be done in order to define the clinical contexts in which single and

combination therapies will be the most successful. Existing FDA-approved chemotherapies and targeted therapies, which are administered systemically and thus act upon normal host cells in addition to cancer cells, can have synergistic or competing effects on the microenvironment that are critical to the ultimate behavior of the tumor and the systemic disease ([19]). In this study, we examine the effects of autophagy inhibition, both genetically within cancer cells and systemically via pharmacological inhibition, on the behavior of the immune and vascular microenvironments of mouse breast tumors and melanomas.

Overview of autophagy in basic biology

Macroautophagy, hereafter referred to as autophagy ("self-eating'), is a multi-faceted cellular program that promotes cellular homeostasis, fitness, and survival, that is intertwined with numerous intracellular vesicular processes. This program that sequesters cytoplasmic components into double-membrane vesicles termed autophagosomes that fuse with a variety of intracellular vesicular compartments. The diverse destinations of autophagy-collected cargo include lysosomes for degradation, endosomes or multivesicular bodies (MVBs) for storage and transport, the plasma membrane for secretion, and MHC-containing vesicles for antigen presentation. Consequently, autophagy is a ubiquitous and highly context-dependent process that intersects with many other cellular pathways. Classic autophagy is an auto-digestive process that degrades proteins and organelles and recycles their basic constituents ([20]). This process promotes fitness and survival by degrading damaged proteins and organelles and replenishing nutrients and metabolites. As a stress response, autophagy

prolongs cell survival during nutrient starvation, ER stress, and hypoxia; because these stresses are often observed in pathologic conditions, autophagy has been implicated in many human diseases, notably in cancer ([21]).

Emerging evidence shows that autophagy modulates protein secretion and trafficking ([22]). Most secreted proteins follow the conventional secretion pathway, in which mRNA transcripts with signal sequences are translated into protein in the endoplasmic reticulum (ER), processed in the Golgi, and packaged into vesicles that traffic to the plasma membrane for release. Professional secretory cells often deliver these vesicles to storage compartments such as granules (e.g. platelets) or secretory lysosomes (e.g. cytotoxic T lymphocytes) to store secretory proteins until bulk release is triggered ([23],[24]). Autophagic machinery is thought to intersect with both constitutive and regulated conventional secretion directly by mediating cytoplasmic vesicular fusion events ([25]).

Unconventional secretion is an alternate mechanism in which proteins lacking an export tag are packaged from the cytoplasm directly into exocytic vesicles, circumventing the ER-Golgi axis ([26]). While several proteins are known to be secreted in this manner (e.g. IL1β, IL18, HMGB1, Acb1), the precise biochemical mechanisms are still being delineated. Golgi Reassembly Stacking Proteins (GRASP55 and GRASP65) are necessary for unconventional secretion by mediating vesicle tethering ([27]), and a subset of unconventionally secreted proteins also requires autophagic machinery, which mediates cytoplasmic capture and vesicular fusion events, a process termed “secretory autophagy” ([25],[28]). This involvement has been demonstrated in autophagy-deficient strains of the yeast *S. cerevisiae* and amoeba *D. discoideum*, which fail to secrete the Acb1 protein ([29]). Furthermore, immunofluorescence has identified puncta in mouse

macrophages with co-localization of LC3 with the cytokine IL1-β, and LC3 with GRASP55, providing cell biological evidence for secretory autophagosomes ([30]). Beyond these few examples, the full scope of cytoplasmic components that may be released from cells via secretory autophagy is still being delineated.

Overview of autophagy in cancer biology

As in basic cell biology, autophagy is highly context-dependent during tumor initiation and progression, with conflicting effects during early versus late stages of cancer. By degrading toxic or mutant cytoplasmic proteins, autophagy can act as a barrier to tumor initiation. In contrast, autophagy facilitates tumor growth, matrix detachment, dormancy and drug resistance by helping cancer cells to withstand various stresses ([31]). Autophagy plays a role in focal adhesion turnover and cell migration ([32]), supporting its role in invasion and metastasis. As a result of studies like these, several clinical trials have combined traditional chemotherapy or targeted therapy with antimalarial lysosomotrophic agents, such as hydroxychloroquine, which block the late stages of autophagic proteolysis ([33],[34],[35],[36],[37],[38],[39],[40]). While targeting autophagy is a rational approach to cancer therapy, it remains a challenge to determine appropriate context and timing.

Until now, autophagy in cancer has been studied largely from a cell-autonomous perspective: aiding cancer cell survival during cellular stress, promoting cancer cell metastasis, drug resistance, and dormancy. In contrast, the role of autophagy in the development and function of the tumor microenvironment, a critical mediator of tumor initiation and progression, has been studied to a much smaller extent. The limited studies

that have been done suggest that autophagy inhibition in tumors may decrease the anti-tumor immune response ([41]), but may increase necrosis and inflammation ([42]). Because systemic autophagy inhibition will limit not only cancer cells' but also normal neighboring cells' abilities to survive the stressful conditions of the tumor microenvironment, defining autophagy's role in tumor-stromal secretory interactions as well as within the stromal fraction of tumors will be critical to delineating the clinical contexts appropriate for autophagy inhibition. This is especially true given the rising interest of inhibiting autophagy in melanoma – a Ras pathway-driven cancer and thus one that may rely upon autophagy – which happens to also be a cancer that is very responsive to cancer immunotherapy.

Overview of cancer immunology and immunotherapy

Cancer immunotherapies are becoming increasingly successful approaches to treating certain cancers due to the durable responses they can achieve by boosting the endogenous antitumor immune response. Tumor-infiltrating T cells, attracted by antigen-presenting cells and inflammatory signals, respond to tumor antigens by turning on an antitumor program that culminates in the cytotoxic activity of CD8+ (cytotoxic) T cells. These cells produce and secrete proteins including Th1 cytokines interferon γ (IFNγ) and tumor necrosis factor α (TNFα), and cytotoxic effectors perforin and granzyme B ([43]). While this program eliminates most early initiated cancer cells, decreased immunogenicity or increased immunosuppression can allow small tumors to reach an equilibrium with, and ultimately escape from, immune control ([44]). Suppressed T cells, while still physically present in overt tumors, express inhibitory surface proteins cytotoxic

T-lymphocyte-associated protein 4 (CTLA4) ([45]) and programmed cell death protein (PD1) ([46]).

The most successful cancer immunotherapies to date have been immune checkpoint blockade, in which monoclonal antibodies inhibit CTLA4 and/or PD1 ([17],[47],[48],[49]). This therapy unleashes existing suppressed T cell responses, and thus is achieving incredible long-term remissions in patients with abundant tumor-associated cytotoxic T cells. Currently, the best indication for a powerful response to these therapies is a high number of cancer-expressed neoantigens, such as in melanomas and lung carcinomas ([50]). Even so, only a portion of patients with these cancers respond well to immunotherapy. With the promise of durable responses comes a pressing need to better understand the clinical contexts in which immunotherapies can be effective. Extensive preclinical studies will be necessary to define tumor microenvironment dynamics that may affect the antitumor immune response across different tumor types. Furthermore, chemotherapies and targeted therapies already used in the clinic are manipulating cellular processes that can affect the antitumor immune response. Thus it may be important to revisit the rationale of such therapies and interrogate their effects on tumor-associated lymphocytes – for example, autophagy inhibition.

Overview of tumor vasculature

In order outgrow the oxygen diffusion limit, tumors must stimulate chronic angiogenesis of their local vasculature, a hallmark of cancer ([3]). The “angiogenic switch” is a major secretory switch of tumor cells to a pro-angiogenic state that is required for small, pre-vascular tumors to become overt and vascularized ([51]). While normal

vasculature has a structured hierarchy of arterioles, capillaries and venules, tumor vasculature is typically disorganized, immature, tortuous, and leaky, exhibiting collagen stripping, gaps between endothelial cells, pericyte detachment, and pools of fluid leaking out into the tissue that are termed “blood lakes” ([52],[53]). Structural and functional dysfunction of tumor-associated blood vessels leads to poorly-perfused and hypoxic tumor microenvironments that are known to stimulate invasion, metastasis and drug resistance ([54],[55]).

Clinically-approved anti-angiogenic therapies include bevacizumab, which inhibits vascular endothelial growth factor (VEGF), and sorafenib, which inhibits several receptor tyrosine kinases including VEGF receptor (VEGFR). These therapies are often initially successful by inhibiting either a highly secreted pro-angiogenic factor or its receptor on vascular cells; this loss of growth signal kills blood vessels and starves the tumor of its oxygen and nutrient supply. However, these initial successes are very often followed by highly aggressive relapses due to the tumor’s ability to circumvent the blockade by altering other aspects of the complex and dynamic angiogenic program ([56]). Even worse, destroying blood vessels creates more vascular disorganization, leaking, and hypoxia, which promote rather than inhibit tumor progression.

Thus, some groups have proposed that normalizing the abnormal tumor vasculature, rather than completely destroying it, might prove to be a better approach to leveraging this aspect of the tumor microenvironment, both because it would diminish areas of vascular leaking and hypoxia, and because more homogenous blood flow would improve drug delivery ([2],[57]). Despite extensive research, targeting the tumor vasculature remains a clinical challenge, and requires deeper mechanistic understanding.

Chapter 2

Anti-cancer T cell response remains intact following autophagy inhibition in tumors

This chapter is a manuscript currently in revision.

Contributions: I performed all the experiments and analyzed all the data with the following exceptions. Jordan Ye performed cell culture, tissue harvests, and tissue processing for experimental repeats. Miranda Broz and Kevin Barry prepared fresh OT-I cells for B78-OVA experiments and assisted with flow cytometry. Juliet Goldsmith assisted with tissue harvests and performed cell culture assays for experimental repeats. Timothy Marsh performed IV injections of Doxorubicin. Fanya Rostker was responsible for mouse husbandry and genotyping; she performed all intra-peritoneal injections, retro-orbital injections, and caliper measurements; she also performed subcutaneous injections for experimental repeats. Matthew Krummel provided consultation on methods in tumor immunology. Jay Debnath supervised the entire project.

Abstract

The rising success of cancer immunotherapy has produced immense interest in defining the clinical contexts that may benefit from this new therapeutic approach. To this end, there is a great need to ascertain how the therapeutic modulation of intrinsic cancer cell programs influences the anticancer immune response. For example, the role of autophagy as a tumor cell survival and metabolic fitness pathway is being therapeutically targeted in ongoing clinical trials of antimalarials involving a broad spectrum of cancers, many of which will likely benefit from immunotherapy. However, our current understanding of the interplay between autophagy and the immune response remains incomplete. Here, using immune-competent mouse models of melanoma and mammary cancer, we evaluate how autophagy inhibition impacts the anti-tumor immune response. We observe equivalent levels of T cell infiltration and function within autophagy-competent and deficient tumors, even upon treatment with the anthracycline chemotherapeutic doxorubicin. Similarly, we see equivalent T cell responses upon systemic treatment of tumor-bearing mice with antimalarials. Our findings demonstrate that anti-tumor adaptive immunity is not adversely impaired by autophagy inhibition in these models, allowing for the future possibility of combining autophagy inhibitors with immunotherapy.

Introduction

Autophagy is a tightly regulated cellular program that results in the engulfment and sequestration of cytoplasmic protein and organelle cargo into double-membrane structures termed autophagosomes, which are subsequently delivered to the lysosome for degradation ([58]). Autophagy occurs both at basal conditions to maintain cellular homeostasis, as well as in response to environmental stresses such as nutrient starvation or hypoxia. Most studies investigating autophagy in cancer have focused on its cell-intrinsic effects, including aiding cancer cell survival during extrinsic stress ([59],[60]) as well as promoting drug resistance ([61]). Importantly, several clinical trials have combined traditional chemotherapy or targeted therapy with antimalarial lysosomotrophic agents, such as hydroxychloroquine, which block the late stages of autophagic proteolysis ([33],[34],[35],[36],[37],[38],[39],[40]). Despite interest in inhibiting autophagy in the clinical oncology setting in combination with chemotherapies or other targeted therapies, emerging evidence has raised questions with regard to the efficacy of such approaches to cancer treatment. It is now appreciated that certain chemotherapies, particularly anthracycline agents, kill tumors through combined cytotoxic and immunogenic mechanisms, via the process of immunogenic cell death (ICD) in which dying cells release damage-associated molecular patterns (DAMPs) to elicit an immune response ([62],[63]). ICD is believed to be an important effector of both chemotherapy and radiation therapy, but the precise contributions of ICD to treatment-mediated tumor killing are varied and context-dependent ([64]).

Importantly, autophagy has been shown to promote certain hallmarks of ICD *in vitro,* including the secretion of ATP and high-motility group protein B1 (HMGB1), both of which act as DAMPs ([41]). In support of the notion that autophagy facilitates anti-tumor immunity *in vivo* are the observations that loss of either autophagy or adaptive immunity impairs the regression of some mouse tumors during anthracycline therapy, and autophagy-deficient mouse colon tumors exhibit modest decreases in recruitment and activation of T cells ([41],[65]).

Overall, these potentially adverse effects on the adaptive immune system argue against the use of autophagy inhibitors in anti-cancer therapy. Nonetheless, autophagy inhibition can be a very useful anti-cancer therapy not only in undermining tumor cell growth but also in preventing the survival of quiescent cells during chemotherapy ([66]). These discrepancies become especially important considerations in light of the recent success of cancer immunotherapies. Notably, immune checkpoint blockade therapies, which leverage monoclonal antibodies targeting cytotoxic T-lymphocyte-associated protein 4 (CTLA4) ([47],[67]) and programmed cell death protein 1 (PD1) ([49],[68]) to reinvigorate existing T cell responses within tumors, have produced long-term remission in certain patients ([17],[69]). Currently, the best indication of a powerful response to these therapies is a high number of cancer-expressed neoantigens; thus, melanomas and smoking-associated lung carcinomas, which carry a high mutational load and express high levels of neoantigens, exhibit the highest response rates to immune checkpoint blockade ([50]). Even so, only a portion of patients with these cancers responds well to immunotherapy. With the promise of the impressive durable responses achieved with these therapeutic modalities comes a pressing need to better define the clinical contexts in which

immunotherapies will be effective ([70]). Furthermore, combining immunotherapies' durable responses with targeted therapies' powerful short-term responses is an alluring approach to further improving cancer treatment outcomes ([71]).

In this study, we sought to delineate more fully the effects of autophagy on the tumor-associated T cell response in order to better ascertain whether autophagy inhibition can be effectively combined with chemotherapy in the clinic. Using established immunogenic models of mouse melanoma and mammary cancer, we assessed the effects of autophagy inhibition on the functional status of tumor-infiltrating T cells, both at baseline and following doxorubicin chemotherapy. We interrogated the functional status of tumor-associated $CD4^+$ T helper cells and $CD8^+$ cytotoxic T cells by flow cytometry for a variety of markers of T cell activation ([43],[72]) as well as immune checkpoint modulators. Our results demonstrate that genetic autophagy inhibition in tumor cells *in vivo* does not significantly impact T cell infiltration, activation, or immune checkpoint regulation. Similarly, we observe no changes in the T cell response upon systemic treatment of tumor-bearing mice with antimalarials that inhibit autophagy. We further confirm that autophagy inhibition does not impact the functional activation of adoptively transferred ovalbumin-specific transgenic T cell receptor (OT-I) $CD8^+$ T cells ([73]) in ovalbumin-expressing tumors. Hence, autophagy does not modulate the anti-tumor T lymphocyte response in multiple immune-competent mouse cancer models. Based on these results, we propose that clinical contexts exist in which autophagy inhibition may be utilized as a therapeutic strategy without adversely affecting the anti-tumor immune response.

Results

Genetic inhibition of autophagy in tumor cells does not alter primary tumor growth.

In order to dissect the effect of tumor cell-intrinsic autophagy on the extrinsic anti-tumor immune response, we generated B16 murine melanoma cells stably expressing short-hairpin RNAs (shRNA) against the essential autophagy-related genes ATG7 and ATG12. Cells expressing non-targeting shRNA (shCTL) served as autophagy-competent controls. Stable ATG7 or ATG12 knockdown (Supplementary Figure 1A) led to reduced autophagic flux, evidenced by reduced LC3-II formation and lysosomal turnover (Supplementary Figure 1B). Control and autophagy-deficient B16 tumors were introduced subcutaneously into C57BL/6 mice, and palpable tumors formed 7 to 10 days post-transplantation. Primary tumor growth was unchanged between autophagy-competent and deficient tumors, based on caliper measurements of tumor area over experimental time course as well as resected tumor mass at experimental endpoint (Figure 1A). Similarly, autophagy inhibition in 4T1 mammary cancer cells, achieved via stable ATG7 or ATG12 knockdown (Supplementary Figure 1A), significantly impaired autophagic flux (Supplementary Figure 1C) but did not impact primary tumor growth following orthotopic transplantation into the mammary fat pad of 6-7 week old female BALB/c mice (Figure 1A). In both models, we confirmed that robust autophagy inhibition was maintained over the duration of the experiment, evidenced by the loss of LC3-II in lysates generated from resected tumors harvested at 2 to 3 weeks post-transplant (Figure 1B).

Autophagy-competent and deficient tumors elicit equivalent T cell responses.

Having developed two models of tumor cell autophagy deficiency in distinct mouse genetic backgrounds, we evaluated the immune response to tumors arising from these cells. To quantify and interrogate the function of tumor-associated T cells, we prepared single cell suspensions from resected tumors and subsequently stained a variety of surface and intracellular markers for flow cytometric analysis. To ensure accurate measurements of intracellular cytokines in T cells, we injected mice with Brefeldin A (BFA) prior to tumor resection in order to prevent cytokine secretion. T cells were identified as the $CD45^+/CD3^+/SSC\text{-}A^{low}$ fraction of total live cells defined by a live/dead marker; from these, $CD4^+$ and $CD8^+$ T cell subpopulations were identified (Figure 2A). Autophagy-deficient B16 and 4T1 tumors did not exhibit significant differences in the infiltration of $CD45^+$ cells, total T cells, or $CD4^+$ or $CD8^+$ subsets, when compared to autophagy-competent controls (Figure 2B-C). While tumors raised in littermates exhibited very similar levels of immune infiltration, quantities varied more between experimental cohorts; even so, statistical analyses of both individual and batched data sets were not significant.

We next assessed the functional activation status of $CD8^+$ and $CD4^+$ T cells that had infiltrated B16 tumors by analyzing cell-surface expression of activation and memory marker, CD44, and intracellular expression of the inflammatory cytokines interferon γ (IFNγ) and tumor necrosis factor α (TNFα). By these measures, we observed no differences in the T cell activation phenotype between control and autophagy-deficient B16 tumors (Figure 3A-B and Supplementary Figure 2A). Similarly, we found no differences between cohorts in the activation of the $CD8^+$ T cell cytotoxic program based on intracellular expression of the serine protease granzyme B (GranzB) (Figure 3A-B and

Supplementary Figure 2A). We also measured the surface expression of the immune checkpoint regulator programmed cell death protein (PD1) and found no differences in either $CD4^+$ or $CD8^+$ T cells between autophagy-competent and deficient tumors (Figure 3A-B and Supplementary Figure 2A). In agreement with these results from B16 tumors, T cell functional status and activation phenotype were unchanged between autophagy-competent and deficient 4T1 tumors (Figure 3C). As before, statistical analyses of both individual and batched data sets were not significant. Together, these findings indicate that reduced tumor cell autophagy in both mouse melanomas and mammary tumors does not influence the ability of the host adaptive immune system to infiltrate and become functionally active within these tumors.

To further corroborate the observation that T cell activation was independent of autophagy status, we generated autophagy-competent and deficient B16 tumors in "IFNγ reporter with endogenous polyA transcript" (GREAT) reporter mice carrying an IFNγ-IRES-eYFP reporter cassette, in which expression of IFNγ and enhanced yellow fluorescent protein (eYFP) are separated by an internal ribosome entry site (IRES) and dually controlled by the endogenous IFNγ promoter/enhancer region ([74]). T cell activation in resected tumors was measured by endogenous eYFP fluorescence, obviating the need for BFA treatment or intracellular staining. No differences in eYFP expression in $CD4^+$ or $CD8^+$ T cells were observed by this method, providing further evidence for an autophagy-independent T cell response (Figure 3D). As expected, the IFNγ response based on eYFP reporter levels was comparable to but slightly higher than that obtained with intracellular IFNγ staining; while IFNγ is a secreted protein, eYFP accumulates intracellularly with each IFNγ transcription event.

To address whether tumor cell autophagy status could modulate immunosuppression, we evaluated the quantity and function of regulatory T cells (TRegs) associated with autophagy-competent and deficient B16 tumors (Supplementary Figure 3A). Neither the number of TRegs ($CD45^+$ $CD3^+$ $CD4^+$ $Foxp3^+$) nor their activation ($CD44^+$) were changed upon genetic autophagy inhibition, further supporting the notion that T cell responses were indifferent to autophagy status in these tumors.

Finally, to assess tumor-associated T cell activation potential, we isolated $CD8^+$ T cells from 4T1 tumors by fluorescence-activated cell sorting (FACS) or negative bead selection and cultured them with CD3 and CD28 antibodies to incite robust *ex vivo* antigen-independent re-stimulation. We measured IFNγ secretion in conditioned medium by enzyme-linked immunosorbent assay (ELISA) and observed equivalent levels of secretion from T cells derived from either autophagy-competent or deficient 4T1 tumors (Supplementary Figure 3B). Thus, we concluded that tumor-associated T cells possess equivalent activation *in situ* as well as equivalent activation potential, regardless of the autophagy status of tumor cells.

Autophagy-competent and deficient OVA-expressing tumors stimulate comparable transgenic T cell responses.

Studies utilizing T cells expressing a transgenic T cell receptor (TCR) matched to a specific antigen (e.g. ovalbumin) have been valuable in defining a tumor-specific adaptive immune response. To ensure cancer cell recognition by T cells rather than relying solely on the endogenous T cell response, we designed autophagy-competent (non-targeting shRNA) and deficient (ATG7 or ATG12 shRNA) B78 melanoma cells (a

variant of B16) expressing ovalbumin (OVA). We confirmed stable ATG7 and ATG12 suppression (Supplementary Figure 4A) and reduced autophagic flux by reduced LC3-II and increased P62/SQSTM1, an autophagic cargo receptor that accumulates upon autophagy inhibition, in cell culture lysates (Supplementary Figure 4B). B78-OVA cells were injected subcutaneously into wildtype C57BL/6 mice and allowed to form palpable primary tumors. Freshly isolated ovalbumin-specific OT-I $CD8^+$ T cells expressing green fluorescent protein (GFP) were then adoptively transferred by retro-orbital injection into tumor-bearing mice, and tumors were resected one week later. Tumor growth kinetics were unchanged between autophagy-competent and deficient groups (Figure 4A). Continued autophagy inhibition was confirmed by the accumulation of P62/SQSTM1 cargo receptor aggregates in B78-OVA cells isolated from digested tumors by antibiotic selection (Figure 4B).

Endogenous and adoptively transferred tumor-associated T cells were defined by flow cytometric analysis based on expression of CD45, CD3, CD4, CD8, and GFP; no differences were observed in the tumor infiltration of total T cells, endogenous $CD4^+$ or $CD8^+$ T cells, or adoptively transferred OT-I $CD8^+$ T cells (Figure 4C). We next measured T cell activation by expression of surface CD44 and intracellular IFNγ, TNFα, and GranzB. We observed no significant differences in expression of activation markers in either OT-I or endogenous populations of T cells between autophagy-competent and deficient B78-OVA tumors (Figure 4D and Supplementary Figure 2B). While we did observe a marginal increase in the percentage of TNFα-expressing T cells associated with autophagy-deficient B78-OVA tumors, this was not statistically significant. Importantly, autophagy deficiency did not blunt the overall T cell response. As expected, the activation of OT-I T

cells was higher than that of endogenous $CD8^+$ T cells, as evidenced by higher percentages of $CD44^+$ and $TNF\alpha^+$ cells. Overall, the T cell response remained intact in both the endogenous and antigen-matched setting upon genetic autophagy inhibition.

Doxorubicin-treated autophagy-competent and deficient tumors stimulate equivalent T cell responses.

Because our results indicated that tumor cell-intrinsic autophagy is dispensable for stimulating a T cell response, we next tested whether autophagy was required for the immune response in tumor-bearing mice following treatment with chemotherapy. Previous work with murine colon cancer suggests that autophagy is necessary for the immunogenic cell death (ICD) associated with the efficacy of anthracycline chemotherapy ([41]). Thus, genetic inhibition of autophagy may hinder the chemotherapeutic drug response by blunting immune responses. We treated autophagy-competent and deficient B16 melanoma cells with the anthracycline doxorubicin (Dox) *in vitro*, and measured the secreted levels of ATP and HMGB1, two immunomodulatory factors implicated in ICD (Figure 5A). Consistent with existing literature, we too observed that Dox treatment induced ATP and HMGB1 secretion, which was attenuated in autophagy-deficient cells as compared to autophagy-competent controls. Interestingly, we noted that Dox treatment also led to a modest, albeit significant, reduction in the surface expression of the immunosuppressive protein, programmed death-ligand 1 (PD-L1) in autophagy-deficient tumor cells (Figure 5A). Because these *in vitro* findings suggested that autophagy status in B16 melanoma cells influenced their expression of some markers of ICD, we evaluated the effects of genetic autophagy inhibition upon ICD *in vivo*.

To assess whether autophagy-competent and deficient B16 melanomas underwent equivalent levels of ICD *in vivo*, we utilized the prophylactic vaccination experimental design described previously by Michaud et al ([41]). After generating dose-response curves to determine appropriate treatment regimens (Supplementary Figure 5A), we pre-treated B16-shCTL and B16-shAtg7 with Dox *in vitro* and injected cocktails subcutaneously into mice in which 70% of cells were apoptotic; Matrigel was injected as a control "vaccination." One week later, healthy wildtype B16 cells were injected subcutaneously into contralateral flanks, and tumor incidence was measured by daily palpation. Tumor-free survival was unchanged between mice vaccinated with Matrigel, B16-shCTL, or B16-shAtg7 cells (Figure 5B). Thus, in spite of expressing classic ICD markers *in vitro*, Dox-treated B16 cells were unable to vaccinate mice against re-challenge irrespective of autophagy status, perhaps because they were insufficiently immunogenic *in vivo* to convey protection. This supports the idea that ICD is a dynamic and context-dependent process ([64]), and by extension, autophagy inhibition may not perturb chemotherapeutic responses in all these contexts.

Of note, B16-shAtg7 cells exhibited higher levels of death upon Dox treatment relative to B16-shCTL cells (Supplementary Figure 5A), indicating their sensitivity to autophagy impairment. We confirmed that autophagy-deficient 4T1 cells also exhibited sensitivity to autophagy impairment by measuring their cellular viability by Crystal Violet staining following 24 hours of Dox treatment (Supplementary Figure 5B).

Next, we sought to evaluate directly the effects of genetic autophagy inhibition on the immune response following *in vivo* Dox treatment. We generated autophagy-competent and deficient B16 melanoma tumors in GREAT reporter mice; following the

development of palpable tumors, mice were treated with Dox. There were no significant differences in tumor growth between cohorts, either by caliper measurements or tumor mass at resection (Figure 5C). Phosphorylated H2a histone family member X (γH2AX) expression, a marker of DNA damage, was significantly elevated in Dox-treated tumors compared to untreated controls, but was unchanged between autophagy-competent versus deficient Dox-treated cohorts (Figure 5D). Thus, this dose regimen and mechanism of administration were appropriate for instigating DNA damage in B16 tumors, a prerequisite for cell death and immunogenic potential. We also confirmed autophagy deficiency in resected tumors by immunoblotting for LC3-II (Figure 5D).

Upon assessment of immune infiltration, we found that percentages of $CD45^+$ cells, total T cells and $CD4^+$ and $CD8^+$ subsets, were equivalent between untreated and Dox-treated cohorts (Figure 5E). As before, T cell activation phenotype was measured by flow cytometry using surface CD44 expression and endogenous eYFP fluorescence as a reporter for IFNγ levels, while T cell immune checkpoint regulation was measured by surface PD1 expression. No differences were observed in the levels of any of these functional markers between Dox-treated tumors (Figure 5E).

Importantly, we observed evidence of a chemotherapy-induced immune response in Dox-treated tumors compared to control tumors. Most strikingly, CD44 expression was significantly elevated in both $CD8^+$ and $CD4^+$ T cell populations, in both Dox-treated B16-shCTL and B16-shAtg7 tumors, as compared to untreated counterparts (Figure 5E). Thus, Dox treatment of B16 tumor-bearing mice elicited immune responses within the tumor site, as evidenced by direct measurement of tumor-associated T cell activation. Because autophagy inhibition did not blunt this enhanced immune response during Dox

treatment, our data suggests that autophagy inhibition and anthracycline chemotherapy can be safely combined in certain tumor types.

Antimalarial treatment of tumor-bearing mice does not alter the anti-tumor T cell response.

Autophagy inhibition is currently accomplished in the clinical setting by systemic treatment with antimalarial drugs such as chloroquine and hydroxychloroquine ([75]). These drugs inhibit acidification of intracellular vesicular compartments such as the lysosome, thereby blocking the terminal stages of autophagic proteolysis. To ascertain the effects of systemic antimalarial treatment on the anti-tumor immune response, we evaluated the effects of chloroquine treatment on subcutaneous B16 melanomas in GREAT reporter mice. Mice bearing palpable tumors were treated with daily intraperitoneal (IP) injections of 60 mg/kg chloroquine or vehicle control for 4 to 5 days prior to tumor resection. As with genetic autophagy inhibition, tumor growth kinetics were unchanged upon pharmacological autophagy inhibition (Figure 6A), which was confirmed by the accumulation of P62/SQSTM1 aggregates in resected tumors (Figure 6B). T cell infiltration and activation, measured by CD44 and eYFP reporter activity, were unchanged in chloroquine-treated B16 melanomas compared to vehicle-treated controls (Figure 6C). In addition, chloroquine treatment did not change the levels of immune checkpoint regulator PD1 (Figure 6C). To extend these results, we generated orthotopic 4T1 mammary tumors in BALB/c mice and evaluated the effects of both chloroquine as well as quinacrine, another FDA-approved antimalarial demonstrated to inhibit autophagy in preclinical models ([66],[76]). Mice bearing palpable tumors were treated with daily IP

injections of either 60 mg/kg chloroquine, 50 mg/kg quinacrine, or vehicle control. Tumor growth was not statistically significant between the three cohorts (Figure 6A). Consistent with our results in B16 melanomas, T cell infiltration and activation were unchanged in both chloroquine- and quinacrine-treated 4T1 mammary tumors compared to vehicle-treated controls (Figure 6D). Overall, these data demonstrate that systemic pharmacological inhibition of autophagy using antimalarials does not adversely impact the anti-tumor T cell response.

Discussion

In this study, we demonstrate that the T cell immune response in preclinical models of melanoma and breast cancer is not dependent on autophagy activity of the tumor cell. This suggests the ability to combine autophagy inhibition with chemotherapy safely during cancer treatment, and opens the possibility of future combination with immunotherapy. While ongoing clinical trials are testing the efficacy of combining autophagy inhibition with chemotherapy in multiple cancer types, some recent studies have argued against such combinations due to autophagic regulation of immunogenic mechanisms associated with chemotherapeutic efficacy ([41],[65],[63]). Because of the limited scope of those studies with regard to interrogating autophagy and T cell functional status, as well as the clinical importance of delineating the consequences of autophagy inhibition, we further addressed this critical issue in a broader array of mouse models.

Our study design included two tumor types: B16 melanoma in C57BL/6 mice and 4T1 mammary cancer in BALB/c mice ([77],[78]). These models have been extensively employed in studies of the tumor microenvironment and immune response and provided us with the opportunity to interrogate the effects of autophagy inhibition in two distinct immune-competent genetic backgrounds. We found that the levels of autophagy within tumor cells did not affect either the quantities of infiltrating T cell populations or their functional status. As a further validation of our measurements of the functional analysis of T cells via antibody staining, we raised B16 melanomas in IFNγ-IRES-eYFP ("GREAT") reporter mice and measured eYFP reporter activity. This model allowed us to employ an entirely parallel technical approach to assessing T cell activity, and eliminated any

technical caveats that could be introduced by the reliance on antibody reagents. Once again, we found equivalent tumor-associated T cell responses as measured by eYFP reporter expression between autophagy-competent and deficient tumors. Supplementing these rigorous analyses of tumor-associated T cells, we also demonstrated that autophagy deficiency did not alter the quantity or quality of regulatory T (TReg) cells associated with B16 tumors, and did not alter the activation potential of re-stimulated $CD8^+$ T cells isolated from 4T1 tumors.

Due to the ongoing efforts in repurposing antimalarials as autophagy inhibitors to treat cancer, we interrogated the effects of these agents on the antitumor T cell response. Similar to genetic autophagy inhibition specifically in tumor cells, systemic treatment with the autophagy-inhibiting antimalarial agents chloroquine and quinacrine produced equivalent quantity and functional phenotype of tumor-infiltrating T cells. Remarkably, antimalarials are used clinically in the treatment of autoimmune disorders, and it has been proposed these agents can act as immune suppressors by interfering with immune cell function ([79],[80]). However, in daily treatments of tumor-bearing mice for a limited duration, we observed no evidence of a blunted T cell response. Our results point to a therapeutic window in which antimalarials may be effectively combined with immunotherapies without antagonistic effects. Future preclinical and clinical studies will be necessary to define such combinatorial approaches.

In addition to assessing the endogenous and heterogeneous T cell response in B16 and 4T1 tumors, we chose to employ a more targeted approach to answering the question of whether autophagy-deficient cancer cells were less inherently immunogenic. It has been speculated that impaired autophagy could lead to changes in antigen

availability, processing, or presentation ([81],[82]), or to changes in immune-modulatory secreted proteins, and such effects could potentially dampen cancer cell immunogenicity and subsequent T cell responses. We thus utilized the antigen-matched OT-I system ([73]), in which OVA-specific OT-I $CD8^+$ T cells expressing a traceable fluorescent marker were adoptively transferred into mice bearing OVA-expressing B78 melanoma tumors, a derivative cell line of the B16 model. While the OT-I cells mounted a stronger anti-tumor response than endogenous T cells, the overall T cell response was comparable between autophagy-competent and deficient B78-OVA tumors. The majority of activation markers measured, most notably IFNγ, were unchanged between tumor types. We observed a marginal trending increase of TNFα-expressing T cells in autophagy-deficient B78-OVA tumors relative to control tumors, but this was not significant when p values were adjusted for multiple comparisons; while the biological significance of this single marker increase is unclear, autophagy inhibition certainly did not impair the anti-tumor T cell response in this model. Taken together, the comparable anti-tumor responses of both endogenous and antigen-matched T cells speak strongly to the autophagy independence of these programs.

Our results differ from previous work demonstrating that tumor cell autophagy promotes T cell infiltration and activation in response to anthracycline chemotherapy. Notably, autophagy promotes the *in vitro* secretion of key factors associated with immunogenic cell death (ICD), including ATP and high-motility group protein B1 (HMGB1) ([64]); consistent with those previous findings, ATP and HMGB1 secretion is impaired in doxorubicin (Dox)-treated autophagy-deficient B16 cells *in vitro*. Despite these differences, neither autophagy-competent nor deficient B16 cells that were 70% apoptotic

were able to vaccinate mice against re-challenge with healthy wildtype B16 cells. However, B16 tumor-bearing mice treated with Dox exhibited significantly elevated immune activation compared to untreated tumor-bearing mice. Importantly, autophagy deficiency did not impact T cell activation *in vivo* in B16 tumors following Dox treatment. This raises the likely possibility that there are specific clinical contexts and/or therapeutic windows in which autophagy-dependent immune modulation will not compromise chemotherapeutic efficacy. Thus, we propose that autophagy inhibition can be safely combined with chemotherapy and still stimulate a productive anti-tumor T cell response in certain tumor types. Future studies analyzing patient-derived T cells from clinical trials of autophagy inhibitors will be crucial to determine if this is truly the case. Finally, our studies raise the possibility that anti-cancer immunotherapies can be combined with autophagy inhibition in the future. Because both autophagy inhibition and immune checkpoint blockade are useful treatments in certain clinical contexts, such a combination would be a dual-pronged complementary treatment strategy that would unleash the power of the immune system upon weakened tumor cells.

Materials and Methods

Antibodies

Commercial antibodies include: eFluor 450, Alexa 700, and APC-Cy7 anti-CD45 (clone 30-F11, 1:400); PE and APC anti-CD3e (clone 145-2C11, 1:400); PE-Cy7 anti-CD4 (clone RM4-5, 1:400); Percp-Cy5.5 anti-CD8a (clone 53-6.7, 1:400); FITC and eFluor 450 anti-PD1 (clone RMP1-30, 1:400); eFluor 660 anti-IFNγ (clone XMG1.2, 1:400); FITC and eFluor 450 anti-TNFα (clone MP6-XT22, 1:400); and eFluor 450 anti-Foxp3 (clone FJK-16s, 1:400) obtained from eBioscience (San Diego, CA, USA). APC-Cy7 anti-CD45 (clone 30-F11, 1:400); FITC anti-CD8a (clone 53-6.7, 1:400); Brilliant Violet 785 anti-CD44 (clone IM7, 1:800); Pacific Blue anti-Granzyme B (clone GB11, 1:400); and Brilliant Violet 421 anti-PDL1 (clone 10F.9G2, 1:800) obtained from Biolegend (San Diego, CA, USA). Anti-ATG7 (2631, 1:500) obtained from Cell Signaling Technology (Danvers, MA, USA). Anti-ATG5 (NB110-53818, 1:2000) obtained from Novus Biologicals (Littleton, CO, USA). Anti-P62 (GP62-C, 1:100 for immunofluorescence and 1:1000 for immunoblotting) obtained from Progen (Heidelberg, Germany). Anti-phospho-histone H2A.X (clone JBW301, 1:1000) and anti-GAPDH (AB2302, 1:5000) obtained from Millipore (Billerica, MA, USA). A rabbit polyclonal anti-LC3 antibody was created using a conserved N-terminal peptide between human, rat, and mouse ([83]), which is also commercially available from Millipore (ABC232, 1:1000).

Cell culture

Lewis Lanier (UCSF) provided B16 murine melanoma cells, 4T1 mammary carcinoma cells were purchased from the American Type Culture Collection (ATCC), and Matthew Krummel (UCSF) provided B78-OVA murine melanoma cells, which express ovalbumin via the mCherry-p2A-OVA sequence ([84]). All cells were cultured in D10 culture medium (DMEM, 10% fetal bovine serum, penicillin/streptomycin), verified to be free of mycoplasma contamination, and authenticated via transplantation in the appropriate syngeneic host. For stable RNA interference, pLKO.1-puro (puromycin) lentiviral plasmids containing non-targeting shRNA (shCTL) or shRNA against mouse ATG7 (NM_028835) and mouse ATG12 (NM_026217) were purchased from Sigma-Aldrich. The target sequence for shRNA directed against mouse ATG7 (TRCN0000092163) is: CCAGCTCTGAACTCAATAATA, and directed against ATG12 (TRCN0000257708) is: TGGTAAACTGGTCCTGCATTA. Viral particles were produced using a third-generation lentiviral packaging system in HEK293T cells, and used to infect B16 murine melanoma, 4T1 mammary carcinoma and B78-OVA murine melanoma cells. Following infection and drug selection, early passage stable pools of ATG knockdown cells were utilized for both *in vitro* and *in vivo* assays. To confirm autophagy deficiency following ATG knockdown, cells were cultured in full growth medium or starvation medium (HBSS), with or without Bafilomycin A (Baf A). Cell lysates were then assessed for autophagic flux by LC3-II turnover via immunoblot. To confirm autophagy deficiency in resected B78-OVA tumors, cancer cells were isolated by *ex vivo* culture of tumor digests in puromycin selection and assessed for P62 accumulation by immunocytochemistry.

For analysis of secreted factors associated with immunogenic cell death, cells were treated with 10uM Doxorubicin (Sigma, 44583) for 24 hours; conditioned medium was collected and analyzed for HMGB1 secretion by ELISA (GENTAUR, ST51011) or ATP secretion by Enliten ATP assay (Promega, FF2000). Viability of Doxorubicin-treated cells was assessed by crystal violet staining. Cultured cells were fixed with 4% paraformaldehyde (PFA) for 10 minutes at room temperature, incubated with 0.3% crystal violet for 20 minutes at room temperature, washed with deionized water, air-dried overnight, and re-solubilized with 45% methanol in deionized water for 30 minutes at room temperature prior to absorbance reading.

For T cell re-stimulation, tissue culture plates were incubated overnight with 1 µg/ml purified CD3 antibody in PBS. Excess antibody was aspirated and plates were blocked with R10 medium (RPMI, 10% calf serum, penicillin/streptomycin) at 4°C. Tumor-associated $CD8^+$ T cells were isolated by FACS and cultured overnight on CD3-coated plates with R10 medium and 0.5 µg/ml purified CD28 antibody. Conditioned medium was collected and analyzed for IFNγ secretion by ELISA (R&D, MIF00). Experiments were also repeated in which untouched tumor-associated $CD8^+$ T cells were isolated by negative bead selection kit (Miltenyi Biotec, 130-104-075).

Animals

Animal studies were performed in accordance with approved UCSF Institutional Animal Care and Use Committee Protocols. Richard Locksley (UCSF, HHMI) generously provided the IFNγ reporter (GREAT) mouse strain (Ifngtm3(EYFP)Lky) that carries a bicistronic IFNγ-IRES-eYFP reporter allele under the control of the endogenous IFNγ

promoter/enhancer region. Murine cells expressing IFNγ also express cytoplasmic eYFP, which can be detected by flow cytometry. Matthew Krummel (UCSF) provided OT-I mice, specific for the ovalbumin peptide SIINFEKL (SL8) in the context of H-2Kb. Wildtype C57BL/6 and BALB/c mice were purchased from Jackson Laboratory.

For the generation of tumor-bearing mice, B16 and B78-OVA cells were injected subcutaneously (150,000 cells per injection in 50% growth factor-reduced Matrigel in PBS) into the back flanks of 6 to 7 week old male and female wildtype C57BL/6 mice or GREAT reporter mice on the C57BL/6 background. Mice bearing 2-week B78-OVA tumors received an adoptive transfer of $2*10^6$ freshly-isolated OT-I T cells expressing CD2-GFP by retro-orbital injection. 4T1 cells were injected orthotopically into mammary fat pads of 6 to 7 week old female wildtype BALB/c mice (100,000 cells per injection in 50% growth factor-reduced Matrigel in PBS). For studies of intracellular cytokine staining, mice were injected by tail vein with 10 ug/g of body weight of Brefeldin A (BFA, Sigma, B6542) at 6 hours prior to tumor resection. Tumors were resected, minced, and subjected to enzymatic digest with Collagenase IV (Sigma C5138, 500 U/ml), Collagenase A (Worthington LS004197, 100 U/ml), and DNase (200 ug/ml) in RPMI medium for 30 minutes at 37°C with shaking followed by passage through a 70-micron cell strainer. BFA was also added to reagents to prevent *ex vivo* secretion during tissue processing.

For prophylactic vaccination, mice were injected subcutaneously with Matrigel or 10^6 B16 cells pre-treated with Doxorubicin to achieve 70% dead and dying cells, as assessed by Annexin V and DAPI staining. Interpolation from a dose-response curve indicated that 24 hours of treatment with 8.8 μM or 7.5 μM Doxorubicin would yield 70% dead and dying cells for B16-shCTL and shAtg7 cells, respectively. One week after

vaccination, mice were injected subcutaneously on the contralateral flank with 100,000 healthy wildtype B16 cells. Tumor incidence was assessed by daily palpation.

For chemotherapy, mice bearing palpable tumors were injected by tail vein with 5 mg/kg of body weight of Doxorubicin (Sigma, 44583) once per 7 days for 2 weeks prior to tumor resection. For antimalarial treatment, mice bearing palpable tumors were injected IP with 60 mg/kg chloroquine, 50 mg/kg quinacrine, or vehicle control, daily for 4 to 6 days prior to tumor resection. B16-bearing mice were treated for either 4-5 consecutive days; 4T1-bearing mice were treated for 3 days on and 2 days off for 6 total injections. Only chloroquine treatment was used for the studies of B16 melanoma in GREAT mice because quinacrine is autofluorescent in a similar range to eYFP.

Flow cytometry and FACS

Red blood cell lysis was performed with 175 mM ammonium chloride on ice. Zombie NIR fixable viability kit (Biolegend, 423105) was applied to cells for 30 minutes on ice. Subsequent steps were performed in flow buffer (PBS, 2% calf serum, penicillin, streptomycin, glutamine, 2 mM EDTA, 0.01% sodium azide). Cells were incubated in flow buffer with FcR blocking reagent (Miltenyi Biotec, 130-092-575), 2% fetal bovine serum, 2% Armenian hamster serum (Innovative Research IGHMA-SER), and antibodies against surface markers for 30 minutes on ice. Cells were then fixed with 2% paraformaldehyde in flow buffer for 15 minutes at 25°C and permeabilized with 0.02% saponin in flow buffer for 10 minutes at 25°C and incubated with 0.02% saponin and antibodies against intracellular markers in flow buffer for 30 minutes at 25°C. Fixation and permeabilization of cells for intracellular Foxp3 staining was performed using the Foxp3 transcription factor

staining buffer set (eBioscience, 00-5523-00). All flow cytometry was performed on a BD LSR II flow cytometer. Flow cytometry data analysis was done using FlowJo software (version 10.1).

Fluorescence-activated cell sorting (FACS) of tumor-associated $CD8^+$ T cells was performed using a Beckman Coulter MoFlo XDP.

Immunoblotting

Cells were lysed in RIPA buffer with 10 mM NaF, 10 mM β-glycerophosphate, 1 mM Na3VO4, 10 nM calyculin A, 0.1 mM E64-D, 10 ug/ml Pepstatin A, and 20 nM Bafilomycin A. Lysates were cleared by centrifugation for 15 minutes at 4°C, boiled in sample buffer, resolved by SDS-PAGE, and transferred to PVDF membrane. Membranes were blocked in 5% milk in PBS with 0.1% TWEEN-20 (PBS-T), incubated with primary antibodies overnight at 4°C in blocking buffer, incubated with HRP-conjugated secondary antibodies, and analyzed by chemiluminescence. Image analysis was performed on raw images, and image brightness was adjusted for publication.

Immunohistochemistry and immunofluorescence

For immunohistochemistry, tumors were resected and fixed in formalin overnight at 4°C, incubated in 30% sucrose for cryo-protection for 24 hours at 4°C, embedded in OCT and stored at -80°C prior to and following tissue sectioning. Thawed tissue slides were incubated in 4% paraformaldehyde for 5 minutes, washed with PBS-T, and incubated in 1X target retrieval solution (Dako, S1699) at 96°C for 20 minutes in a plastic Coplin jar submerged in a beaker of boiling water. Slides were cooled for 20 minutes at

25°C, washed with PBS-T, blocked with 10% goat serum in PBS-T, and incubated with primary antibody in blocking serum overnight at 4°C. Slides were washed with PBS-T and incubated with fluorescent secondary antibody for 1 hour at 25°C, washed with PBS-T, incubated with 10 mg/ml Hoechst 33342 nuclear stain (ThermoFischer Scientific, H1399) for 5 minutes at 25°C, and washed with PBS-T and distilled water. Coverslips were mounted with Prolong Gold antifade mountant (ThermoFischer Scientific, P36934) and sealed with nail polish.

For immunofluorescence, cells were cultured on fibronectin-coated coverslips for 24 hours. Cells were fixed with 4% paraformaldehyde (PFA) for 10 minutes at 25°C, incubated with 0.1M glycine in PBS for 5 minutes at 25°C to quench PFA autofluorescence, permeabilized with 0.5% Triton X-100 for 5 minutes at 25°C, and blocked for 1 hour at 25°C with 10% goat serum in PBS. Primary antibody incubation was performed overnight at 4°C, secondary antibody incubation for 1 hour at 25°C, and nuclei were stained with Hoechst 33342 nuclear stain (ThermoFischer Scientific, H1399) for 10 minutes at 25°C. Coverslips were mounted with Prolong Gold antifade mountant (ThermoFischer Scientific, P36934) and sealed with nail polish. Washes were performed between each incubation with 1X immunofluorescence wash buffer (PBS, 0.1% BSA, 0.2% Triton X-100, 0.04% Tween-20).

Fluorescence imaging was performed using a Zeiss Axiovert 200 microscope equipped with a SPOT RT camera (Diagnostic Instruments) and mercury lamp; images were acquired and prepared using SPOT and ImageJ software. Image analysis was performed on raw images, and image brightness was adjusted for publication.

Statistics

Where representative images are shown, experiments were performed at least three times and no data were excluded from analysis. Statistical analysis was done using GraphPad Prism software (version 7.01). Error bars represent standard deviations from at least triplicate experimental conditions. P values were determined by unpaired T-Test for comparisons of two groups or by two-way ANOVA for multiple comparisons as indicated. When ANOVA results were significant, multiple T-Tests were performed and p values were adjusted for multiple comparisons using the Holm-Sidak method. P values are indicated as * ($p \leq 0.05$), ** ($p \leq 0.01$), and *** ($p < 0.001$).

Figure 1. Genetic models of autophagy deficiency in mouse melanoma and mammary cancer.

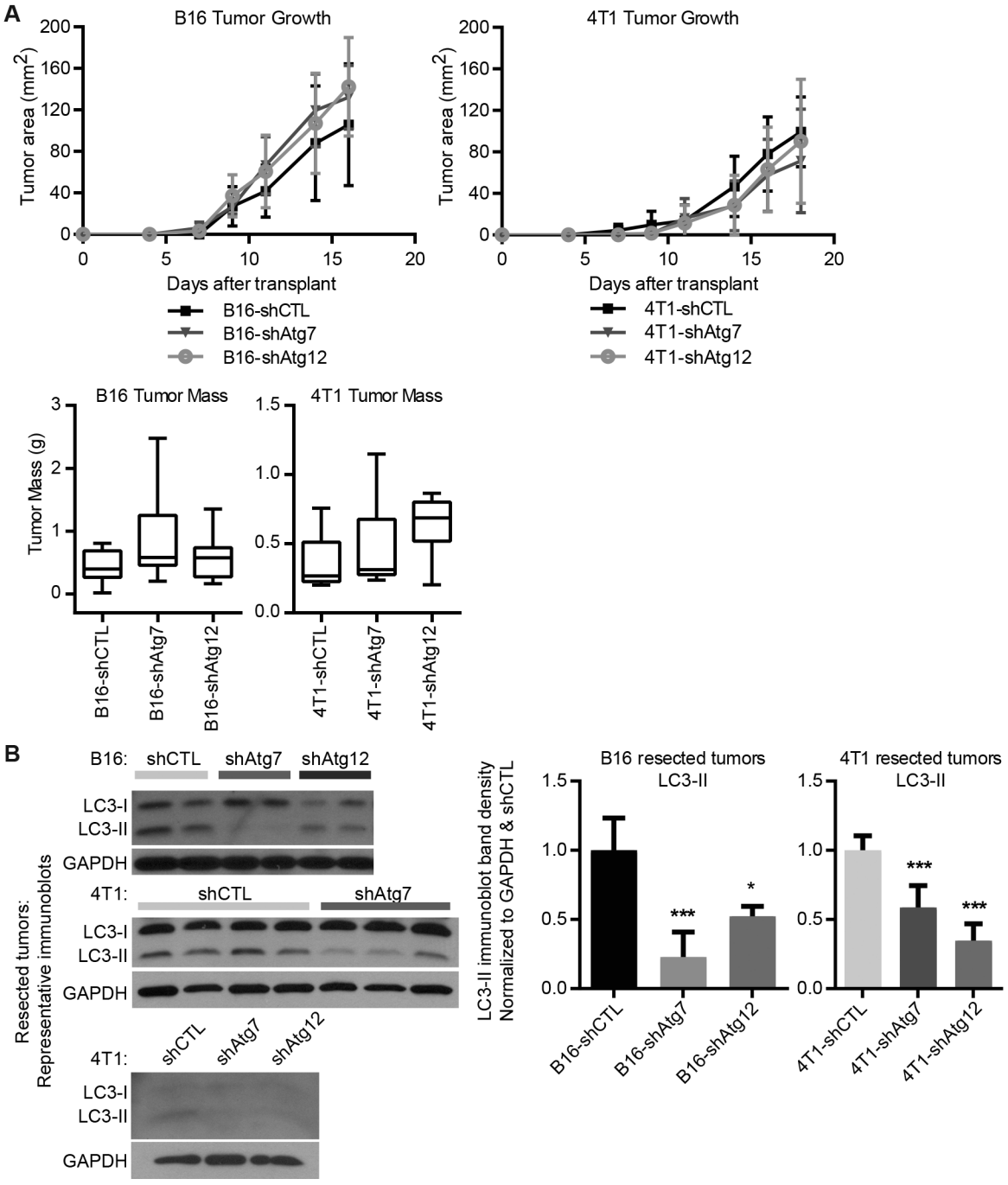

Figure 1. Genetic models of autophagy deficiency in mouse melanoma and mammary cancer. B16 mouse melanoma and 4T1 mouse mammary cancer cells bearing non-targeting shRNA (shCTL) or shRNAs directed against autophagy-related genes (ATGs) were transplanted into immune-competent host mice. (A) Top: Primary tumor growth of autophagy-competent and deficient subcutaneous B16 tumors and orthotopic 4T1 tumors in syngeneic host mice, as assessed by caliper measurements of tumor area (N=5-8). Error bars represent standard deviation. Bottom: Tumor mass at experimental endpoint (day 16-18). Box and whisker plots indicate minimum, median, and maximum values. Two-way ANOVA tests were not significant. (B) Lysates from resected tumors were assessed for continued autophagy deficiency by α-LC3 immunoblotting; band densities for LC3-II were normalized to GAPDH and to the control average within each experiment. Error bars represent standard deviation and T-Test results are indicated as * ($p \leq 0.05$) or *** ($p \leq 0.001$).

Figure 2. T cell infiltration is unchanged in autophagy-deficient mouse tumors.

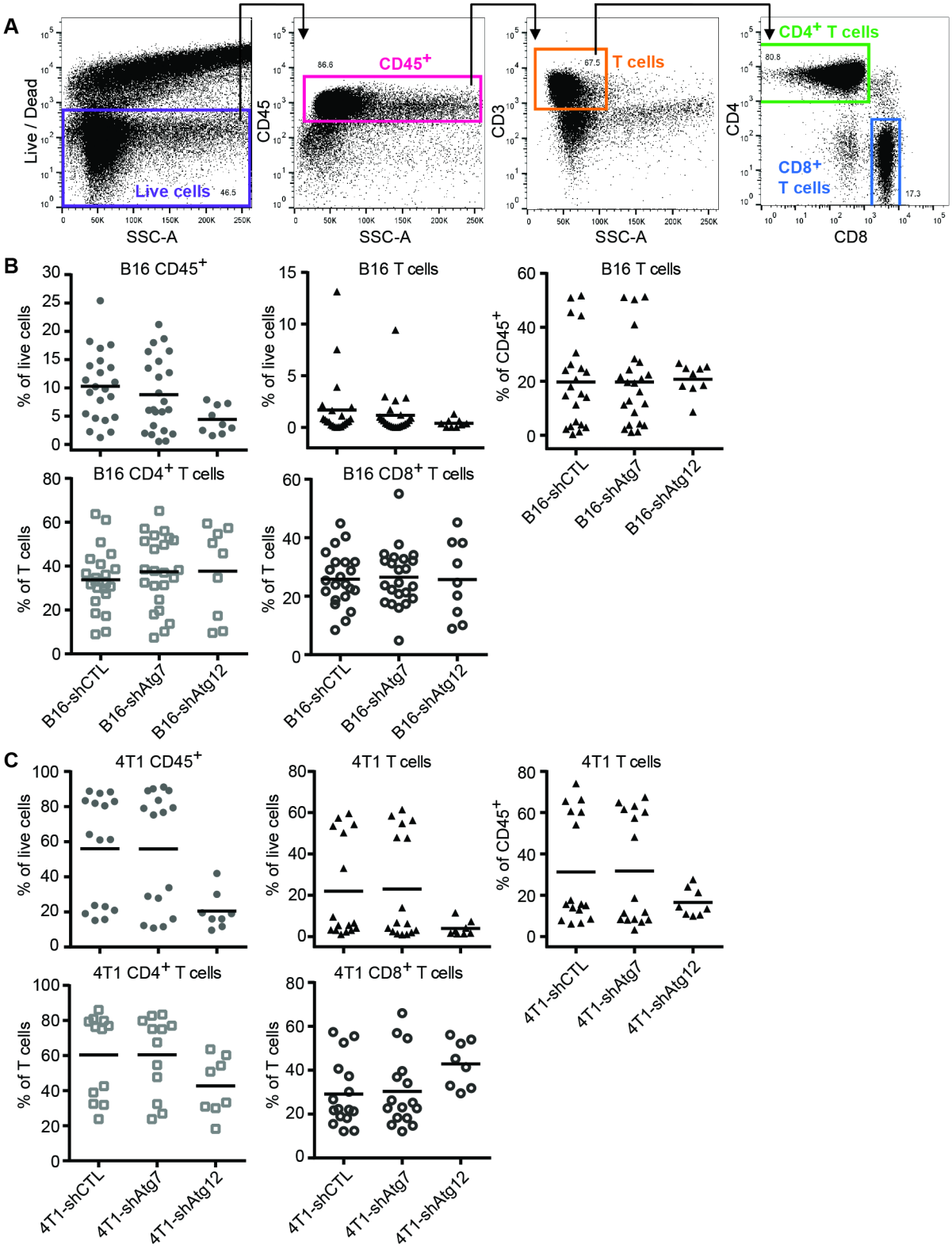

Figure 2. T cell infiltration is unchanged in autophagy-deficient mouse tumors. Subcutaneous B16 and orthotopic 4T1 tumors were allowed to form tumors for 2-3 weeks. Tumors were resected and digested enzymatically, and T cell infiltration was measured by flow cytometry. (A) Representative flow cytometry gating strategy to define T cell populations. A live/dead marker was used to define live cells as a subset of singlets. $CD45^+$ cells were defined from live cells and T cells were defined as the $CD3^+$ SSC-A^{low} fraction of $CD45^+$ cells. $CD4^+$ and $CD8^+$ single-positive T cell populations were subdivided from total T cells. (B) Infiltration of $CD45^+$ cells and T cell populations into primary mouse tumors in autophagy-competent and deficient B16 melanomas. Each data point represents a distinct tumor from a distinct host mouse. Bars represent mean values and two-way ANOVA tests were not significant. (C) Infiltration of $CD45^+$ cells and T cell populations into primary mouse tumors in autophagy-competent and deficient 4T1 mammary tumors. Each data point represents a distinct tumor from a distinct host mouse. Bars represent mean values and two-way ANOVA tests were not significant.

Figure 3. T cell functional status is unchanged in autophagy-deficient mouse tumors.

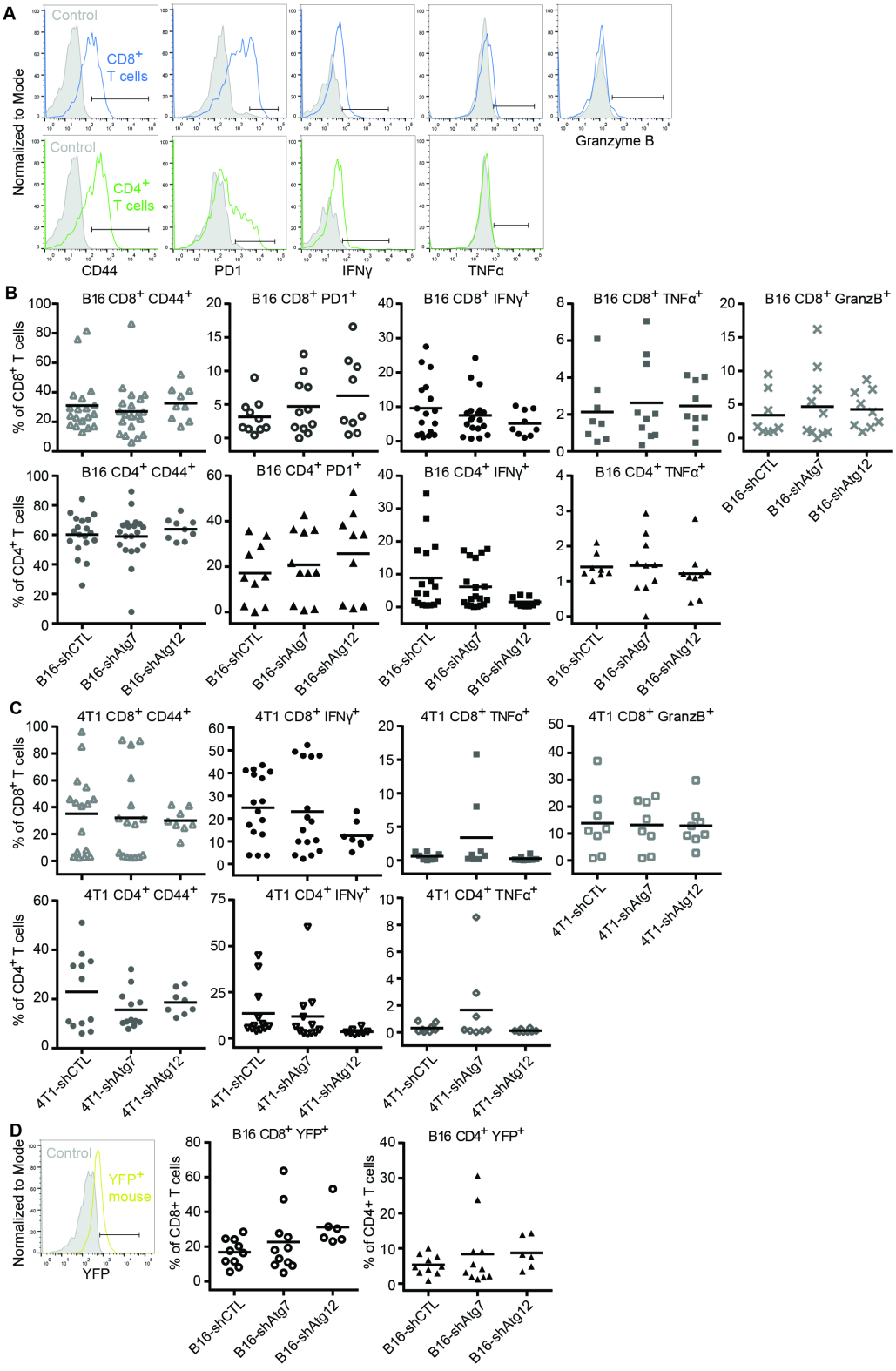

Figure 3. T cell functional status is unchanged in autophagy-deficient mouse tumors. Expression of T cell activation markers (CD44, IFNγ, TNFα, Granzyme B) and immune checkpoint marker PD1 were measured by flow cytometry in $CD8^+$ and $CD4^+$ T cell populations. (A) Representative histograms of functional marker staining of $CD8^+$ and $CD4^+$ T cell populations. Solid gray plots represent unstained controls (for staining of CD44) and isotype controls (for stains of PD1, IFNγ, TNFα, GranzB). Positive staining is indicated by gate and was defined as that above the unstained or isotype control. (B) Functional status of T cells isolated from autophagy-competent (shCTL) and deficient (shAtg7 or shAtg12) B16 tumors. Each data point represents a distinct tumor from a distinct host mouse. Bars represent mean values and two-way ANOVA test was not significant. (C) Functional status of T cells isolated from autophagy-competent (shCTL) and deficient (shAtg7 or shAtg12) 4T1 tumors. Two-way ANOVA test was not significant. (D) B16 tumors were grown in GREAT reporter mice bearing the IFNγ-IRES-eYFP reporter cassette. Representative histogram shows a YFP-negative control (solid gray plot) and cells isolated from a GREAT reporter mouse (yellow plot). Positive signal was defined as that above the control and is indicated by a gate. Endogenous eYFP expression was measured in tumor-infiltrating T cell populations by flow cytometry without BFA injection. T-Test results were not significant.

Figure 4. Transgenic OT-I cell activation is unchanged in autophagy-deficient OVA-expressing tumors.

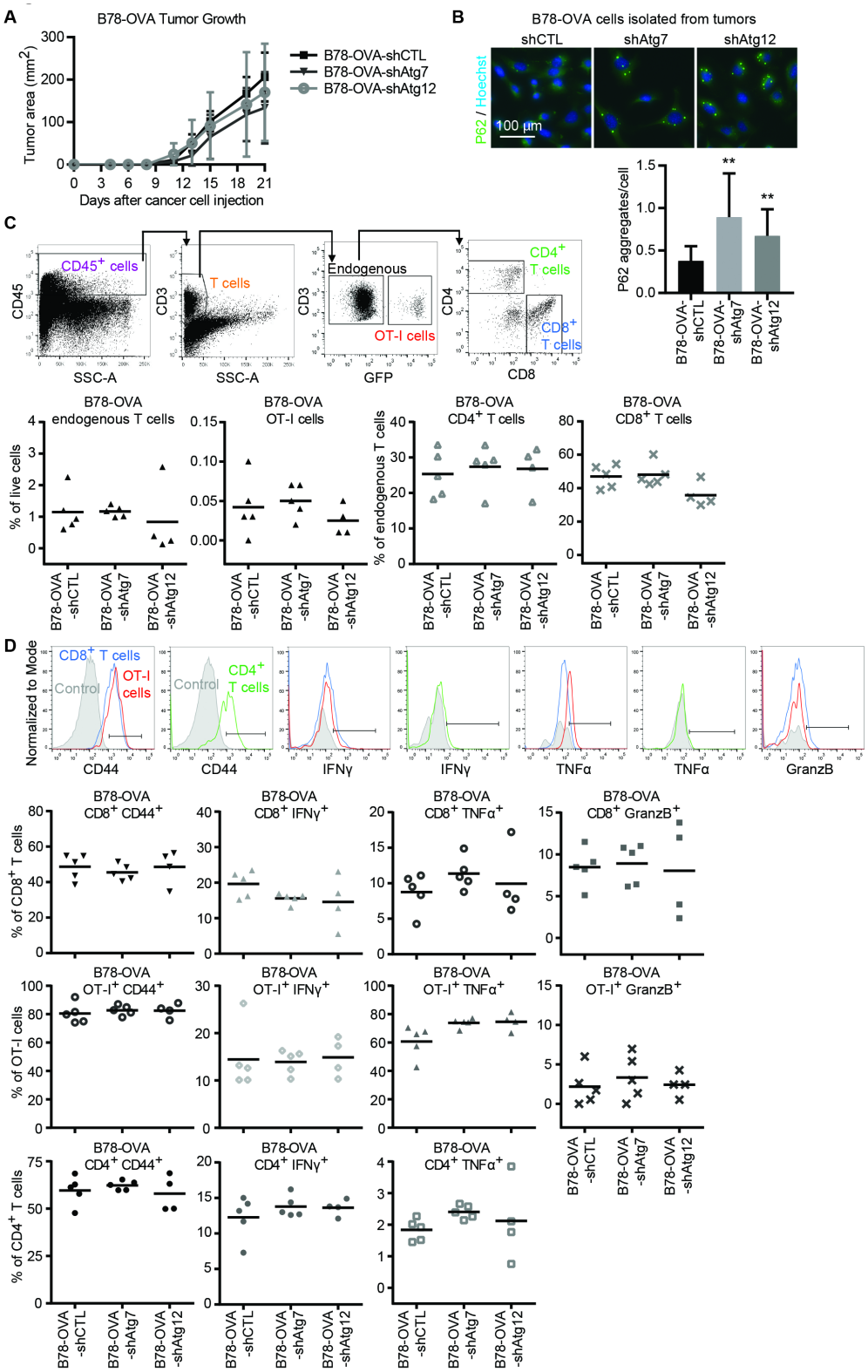

Figure 4. Transgenic OT-I cell activation is unchanged in autophagy-deficient OVA-expressing tumors. Freshly isolated transgenic OT-I $CD8^+$ T cells expressing GFP were adoptively transferred by retro-orbital injection into mice bearing two-week subcutaneous autophagy-competent and deficient B78 melanomas expressing ovalbumin (OVA). (A) Primary tumor growth of autophagy-competent and deficient subcutaneous B78-OVA tumors in syngeneic host mice, as measured by tumor area over experimental time course (N=5). (B) Autophagy deficiency was confirmed in B78-OVA cells isolated from digested tumors cultured in drug selection, by immunofluorescence for the autophagic cargo receptor P62/SQSTM1. Accumulation of p62 aggregates was quantified relative to nuclei. Error bars represent standard deviation and T-Test results are indicated as ** ($p \leq 0.01$). (C) Total T cells were defined as the $CD45^+$ $CD3^+$ SSC-A^{low} fraction of live cells and were further subdivided into OT-I (GFP^+) and endogenous (GFP^-) populations; the latter was analyzed for CD4 and CD8 surface expression. Endogenous and OT-I T cell populations were equivalent between autophagy-competent (shCTL) and deficient (shAtg12) B78-OVA tumors. Error bars represent standard deviation and two-way ANOVA tests were not significant. (D) Activation status was measured by surface CD44 and intracellular IFNγ, TNFα, and Granzyme B expression in endogenous and OT-I T cell populations from autophagy-competent and deficient B78-OVA tumors. Representative histograms of functional marker staining of endogenous and OT-I T cell populations: solid gray plots represent unstained controls (for surface staining of CD44) and isotype controls (for intracellular stains of IFNγ, TNFα, Granzyme B). Positive staining was defined as that above the unstained or isotype control and is indicated by gates. In graphs, each data point represents a distinct tumor from a distinct host mouse and bars represent mean

values. Two-way ANOVA was significant ($p=0.03$) but no T-Test p values were significant after correction for multiple comparisons.

Figure 5. Doxorubicin-treated autophagy-deficient tumors elicit equivalent T cell responses despite altered secretion of immunomodulatory factors.

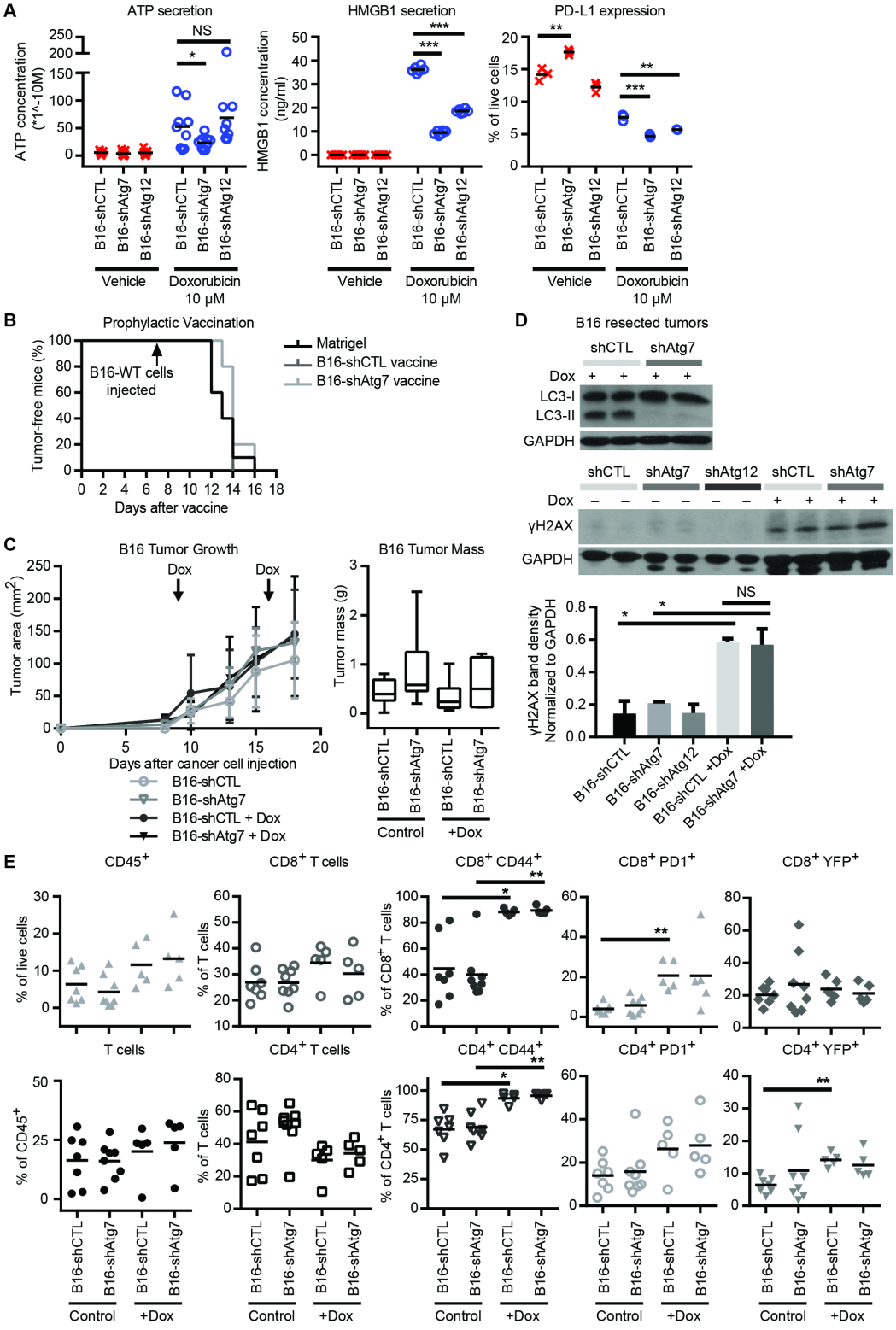

Figure 5. Doxorubicin-treated autophagy-deficient tumors elicit equivalent T cell responses despite altered secretion of immunomodulatory factors. (A) Autophagy-competent (shCTL) and deficient (shAtg7 or shAtg12) B16 cells were treated *in vitro* with 10 μM doxorubicin (Dox) or vehicle control. ATP and HMGB1 secretion were assessed in conditioned medium. The immune-suppressive cell surface marker PD-L1 was measured by flow cytometry. Data points represent biological replicates, bars represent mean values, and T-Test results are indicated as * ($p \leq 0.05$), ** ($p \leq 0.01$), *** ($p \leq 0.001$), or not significant (NS). (B) Autophagy-competent (shCTL) and deficient (shAtg7) B16 cells were treated for 24 hours with 8.8 μM and 7.5 μM Doxorubicin, respectively, and subsequently injected subcutaneously into wildtype C57BL/6 mice (N=5). Control mice were injected with Matrigel (N=10). One week later, wildtype B16 cells were injected subcutaneously into the contralateral flank. Tumor incidence was monitored by daily palpation. (C) Autophagy-competent and deficient B16 cells were injected subcutaneously into GREAT reporter mice and allowed to form palpable tumors. Mice were then treated with 5 mg/kg Dox once a week for two weeks. Growth was assessed by caliper measurements of tumor area (N=6-8); arrows indicate Dox treatment and error bars represent standard deviation. Tumor area and resected tumor mass are shown at experimental endpoint (day 18); box and whisker plots indicate minimum, median, and maximum values. Measurements of untreated tumors are also used in Figure 1A. (D) Dox-treated tumors were harvested and digested; autophagy deficiency was confirmed in resected tumors by α-LC3 immunoblotting. Lysates were also analyzed for DNA damage marker γH2AX by immunoblot. Expression was quantified by densitometry and normalized to GAPDH. Error bars represent standard deviation and T-Test results are

indicated as * ($p \leq 0.05$) or not significant (NS). (E) T cell infiltration and functional status (CD44, PD1, eYFP) in control and Dox-treated autophagy-competent and deficient B16 tumors. Bars represent mean values. Two-way ANOVA was significant ($p<0.0001$) and T-Test results between Dox-treated tumors and the corresponding untreated tumor of the same hairpin are indicated as * ($p \leq 0.05$) and ** ($p \leq 0.01$), after adjustment for multiple comparisons. Measurements between untreated cohorts and those between Dox-treated cohorts were not significantly different. Measurements of untreated tumors are also used in Figure 2B and 3B.

Figure 6. Antimalarial-treated tumors elicit equivalent T cell responses.

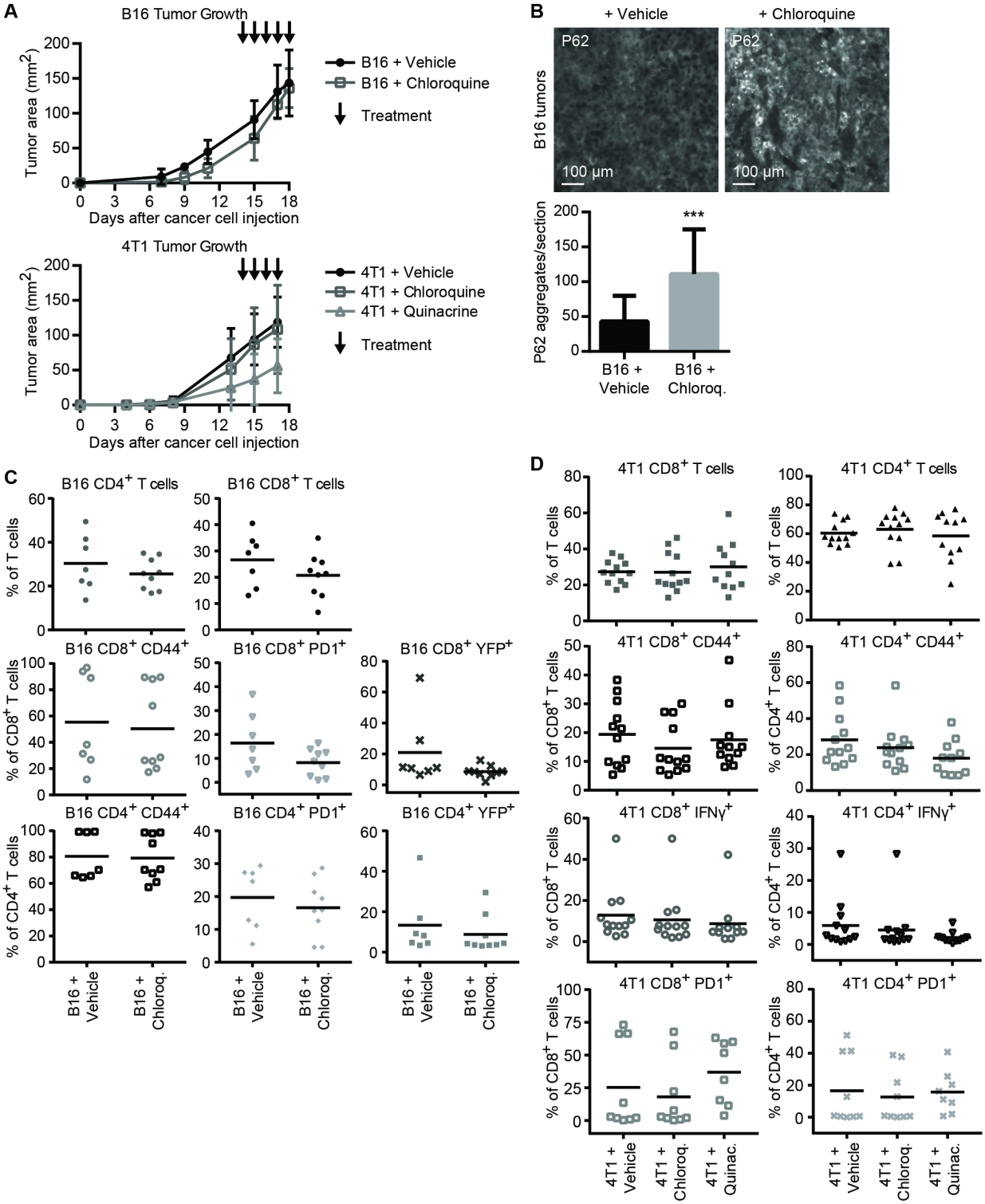

Figure 6. Antimalarial-treated tumors elicit equivalent T cell responses. Subcutaneous B16 melanomas were raised in GREAT reporter mice and orthotopic 4T1 mammary tumors were raised in wildtype BALB/c mice. Cells were allowed to form primary tumors for 7-10 days and were subsequently treated daily with chloroquine, quinacrine, or vehicle control by IP injection for 4-6 days prior to tumor resection. (A) Primary tumor growth of B16 (N=5) and 4T1 tumors (N=8-9) as assessed by caliper measurements of tumor area. Error bars represent standard deviation and arrows indicate treatment days (4-5 days for these experimental cohorts). (B) Autophagy deficiency was confirmed in resected B16 tumors by immunofluorescence for P62/SQSTM1 and accumulation of P62 aggregates was quantified. Error bars represent standard deviation and T-Test results are indicated as *** ($p \leq 0.001$). (C) Infiltration and functional phenotype of $CD4^+$ and $CD8^+$ T cell populations were measured by flow cytometry in vehicle- and chloroquine-treated B16 tumors. Data points represent distinct tumors from distinct mice and bars represent mean values. Two-way ANOVA test was not significant. (D) Infiltration and activation of $CD4^+$ and $CD8^+$ T cell populations were measured by flow cytometry in vehicle-, chloroquine-, and quinacrine-treated 4T1 tumors. Two-way ANOVA test was not significant.

Supplementary Figure 1. Validation of autophagy deficiency in B16 melanoma and 4T1 mammary cancer cells.

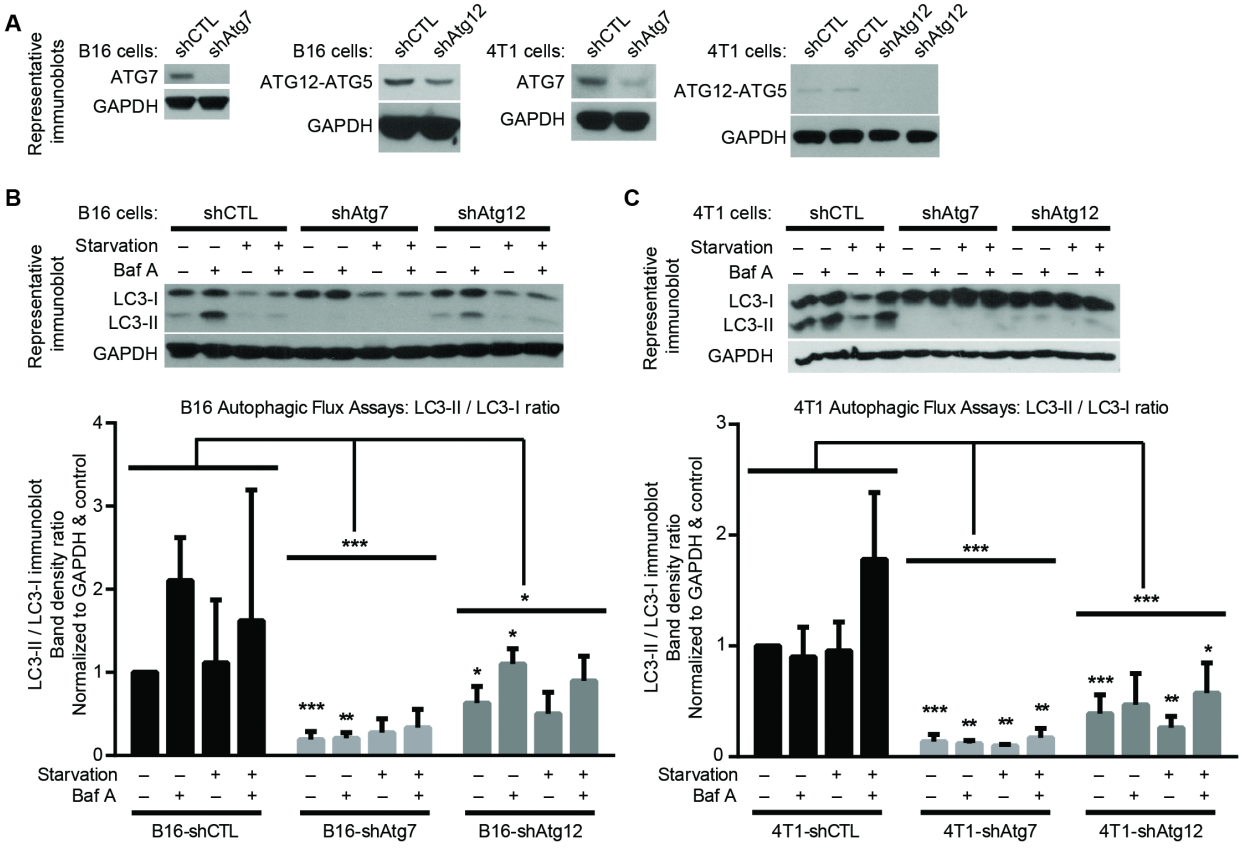

Supplementary Figure 1. Validation of autophagy deficiency in B16 melanoma and 4T1 mammary cancer cells. B16 mouse melanoma and 4T1 mouse mammary cancer cells were infected with lentivirus carrying either non-targeting (shCTL), ATG7, or ATG12 shRNA. (A) ATG7 and ATG12 knockdown was confirmed by immunoblotting. Autophagy flux assays were performed with full medium and starvation conditions, with or without Bafilomycin A (Baf A), with (B) B16 and (C) 4T1 cells. Autophagy deficiency was confirmed by reduction in the ratio of LC3-II/LC3-I. Band density was quantified from α-LC3 immunoblotting of cell lysates from three independent experiments and normalized to GAPDH and control cells grown in full medium without Baf A. Error bars represent standard deviation and T-Test results are indicated as * ($p \leq 0.05$), ** ($p \leq 0.01$), or *** ($p \leq 0.001$).

Supplementary Figure 2. Representative dot plots of T cell functional markers.

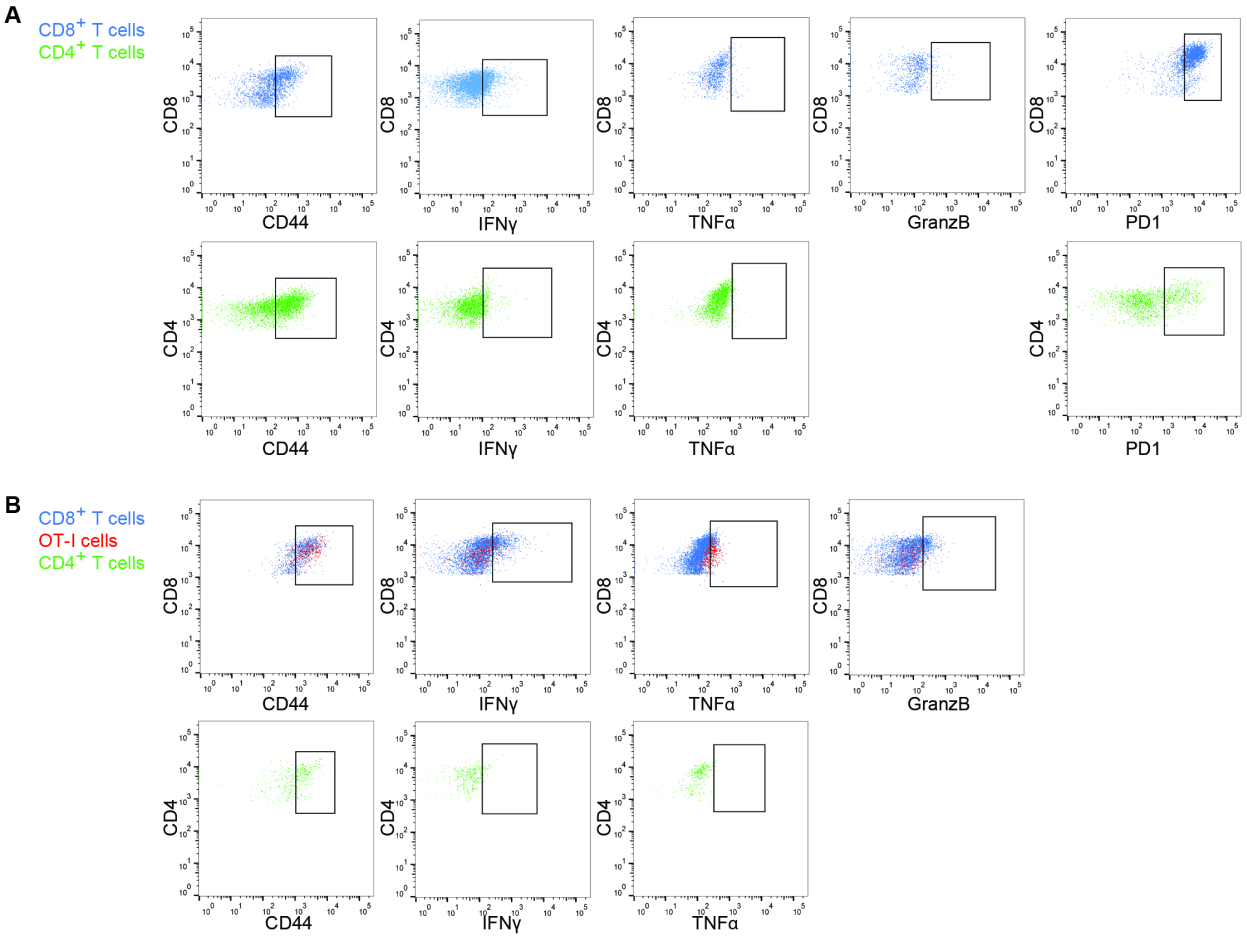

Supplementary Figure 2. Representative dot plots of T cell functional markers. (A) Dot plots correspond to histograms in Figure 3A. Expression of T cell activation markers (CD44, IFNγ, TNFα, Granzyme B) and immune checkpoint marker PD1 were measured by flow cytometry in $CD8^+$ (blue) and $CD4^+$ (green) T cell populations. (B) Dot plots correspond to histograms in Figure 4D. Expression of T cell activation markers (CD44, IFNγ, TNFα, Granzyme B) were measured by flow cytometry in endogenous $CD8^+$ T cells (blue), adoptively transferred OT-I cells (red), and endogenous $CD4^+$ T cells (green).

Supplementary Figure 3. T cell suppression and activation potential are unchanged in autophagy-deficient mouse tumors.

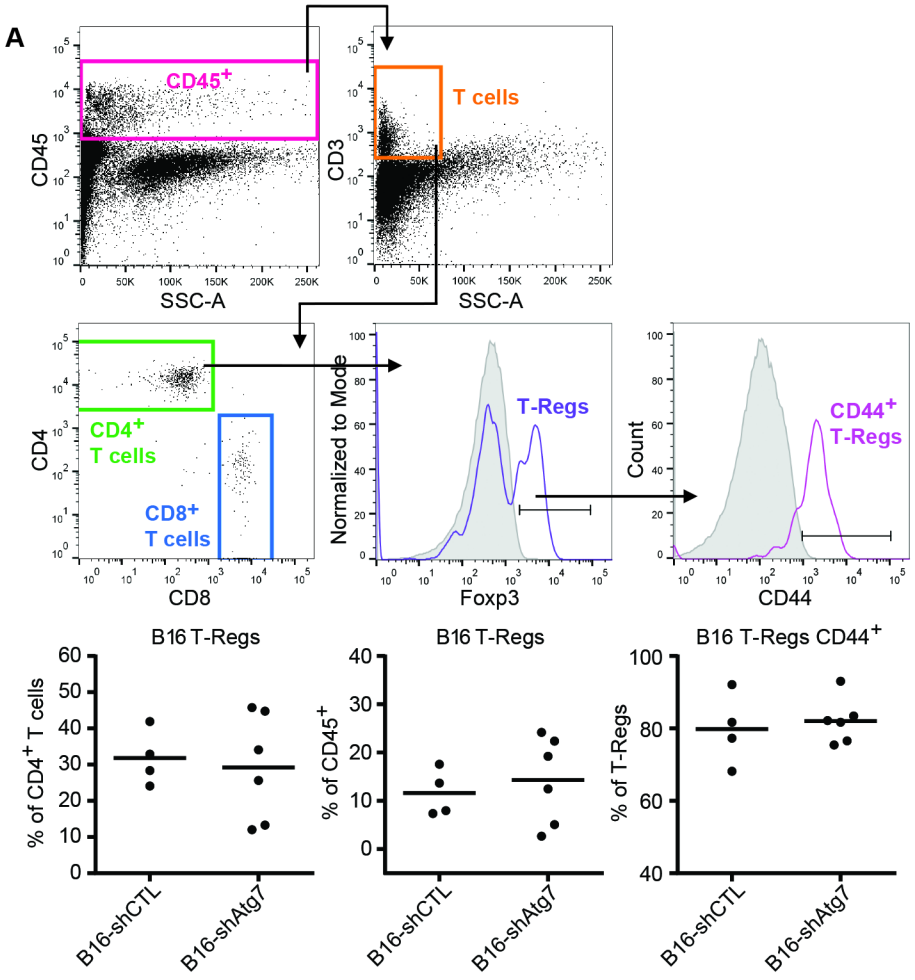

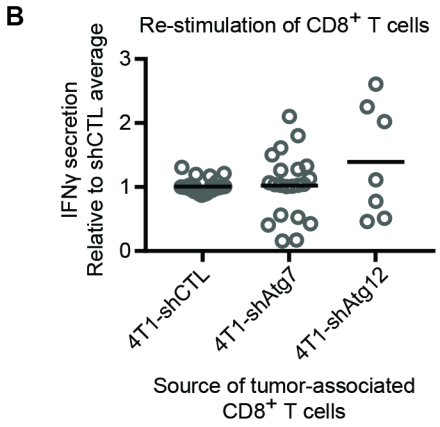

Supplementary Figure 3. T cell suppression and activation potential are unchanged in autophagy-deficient mouse tumors. Subcutaneous B16 were allowed to form tumors for 2 weeks. Tumors were resected and digested enzymatically, and Regulatory T (TReg) cell infiltration and functional status were measured by flow cytometry. (A) Top: Representative flow cytometry gating strategy to define TReg cell populations. A live/dead marker was used to define live cells as a subset of singlets. $CD45^+$ cells were defined from live cells and T cells were defined as the $CD3^+$ SSC-A^{low} fraction of $CD45^+$ cells. $CD4^+$ and $CD8^+$ single-positive T cell populations were subdivided from total T cells, and TRegs were defined as the $Foxp3^+$ fraction of $CD4^+$ cells. TReg activation was measured by surface CD44 expression. Solid gray plots represent isotype control (for stain of Foxp3) and unstained control (for stain of CD44). Positive staining was defined as that above the unstained or isotype control. Bottom: on graphs, each data point represents a distinct tumor from a distinct host mouse. Bars represent mean values and two-way ANOVA test was not significant. (B) $CD8^+$ T cells isolated from autophagy-competent and deficient 4T1 tumors are re-stimulated to equivalent activation levels. Orthotopic autophagy-competent (shCTL) and deficient (shAtg7 and Atg12) 4T1 tumors were allowed to form tumors for 2-3 weeks. Tumors were resected and digested enzymatically. $CD8^+$ T cells were isolated by either FACS or negative bead selection, and re-stimulated in overnight culture with CD3 and CD28 antibodies. Conditioned medium from T cell cultures was analyzed for IFNγ secretion by ELISA. T cell isolation was performed 5 separate times; each data point represents a distinct conditioned medium sample and bars represent means. T-Test results were not significant.

Supplementary Figure 4. Validation of autophagy deficiency in B78-OVA mouse melanoma cells.

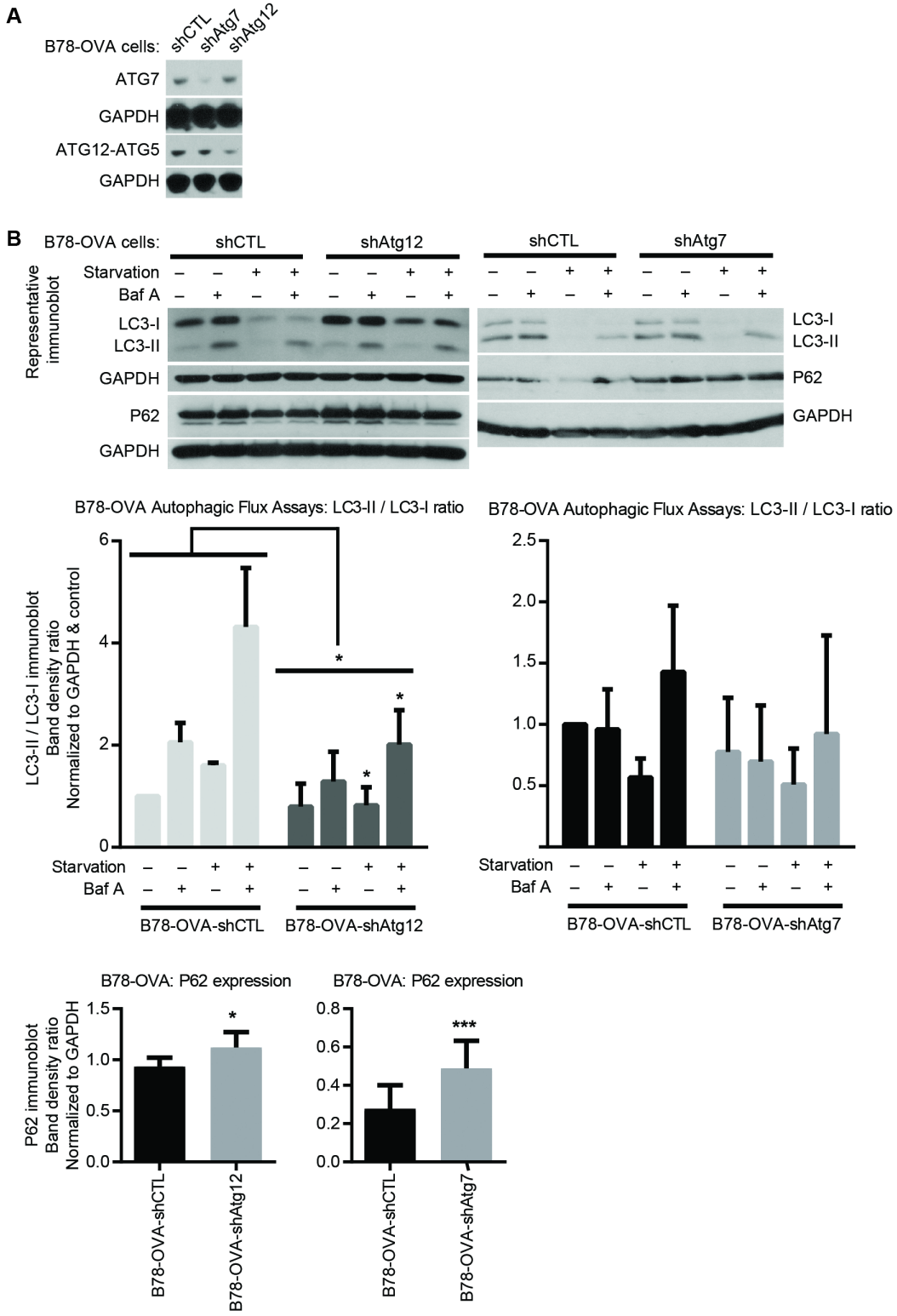

Supplementary Figure 4. Validation of autophagy deficiency in B78-OVA mouse melanoma cells. B78-OVA melanoma cells were infected with lentivirus carrying either non-targeting (shCTL), ATG7, or ATG12 shRNA. (A) ATG7 and ATG12 knockdown were confirmed by immunoblotting. (B) Autophagy flux assays were performed with full medium and starvation conditions, with or without Bafilomycin A (Baf A). Autophagy flux deficiency was confirmed by reduction in the ratio of LC3-II/LC3-I and an increase in P62 expression. Band density was quantified from α-LC3 immunoblotting of cell lysates from three independent experiments and normalized to GAPDH and control cells grown in full medium without Baf A. Error bars represent standard deviation and T-Test results are indicated as * ($p \leq 0.05$). Band density was quantified from P62 immunoblotting of cell lysates and normalized go GAPDH. Error bars represent standard deviation and T-Test results are indicated as * ($p \leq 0.05$) and *** ($p \leq 0.001$).

Supplementary Figure 5. Autophagy-deficient cells are more sensitive to Doxorubicin treatment.

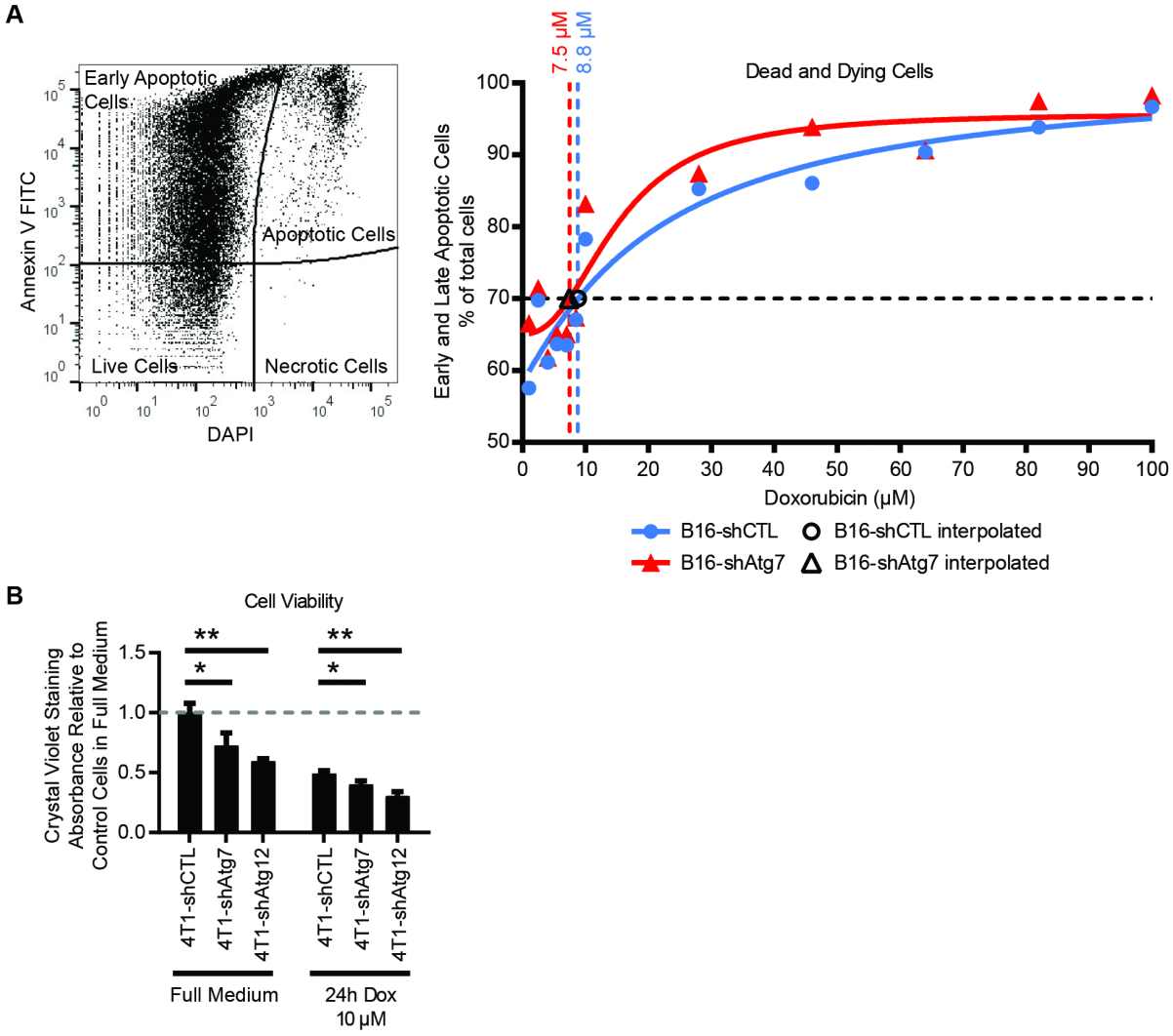

Supplementary Figure 5. Autophagy-deficient cells are more sensitive to Doxorubicin treatment. (A) Autophagy-competent (shCTL) and deficient (shAtg7) B16 melanoma cells were cultured for 24 hours with various doses of Doxorubicin. Floating and adherent cells were collected and stained with an Annexin V kit and DAPI. Singlet cells were analyzed by flow cytometry and divided into quartiles: live cells (Annexin V^{low} $DAPI^{low}$), early apoptotic cells (Annexin V^{high} $DAPI^{low}$), apoptotic cells (Annexin V^{high} $DAPI^{high}$), and necrotic cells (Annexin V^{low} $DAPI^{high}$). Dead and dying cells were defined as early and late apoptotic populations; dosages that achieved 70% of dead and dying cells were interpolated from a dose-response curve. (B) Autophagy-competent (shCTL) and deficient (shAtg7 or shAtg12) 4T1 mammary carcinoma cells were cultured for 24 hours in full medium or 10 μM Doxorubicin. Cell viability was measured by crystal violet staining. Error bars represent standard deviation and T-Test results are indicated as * ($p \leq 0.05$) and ** ($p \leq 0.01$).

Chapter 3

Abnormal vascular leaking is normalized following autophagy inhibition in tumors

This chapter describes unpublished work.

Contributions: I performed all the experiments and analyzed all the data with the following exceptions. Fanya Rostker was responsible for mouse husbandry and genotyping and performed caliper measurements of tumors. Jennifer Rudnick and Juliet Goldsmith assisted with mouse surgeries. Jay Debnath supervised the entire project.

Abstract

Cancer cells utilize protein secretion to hijack neighboring host cells to support tumor growth and progression. Secretory autophagy is the process by which unconventionally secreted cytoplasmic proteins are captured and secreted utilizing autophagic machinery. While poorly understood, such a mechanistic overlap between an intracellular stress response and an extracellular form of communication could prove to be important for a tumor undergoing environmental stress and requiring the recruitment of external aid. Modulating autophagy in cancer cells therefore presents an opportunity to modulate a secretory program, and as a result disrupt a collection of factors involved in tumor-stromal interactions. Autophagy-deficient 4T1 mouse mammary tumors exhibited decreased vascular leaking as compared to autophagy-competent controls *in vivo*. This phenotype was replicated in 4T1 tumors overexpressing the P62/SQSTM1 autophagic cargo receptor but not by global ablation of unconventional secretion by knockdown of the essential gene GRASP55. Autophagy-deficient 4T1 mammary cells secreted lower levels of several angiogenic and inflammatory cytokines as compared to autophagy-competent controls *in vitro*, and stimulated less branching of HUVECs *in vitro*. This study presents a novel approach to disrupting tumor-stromal secretory interactions via the inhibition of the intracellular program at their source.

Introduction

Cancer cells rely largely on secretion to communicate with their microenvironments and hijack neighboring cells to support tumor growth and progression. While there is good rationale to target the tumor microenvironment via inhibition of secreted signal, the predominant pharmacological approach has been to identify and inhibit one “key” biomarker in a particular tumor-stromal interaction, such as VEGF for angiogenesis and CSF1 for inflammation, these approaches face two risks: first, that tumors will rescue the stromal interaction by increasing secretion of a different cytokine with redundant function ([56]), or second, that this inherent redundancy will render the therapy only partially effective. Thus, to ablate a tumor’s ability to stimulate angiogenic or inflammatory microenvironments, a more potent approach would be to target an entire secreted program. However, with dozens if not hundreds of factors involved in these programs, in practice this is not feasible at the present moment.

Cellular secretion is now known to fall into two major categories: conventional secretion of proteins translated in the endoplasmic reticulum and transported through the Golgi apparatus to the plasma membrane, and unconventional secretion of cytoplasmic protein engulfed by vesicles and transported to the plasma membrane. A subset of unconventionally-secreted proteins also requires autophagic machinery, which mediates cytoplasmic capture and vesicular fusion events, a process termed “secretory autophagy” ([25],[28]). Modulating autophagy in tumors could therefore undermine an entire set of secreted factors, achieving what would otherwise require a cocktail of therapeutics targeting individual secreted factors.

This could prove especially important for the interaction between cancer cells and their neighboring vasculature, which is controlled by an extensive angiogenic secretome consisting of dozens of stimulatory and inhibitory factors. While studies have yet to define the set of proteins secreted by unconventional autophagic secretion, I hypothesized that autophagy, a cellular stress response overlapping with secretion, might modulate a particular secretory program that could recruit a nourishing vasculature to a tumor experiencing environmental stress (e.g. hypoxia and nutrient starvation). Thus, depriving a tumor of autophagy might disrupt its ability to utilize this mechanism secretion-mediated compensation to survive environmental stress.

Because overt tumors secrete pro-angiogenic signals incessantly, the blood vessels that form in their microenvironments are constantly sprouting and never able to fully mature, structurally or functionally ([85]). Constant sprouting leaves gaps between endothelial cells, and thus tumor vasculature is often leaky, leading to heterogenous blood flow that floods some areas of the tumor in blood lakes ([52],[53]), while leaving other areas with poor perfusion that results in hypoxia ([54],[55]).

Anti-angiogenic therapies, while initially successful in shrinking tumors by depriving them of a supportive network of blood vessels, have often resulted in aggressive relapses due to their tendency to increase structural and functional abnormalities ([56]). Thus, some have proposed that vascular normalization might prove to be a better approach to leveraging this aspect of the tumor microenvironment, by improving drug delivery ([2],[57]). Despite extensive research, targeting the tumor vasculature remains a clinical challenge, and requires deeper mechanistic understanding.

In this study, I sought to explore whether autophagy in cancer cells could modulate the angiogenic secretome and as a result the structure or function of tumor-associated vasculature. I discovered that vascular leaking was decreased in autophagy-deficient 4T1 mouse mammary tumors as compared to autophagy-competent controls, but this phenotype was specific to the 4T1 mammary tumor model and did not apply to other tumor types I tested. Subsequent mechanistic studies demonstrated that this phenotype could be replicated in 4T1 tumors overexpressing the P62/SQSTM1 autophagic cargo receptor but not by global ablation of unconventional secretion by knockdown of the essential gene GRASP55. I also identified multiple changes in the angiogenic secretome of autophagy-deficient 4T1 cells that suggested a complex mechanism underlying this vascular normalization phenotype. By demonstrating that autophagy inhibition could alter numerous angiogenic and inflammatory cytokines, and alter the *in vivo* function of tumor vasculature, this study presents a novel approach to disrupting tumor-stromal secretory interactions via the inhibition of the intracellular program at the source of those numerous signals.

Results

Autophagy inhibition reduces necrosis and increases metastasis in 4T1 mammary cancer.

In order to dissect the effect of tumor cell-intrinsic autophagy on the development and function of the tumor microenvironment, I utilized autophagy-competent and deficient lines of 4T1 mouse mammary carcinoma described in Chapter 2. Stable knockdown of ATG7 or ATG12, essential autophagy genes (Chapter 2, Supplementary Figure 1A), led to significantly decreased autophagic flux (Chapter 2, Supplementary Figure 1C), as compared to non-targeting control hairpins. Stable autophagy inhibition was also confirmed in resected tumors (Chapter 2, Figure 1B). Primary tumor growth was unchanged between autophagy-competent and deficient 4T1 tumors (Chapter 2, Figure 1A).

Despite their equivalent tumor size, autophagy-competent and deficient 4T1 tumors exhibited strikingly different tissue morphologies. While autophagy-competent tumors exhibited extensive areas of necrosis on tissue section stained with Masson's Trichrome, this was significantly reduced in both autophagy-deficient tumor groups (Figure 1A). This apparent improvement in viability *in vivo* was particularly intriguing when taken in the context of reduction in cellular viability *in vitro* of autophagy-deficient 4T1 cancer cells (Chapter 2, Supplementary Figure 5B). Furthermore, our observations contradicted existing scientific literature proposing that autophagy deficiency would increase necrosis ([42],[86]). Even more intriguing was the observation that autophagy deficiency enhanced *in vivo* lung metastasis of 4T1 mammary carcinoma cells (Figure

1B). Because of autophagy's role in promoting cellular health and survival of extrinsic stress, it has been hypothesized that autophagy would support cancer cells' ability to survive the highly stressful processes of the metastatic cascade ([87]), yet in our 4T1 tumors, autophagy appeared to suppress metastasis. Furthermore, elevated necrosis in the tumor microenvironment is typically associated with elevated hypoxia and metastasis ([88]), whereas in our 4T1 tumors the phenotypes were changing in opposite directions.

Taken together, these unexpected results could not be explained solely by autophagy's cell autonomous role in cancer cell homeostasis and survival. Instead, they strongly suggested a non-cell autonomous role for cancer cell autophagy in modulating tumor microenvironment interactions. I hypothesized that such interactions could recruit more support from the extrinsic environment and compensate for any intrinsic impairment in cellular health.

Autophagy-competent and deficient 4T1 mammary tumors recruit comparable quantities of stromal cells.

I began characterizing the tumor microenvironment of autophagy-competent and deficient 4T1 tumors by assessing the infiltration of stromal cells known to be important for supporting tumor growth and progression ([16]). I observed that autophagy-competent and deficient tumors recruited comparable quantities of fibroblasts and macrophages, as measured by immunohistochemical analysis of alpha-smooth muscle actin (SMA) and cell surface glycoprotein F4/80 (Figure 2A).

I next measured the infiltration of vascular endothelial cells by immunostaining for a pan-endothelial cell antigen (MECA32), and observed no change in microvessel density

between tumor types (Figure 2B). However, higher numbers of extravascular red blood cells were evident in autophagy-competent control tumors as compared to autophagy-deficient tumors on Masson's Trichrome stains (Figure 1A), and thus I was interested in dissecting the function of tumor-associated blood vessels more closely.

Autophagy deficiency reduces vascular leaking in 4T1 mammary tumors.

To study vascular function, I raised autophagy-competent and deficient 4T1 tumors in wildtype BALB/c mice for two to three weeks and injected the mice with FITC-conjugated dextran by tail vein two hours before tumor resection. In order to evaluate the permeability of the tumor vasculature, I chose a large molecular weight of FITC-Dextran (2,000,000) that would remain restricted to the lumen of normal blood vessels but would extravasate into the tissue wherever abnormally large gaps between endothelial cells occurred. Vascular endothelium was visualized by immunostaining for the vascular endothelium for the endothelial marker MECA32. While I observed extensive areas of extravascular FITC-Dextran in the tissue of control 4T1 tumors, FITC fluorescence was almost entirely restricted to the blood vessels of autophagy-deficient 4T1 tumors, indicating a striking decrease in leaking associated with vascular normalization (Figure 3A). Quantification of FITC fluorescent intensity across multiple tumors showed that this decrease was statistically significant (Figure 3A).

Normal blood vessels in healthy tissues exhibit a tight "sandwich" of three structural layers: endothelial cells lining the blood vessel lumen are coated with a basement membrane abundant in collagen IV, with pericytes wrapped around the outside to aid with vessel contraction ([89]). Blood vessels bathed in perpetual pro-growth signals,

such as those within aggressively-growing tumors, are often unable to reach appropriate structural maturity, and are thus prone to various structural abnormalities including endothelial gaps and denuded endothelium where pericyte and basement membrane coverage is lost ([89]). To evaluate the structure of blood vessels associated with 4T1 tumors, I immunostained for alpha-smooth muscle actin (SMA) expressed by pericytes, MECA32 expressed by endothelial cells, and collagen IV, and observed normal adherence of these three layers in both autophagy-competent and deficient tumors (Figure 3B). Thus, vascular normalization was not occurring as a result of changes in basement membrane or pericyte coverage of blood vessels.

Vasculature associated with B16 tumors is less leaky than in 4T1 tumors.

Next, I wished to determine whether vascular normalization would occur in other models of autophagy-deficiency in tumors. I utilized autophagy-competent and deficient lines of B16 mouse melanoma described in Chapter 2, in which stable knockdown of ATG7 (Chapter 2, Supplementary Figure 1A) leads to a significant decrease in autophagic flux (Chapter 2, Supplementary Figure 1B), and this decrease is maintained during *in vivo* tumor growth as measured by reduction in LC3-II in resected tumors (Chapter 2, Figure 1B). As with 4T1 tumors, B16 tumors grew with similar kinetics independent of autophagy status (Chapter 2, Figure 1A).

To assess vascular leaking, I raised autophagy-competent and deficient B16 tumors in wildtype C57BL/6 mice for two weeks and introduced FITC-Dextran with a molecular weight of 2,000,000 into the blood stream by intravenous injection two hours prior to tumor resection. Unlike control 4T1 tumors, control B16 tumors did not exhibit

extensive vascular leaking by extravascular FITC-Dextran (Figure 3C), indicating that B16 tumor-associated blood vessels lacked the abnormally large endothelial gaps of 4T1 tumors that permitted extravasation of high molecular weight dextran. FITC-Dextran fluorescence was limited to the lumen of MECA32^{+} blood vessels in both autophagy-competent and deficient B16 tumors as assessed by immunohistochemistry (Figure 3C). While it was possible that smaller endothelial gaps existed in control B16 tumors that might be normalized by autophagy deficiency, a phenotype that could be visualized by injecting a smaller molecular weight of fluorescently-labeled dextran, Masson's Trichrome stains of B16 tumors did not exhibit extensive extravascular red blood cells (data not shown), and thus I returned my attention to the study of vascular normalization in autophagy-deficient 4T1 tumors.

Autophagy deficiency attenuates the angiogenic secretome of 4T1 mammary carcinoma cells.

The most likely cause of decreased vascular leaking would be attenuated pro-angiogenic signaling from autophagy-deficient 4T1 cancer cells are compared to autophagy-competent control cells. To test this hypothesis, I collected conditioned medium from autophagy-competent and deficient 4T1 cells cultured in 0.5% serum for 24 hours and evaluated a panel of angiogenic cytokines by commercial membrane-based cytokine array (Figure 4A). I identified five angiogenic cytokines with significantly decreased levels in grouped autophagy-deficient (ATG7 and ATG12 knockdown) secretomes as compared to controls (G-CSF, IL12 p40/70, MCP-1, M-CSF, and PF4)

(Figure 4A). Several other factors also followed this trend of decrease upon autophagy deficiency, but were not statistically significant for both independent hairpins.

Interestingly, the largest differences in secretion levels were observed in cytokines not involved in direct signaling to vascular cells, but acted through an intermediate cell type associated with inflammation or wound repair. For example, MCP-1 (monocyte chemoattractant protein 1, also referred to as CCL2) recruits myeloid cells and lymphocytes to sites of inflammation, and M-CSF (macrophage colony-stimulating factor, also referred to as CSF1) modulates macrophage functional differentiation ([90]). Puzzlingly, a reduction in secretion of these factors has previously been correlated to reduced metastasis ([90]), yet in my model, these two phenotypes were uncoupled.

To determine the direct effects of angiogenic secretomes of autophagy-competent and deficient cells upon vasculature, I employed the classic experimental model of culturing human umbilical vein endothelial cells (HUVECs) on Matrigel in conditioned medium collected from autophagy-competent and deficient 4T1 cancer cells cultured in full growth medium containing 10% serum. While unstimulated HUVECs adhered to the Matrigel individually or in clusters, those stimulated by pro-angiogenic signals formed rudimentary vessel-like branch structures between cells (Figure 4B). Quantification of branch points revealed that autophagy-deficient 4T1 cells produced a secretome that stimulated less angiogenesis *in vitro* as compared to autophagy-competent cells (Figure 4B). Thus, the mix of growth factors in autophagy-deficient 4T1 secretomes, while pro-angiogenic to the point of stimulating some HUVEC branching, was attenuated compared to controls.

My next aim was to determine whether endothelial cell junctions formed differently when receiving signals from autophagy-competent or deficient secretomes *in vitro*, as this could provide mechanistic insight to the difference in vascular leaking *in vivo*. I seeded HUVECs into their own culture medium to allow them to form cell-cell junctions normally, and then switched their culture medium to conditioned medium from either autophagy-competent or deficient 4T1 cancer cells, thus exposing them to pro-angiogenic signals. Immunostaining for vascular endothelial cadherin (VE-Cadherin), an adherens junction protein that tethers endothelial cells to each other ([91]), showed equally tight cell-cell junctions in all three conditions (Figure 4C). Similarly, immunostaining for β-catenin, an intracellular protein that binds to VE-Cadherin at the plasma membrane, exhibited similar staining patterns in all three conditions (Figure 4C). Thus, endothelial adherens junctions were not disrupted by culture in 4T1 conditioned medium.

Pro-angiogenic factors such as vascular endothelial growth factor (VEGF) induce blood vessel growth by disrupting endothelial junctions, creating space for a new vascular sprout to form. This signaling induces phosphorylation of VE-Cadherin, leading to its internalization and junction breakdown ([91]). To assess the stability of adherens junctions in endothelial cells subjected to angiogenic signals derived from autophagy-competent and deficient 4T1 cancer cells, I cultured “VeraVec” C57BL/6 mouse liver microvascular endothelial cells ([92]) in 4T1 conditioned medium and immunoblotted cell lysates for total and phosphorylated VE-Cadherin proteins (Figure 4C). I did not observe any major change in VE-Cadherin phosphorylation on either tyrosine 658 or tyrosine 685 residues (Figure 4C). Taken together, these data indicate that endothelial cell junctions are

comparable between vasculature associated with autophagy-competent and deficient 4T1 tumors.

Immune deficiency reduces vascular leaking in 4T1 mammary tumors.

The complex network of interactions between cell types in the tumor microenvironment modulates many of the abnormal mechanisms and phenotypes that bolster tumor growth and progression. The quantity and function of immune cells within the tumor microenvironment, particularly macrophages and T cells, play a large role in the pro-growth and pro-angiogenic stimuli within that environment. To address the possibility of immune cell involvement in the mechanism of vascular normalization in autophagy-deficient 4T1 tumors, I raised autophagy-competent and deficient 4T1 tumors in Rag1 null (Rag1-KO) mice for two weeks and injected FITC-Dextran intravenously two hours prior to tumor resection.

Intriguingly, I observed that 4T1 tumors raised in these mice, which lacked functional T or B lymphocytes, did not exhibit any extravascular FITC-Dextran, regardless of autophagy status within the cancer cell fraction (Figure 5A). Furthermore, when autophagy-competent and deficient 4T1 tumors were raised in wildtype C57BL/6 mice and treated with purified anti-CD8 antibodies, extravascular FITC-Dextran also decreased relative to tumors treated with control IgG antibody, independent of autophagy status (Figure 5B).

Thus, autophagy and lymphocyte deficiency, more specifically a loss of $CD8^+$ T cells, could all produce an identical vascular normalization with regard to blood vessel leaking (Figure 5B). If these deficiencies were acting in one mechanistic pathway – in

other words, if autophagy deficiency in 4T1 tumors were leading to a T cell deficiency which in turn modulated the inflammatory and vascular tumor microenvironment – then autophagy-deficient tumors might exhibit altered T cell infiltration or function. I evaluated this hypothesis extensively and rigorously (Chapter 2) and found that T cell recruitment and functional status was equivalent between 4T1 tumors as well as other cancer models. Thus, I concluded that autophagy deficiency and $CD8^+$ T cell deficiency could independently lead to a reduction in vascular leaking in 4T1 tumors, perhaps by acting upon similar mechanisms within the microenvironment.

Accumulation of P62/SQSTM1 and inhibition of unconventional secretion have opposite effects on vascular leaking in 4T1 tumors.

In search of a mechanism responsible for my observations of reduced vascular leaking in autophagy-deficient 4T1 tumors relative to autophagy-competent controls, I turned my attention to evaluating the immediate intracellular consequences of autophagy deficiency that could lead to an altered angiogenic secretome. Specifically, I was interested in assessing whether vascular normalization could be achieved by overexpressing P62/SQSTM1, an autophagic cargo receptor that has been implicated in inflammatory secretion via interaction with transcription factors NF-κB and NRF2 ([93],[94]). I generated 4T1 mammary carcinoma cells stably expressing high levels of HA-tagged wildtype P62 (P62-WT), a mutant form of P62 (W338A) that lacks the LC3-interacting region (LIR) and thus is resistant to autophagic degradation (P62-LIR) ([95]), or an empty vector. I confirmed P62 expression by immunoblotting for the HA tag, and as expected observed higher expression levels with mutant P62-LIR (Figure 6A). I then injected these

orthotopically into BALB/c mice, allowed tumors to form for two weeks, and injected FITC-Dextran intravenously two hours before tumor resection. As with ATG knockdown, upregulation of P62 did not alter tumor mass at resection compared to control 4T1 tumors (Figure 6A).

As I observed with control 4T1 tumors expressing a non-targeting RNA hairpin, control 4T1 tumors expressing an empty vector plasmid exhibited areas of extravascular FITC-Dextran (Figure 6B). I also observed a reduction in this extravascular fluorescent signal in 4T1-P62-WT tumors, and a greater reduction in 4T1-P62-LIR tumors that reached statistical significance (Figure 6B). These preliminary results suggest that elevated levels of the P62 protein, which occur during autophagy deficiency, could independently lead to vascular normalization in 4T1 mammary carcinomas *in vivo*. A larger study would be necessary to increase confidence in the conclusion that P62 modulates tumor-vascular interactions. However, the observation of the dose-dependence of vascular normalization based on levels of P62 overexpression gives credence to a mechanism involving P62 in the tumor angiogenesis program.

Ablation of unconventional secretion increases vascular leaking in 4T1 mammary tumors.

Lastly, I aimed to determine whether unconventional secretion played a role in the vascular alterations observed in autophagy-deficient 4T1 mammary tumors. Because the angiogenic and inflammatory programs contain hundreds of secreted factors, even ruling in P62 as a mediator of this mechanism of vascular normalization by autophagy would not necessarily rule out other mediators downstream of autophagy deficiency. To

evaluate this possibility, I generated 4T1 mammary cancer cells stably expressing hairpins against GRASP55, a protein necessary for unconventional secretion, and selected a hairpin that achieved robust protein reduction as compared to a control hairpin (Figure 6C). I then injected these orthotopically into the mammary glands of BALB/c mice and allowed them to form tumors for 11 days in one experimental cohort, and 20 days in another. Unlike autophagy deficiency, ablation of unconventional secretion by GRASP55 blockade resulted in significant increases in tumor size at both time points, as measured by tumor mass at resection (Figure 6C). This result suggested that impairing autophagy or unconventional secretion had different effects on 4T1 tumor growth.

Next, I assessed the tissue architecture of 4T1-shGRASP55 tumors. Again showing phenotypic divergence from autophagy deficiency, these 4T1 tumors exhibited extensive necrotic areas, often surrounded by a border of immune cells and matrix deposition (Figure 6D). Finally, histological analysis of extravascular FITC-Dextran revealed even more extensive vascular leaking than observed previously in any control 4T1 tumors (Figure 6D). While intriguing and worthy of detailed follow-up, this finding did not mimic the vascular normalization I observed in autophagy-deficient 4T1 tumors, and thus was beyond the scope of this study. Notably, while a global defect in unconventional secretion did not mimic autophagy deficiency, this observation could nonetheless not rule out the involvement of autophagic secretion, which is a small subset of all unconventional secretion.

Discussion

In this study, I demonstrate that the abnormal vasculature in a preclinical model of triple-negative breast cancer (4T1) is at least partially sustained by the autophagy program within cancer cells. Specifically, autophagy modulates aspects of the angiogenic and inflammatory secretomes that produce a highly perforated vasculature that allows for extensive extravascular leaking. Inhibition of autophagy reduces this leaking by attenuating the pro-angiogenic secretome, producing a more normalized vasculature as compared to that of autophagy-competent tumors. I demonstrate this by the significant decrease of extravascular FITC-Dextran in autophagy-deficient 4T1 tumors with two independent hairpins (ATG7 and ATG12) as compared to autophagy-competent controls. Analysis of the 4T1 secretome *in vitro* identifies decreases in several angiogenic and inflammatory secreted factors, and a decreased ability to stimulate HUVEC branching.

I also implicate P62/SQSTM1 as an intermediate step in the mechanism between autophagy inhibition and vascular normalization. Increased levels of P62 have been correlated with poor prognosis for breast cancer patients, including increased aggressiveness and metastasis ([96]). Despite its negative impact on long-term prognosis, P62 accumulation may provide a narrow yet exploitable therapeutic window for these patients by modulating a short-term normalization effect on the tumor vasculature, which can improve uniformity of drug delivery and thereby improve clinical responses. It is possible that breast cancer patients exhibiting high levels of P62 by immunohistochemistry, along with low levels of fibrinogen – a clotting factor that can act as a surrogate marker for plasma leakage – would respond well to chemotherapy and

targeted agents as a result of improved drug delivery. This could provide a novel method of stratification of a poor prognosis patient population. Future clinical studies would be necessary to test this hypothesis. Furthermore, this would provide strong clinical rationale for future clinical and pre-clinical studies of the relationship between the autophagy-P62 pathway and the structure and function of tumor vasculature.

My study of the tumor vasculature in autophagy-deficient tumors also included B16 melanoma and R221A polyoma middle-T antigen (PyMT) luminal breast cancer (data not shown). Interestingly, neither of these tumor types exhibited the same phenotypes with regard to vascular leaking and its normalization in autophagy deficiency. Thus, while autophagic support of an angiogenic and inflammatory secretome associated with abnormal tumor vasculature is a context-specific process. Intriguingly, a recent study observed that B16 tumors treated with chloroquine exhibited a reduction in blood vessel leaking as measured by fluorescently-labeled dextran (40 kDa), but this decrease did not occur in ATG-silenced B16 tumors, which exhibited unchanged vessel leaking and increased necrosis ([97]). This further supports the notion that autophagic control of tumor vascular function is highly context-dependent. It would be important to identify additional tumor models with vascular leaking and evaluate the effects of autophagy inhibition, before drawing broader conclusions about autophagy's general involvement in angiogenic secretion and tumor-vascular crosstalk.

Although I initially hypothesized that autophagy could modulate the interactions of cancer cells and their microenvironments via unconventionally-secreted proteins, inhibiting the entire unconventional secretion program via knockdown of the GRASP55 protein in 4T1 cancer cells lead to an increase, rather than normalization, of vascular

leaking. 4T1-shGRASP55 tumors also exhibited vast expanses of necrosis and were significantly larger than control tumors. On its own, this finding indicates that some unconventionally-secreted proteins play an important tumor suppressive role. The entire spectrum of unconventionally-secreted proteins has not yet been characterized, with only a handful of proteins shown to be secreted by this mechanism. Thus, basic studies would be required before it would be possible to implicate a specific factor or set of factors in this role in tumor biology. Notably, the observation that global inhibition of unconventional secretion increases vascular leaking does not rule out the involvement of a subset of unconventionally-secreted proteins in the mechanism by which autophagy inhibition decreases it. The angiogenic and inflammatory secretomes are vast programs encompassing hundreds of factors that hold each other in a delicate balance; inhibition of all unconventionally-secreted proteins by blockade of GRASP55 disrupts this balance to create a more pro-angiogenic and pro-leaking program. However, the subset of unconventionally-secreted proteins that are autophagically-secreted may still play a role in vascular normalization, and are simply eclipsed by the other effects of GRASP55 knockdown. Again, without basic studies defining the set of proteins secreted by unconventional and autophagic mechanisms, it would be difficult to perform detailed mechanistic studies to unravel these competing effects.

The complex and dynamic matrix of interactions within the tumor microenvironment has many competing and overlapping effects that are challenging to separate and study individually. I observed several confounding phenotypes in 4T1 tumors including autophagy deficiency coupled with decreased necrosis (previous work has correlated autophagy deficiency with increased necrosis), increased metastasis

(previous work has correlated decreased necrosis with decreased metastasis), and decreased vascular leaking (previous work has correlated increased vascular leaking with increased metastasis). My study appears to identify a context in which autophagy deficiency uncouples processes that have been observed in other studies to increase and decrease together. This discovery could potentially be leveraged in the clinic to disrupt intertwined processes that support breast tumor progression.

Materials and Methods

Antibodies

Commercial antibodies include: Anti-SMA (VP-S281, 1:50) obtained from Vector Labs (Burlingame, CA). Anti-F4/80 (MCA497A488T, 1:50) obtained from Bio-Rad (Raleigh, NC). Anti-MECA32 (1:25) obtained from the Developmental Studies Hybridoma Bank of the University of Iowa (Iowa City, IA). Anti-Collagen IV (ab6586, 1:200); Anti-VE-Cadherin (ab7047, 1:50); Anti-VE-Cadherin p-Y658 (ab27775, 1:500); Anti-VE-Cadherin p-Y685 (ab119785, 1:500) obtained from Abcam (Cambridge, UK). Anti-β-catenin (610154, 1:100) obtained from BD Biosciences (San Jose, CA). Anti-HA.11 (MMS-101R, 1:1000) obtained from Covance (Princeton, NJ). Anti-GAPDH (AB2302, 1:5000) obtained from Millipore (Billerica, MA, USA). Anti-GRASP55 (10598-1-AP, 1:1000) obtained from Proteintech (Chicago, IL). Purified rat IgG and purified anti-CD8 monoclonal antibodies were purchased from the UCSF monoclonal antibody core.

Cell culture

Zena Werb (UCSF) provided 4T1 murine mammary carcinoma cells and Lewis Lanier (UCSF) provided B16 murine melanoma cells. All cells were cultured in D10 culture medium (DMEM, 10% fetal bovine serum, penicillin/streptomycin). For stable RNA interference, pLKO.1-puro (puromycin) lentiviral plasmids containing non-targeting shRNA (shCTL) or shRNA against mouse ATG7 (NM_028835) and mouse ATG12 (NM_026217) were purchased from Sigma-Aldrich. The target sequence for shRNA directed against mouse ATG7 (TRCN0000092163) is: CCAGCTCTGAACTCAATAATA,

and directed against ATG12 (TRCN0000257708) is: TGGTAAACTGGTCCTGCATTA. Viral particles were produced using a third-generation lentiviral packaging system in HEK293T cells, and used to infect 4T1 mammary carcinoma and B16 murine melanoma. Following infection and drug selection, early passage stable pools of ATG knockdown cells were utilized for both *in vitro* and *in vivo* assays. To confirm autophagy deficiency following ATG knockdown, cells were cultured in full growth medium or starvation medium (HBSS), with or without Bafilomycin A (Baf A). Cell lysates were then assessed for autophagic flux by LC3-II turnover via immunoblot.

For analysis of secreted factors, 4T1 mammary cancer cells were cultured in DMEM with 0.5% fetal bovine serum and penicillin/streptomycin for 24 hours; conditioned medium was collected and cells were counted. Conditioned medium was incubated with a commercial membrane-based mouse angiogenesis array following the kit protocol (RayBiotech AAM-ANG-1). Chemiluminescent signal was collected and analyzed by a Bio-Rad ChemiDoc imaging system.

For endothelial branching (*in vitro* angiogenesis) assays, conditioned medium was collected from 4T1 mammary cells cultured in D10 for 24 hours. HUVECs were purchased from Lonza (CC-2517) and cultured on tissue culture-treated plastic dishes in culture medium with supplements in the EGM2 Bullet Kit by Lonza (CC-3214). Equal numbers of cells were then transferred onto 96 well plates with solidified 90% EC Matrix in diluent buffer (Fisher 5056837) and cultured in 4T1 conditioned medium for 7 hours. Brightfield images were collected using a Zeiss Axiovert 200 microscope equipped with a SPOT RT camera (Diagnostic Instruments); images were acquired and prepared using SPOT and ImageJ software.

"VeraVec" C57BL/6 mouse liver microvascular endothelial cells were cultured in VeraVec medium developed and optimized by Angiocrine Bioscience: DMEM/F12 medium with 50 µg/ml endothelial cell supplement (Biomedical Technologies BT-203), 20% fetal bovine serum, 1X antibiotic-antimycotic (Invitrogen 15240-062), 10 mM HEPES buffer, 5 µM SB431542 small molecule (R&D 1614), 50 µg/ml heparin (Sigma H3149-100KU), 1X glutamax (Life Technologies 35050061), 1X non-essential amino acids (Life Technologies 11140050), 20 ng/ml human FGF-2 (Peprotech 100-18B, added fresh when changing medium), and 10 ng/ml mouse VEGF (Peprotech 450-32, added fresh when changing medium).

Animals

Animal studies were performed in accordance with approved UCSF Institutional Animal Care and Use Committee Protocols. Gabriele Bergers (UCSF) generously provided Rag1 null ($Rag1^{tm1Mom}$) mice on the FvB/N background, in which a Neo cassette replaces a 1356 base pair genomic fragment of the Rag1 gene ([98]). Wildtype C57BL/6 and BALB/c mice were purchased from Jackson Laboratory.

For the generation of tumor-bearing mice, 4T1 cells were injected orthotopically into mammary fat pads of 6 to 7-week old female wildtype BALB/c mice or female Rag1 null mice (100,000 cells per injection in 50% growth factor-reduced Matrigel in PBS). B16 cells were injected subcutaneously (150,000 cells per injection in 50% growth factor-reduced Matrigel in PBS) into the back flanks of 6-7 week old male and female wildtype C57BL/6 mice.

For evaluation of vascular leaking, tumor-bearing mice were injected intravenously by tail vein with 2 mg of FITC-Dextran (molecular weight 2,000,000) two hours prior to tumor resection and formalin fixation. FITC fluorescence was assessed by microscopy as described below.

For depletion of $CD8^+$ T cells in 4T1 tumor-bearing mice, mice were injected intraperitoneally (IP) once weekly with 200 μg of a purified anti-CD8 monoclonal antibody or a purified rat IgG control.

Immunoblotting

Cells were lysed in RIPA buffer with 10 mM NaF, 10 mM β-glycerophosphate, 1 mM Na3VO4, 10 nM calyculin A, 0.1 mM E64-D, 10 ug/ml Pepstatin A, and 20 nM Bafilomycin A. Lysates were cleared by centrifugation for 15 minutes at 4°C, boiled in sample buffer, resolved by SDS-PAGE, and transferred to PVDF membrane. Membranes were blocked in 5% milk in PBS with 0.1% TWEEN-20 (PBS-T), incubated with primary antibodies overnight at 4°C in blocking buffer, incubated with HRP-conjugated secondary antibodies, and analyzed by chemiluminescence. Image analysis was performed on raw images, and image brightness was adjusted for publication.

Histology

Tumors and lungs were resected and fixed in formalin overnight at 4°C, embedded in paraffin utilizing a tissue processor and embedding station, sectioned, and stored at 25°C. Hematoxylin and eosin (H&E) staining and Masson's Trichrome staining were

performed by the UCSF Mouse Pathology Core on paraffin-embedded tissue. Bright-field imaging was performed using an Aperio ScanScope whole slide scanner.

Immunohistochemistry and immunofluorescence

For immunohistochemistry of frozen tissue, formalin-fixed tumors were incubated in 30% sucrose for cryo-protection for 24 hours at 4°C, embedded in OCT and stored at -80°C prior to and following tissue sectioning. Thawed tissue slides were incubated in 4% paraformaldehyde for 5 minutes, washed with PBS-T, and incubated in 1X target retrieval solution (Dako, S1699) at 96°C for 20 minutes in a plastic Coplin jar submerged in a beaker of boiling water. Slides were cooled for 20 minutes at 25°C, washed with PBS-T, blocked with 10% goat serum in PBS-T, and incubated with primary antibody in blocking serum overnight at 4°C. Slides were washed with PBS-T and incubated with fluorescent secondary antibody for 1 hour at 25°C, washed with PBS-T, incubated with 10 mg/ml Hoechst 33342 nuclear stain (ThermoFischer Scientific, H1399) for 5 minutes at 25°C, and washed with PBS-T and distilled water. Coverslips were mounted with Prolong Gold antifade mountant (ThermoFischer Scientific, P36934) and sealed with nail polish.

For immunohistochemistry of paraffin-embedded tissue, tissue slides were incubated at 60°C for 5 minutes, washed twice in xylene for 4 minutes, washed in a series of decreasing ethanol dilutions from 100% to 70%, and washed in distilled water. They were then transferred to target retrieval and followed the same protocol as described above for frozen tissue.

For immunofluorescence, cells were cultured on fibronectin-coated coverslips for 24 hours. Cells were fixed with 4% paraformaldehyde (PFA) for 10 minutes at 25°C,

incubated with 0.1M glycine in PBS for 5 minutes at 25°C to quench PFA autofluorescence, permeabilized with 0.5% Triton X-100 for 5 minutes at 25°C, and blocked for 1 hour at 25°C with 10% goat serum in PBS. Primary antibody incubation was performed overnight at 4°C, secondary antibody incubation for 1 hour at 25°C, and nuclei were stained with Hoechst 33342 nuclear stain (ThermoFischer Scientific, H1399) for 10 minutes at 25°C. Coverslips were mounted with Prolong Gold antifade mountant (ThermoFischer Scientific, P36934) and sealed with nail polish. Washes were performed between each incubation with 1X immunofluorescence wash buffer (PBS, 0.1% BSA, 0.2% Triton X-100, 0.04% Tween-20).

Fluorescence imaging was performed using a Zeiss Axiovert 200 microscope equipped with a SPOT RT camera (Diagnostic Instruments) and mercury lamp; images were acquired and prepared using SPOT and ImageJ software. Image analysis was performed on raw images, and image brightness was adjusted for publication.

Statistics

Where representative images are shown, experiments were performed at least three times and no data were excluded from analysis. Statistical analysis was done using GraphPad Prism software (version 7.01). Error bars represent standard deviations from at least triplicate experimental conditions. P values were determined by unpaired T-Test for comparisons of two groups or by two-way ANOVA for multiple comparisons as indicated. When ANOVA results were significant, multiple T-Tests were performed and p values were adjusted for multiple comparisons using the Holm-Sidak method. P values are indicated as * ($p \leq 0.05$), ** ($p \leq 0.01$), and *** ($p < 0.001$).

Figure 1. Autophagy deficiency decreases necrosis but increases lung metastasis in 4T1 mammary cancer.

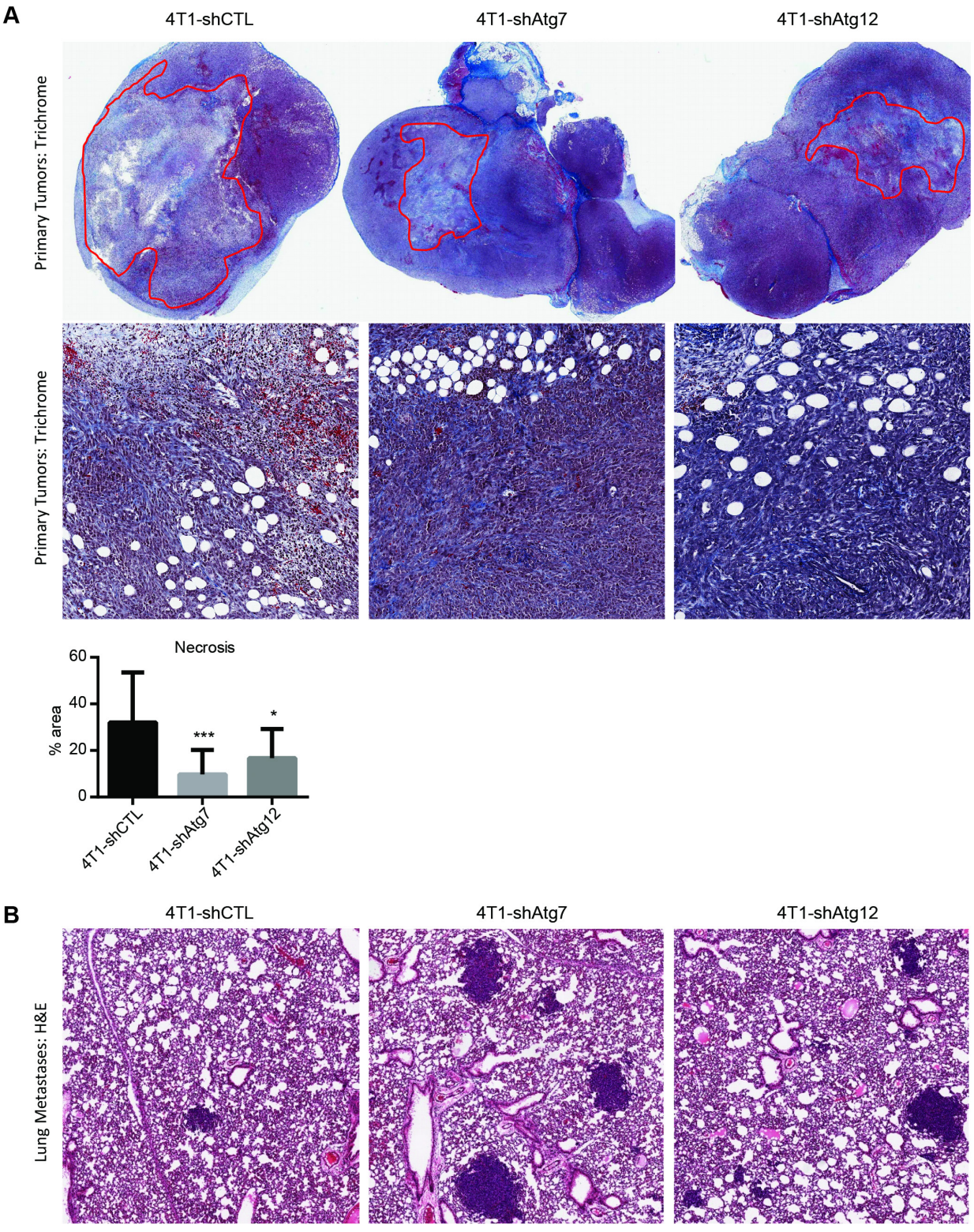

Figure 1. Autophagy deficiency decreases necrosis but increases lung metastasis in 4T1 mammary cancer. 4T1 mammary cancer cells expressing non-targeting control (shCTL), ATG7 (shAtg7), or ATG12 (shAtg12) hairpins were injected orthotopically into mammary fat pads of female 6 to 7 week old wildtype BALB/c mice and allowed to form tumors for 3 weeks. (A) Top: Gross histology of primary mammary tumors stained with Masson's Trichrome (red: red blood cells; blue: collagen; purple: nuclei). Areas of necrosis are outlined in red and quantified below. Student's t-test results are shown as * ($p \leq 0.05$) and *** ($p < 0.001$). Bottom: Masson's Trichrome staining of primary tumors at 20X resolution. (B) Lung tissue resected from autophagy-competent and deficient 4T1 mammary tumor-bearing mice.

Figure 2. Infiltration of stromal cell types is equivalent between autophagy-competent and deficient 4T1 mammary tumors.

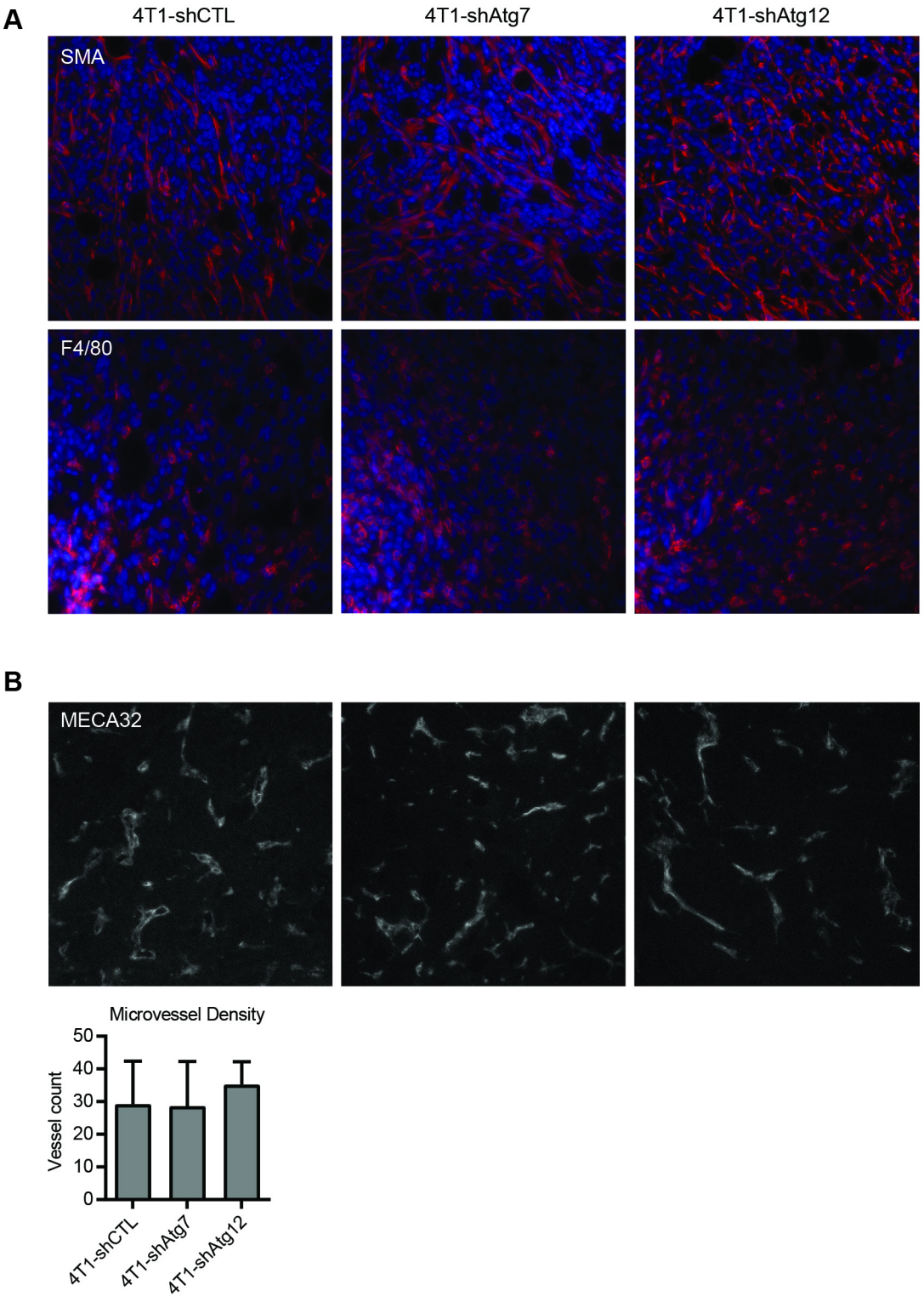

Figure 2. Infiltration of stromal cell types is equivalent between autophagy-competent and deficient 4T1 mammary tumors. Resected autophagy-competent and deficient 4T1 mammary tumors were fixed and stained by fluorescent immunohistochemistry for markers of stromal cell types. (A) Top: staining of fibroblasts and pericytes by alpha-smooth muscle actin (SMA) (red). Bottom: staining of macrophages by F4/80 (red). Nuclei were counter-stained with Hoechst (blue). (B) Staining of endothelial cells by pan-endothelial cell antigen (MECA32) (white) and quantification of microvessel density. Vessels were quantified manually and one-way ANOVA was not significant.

Figure 3. Autophagy deficiency leads to decreased vascular leaking in 4T1 mammary tumors but not B16 melanomas.

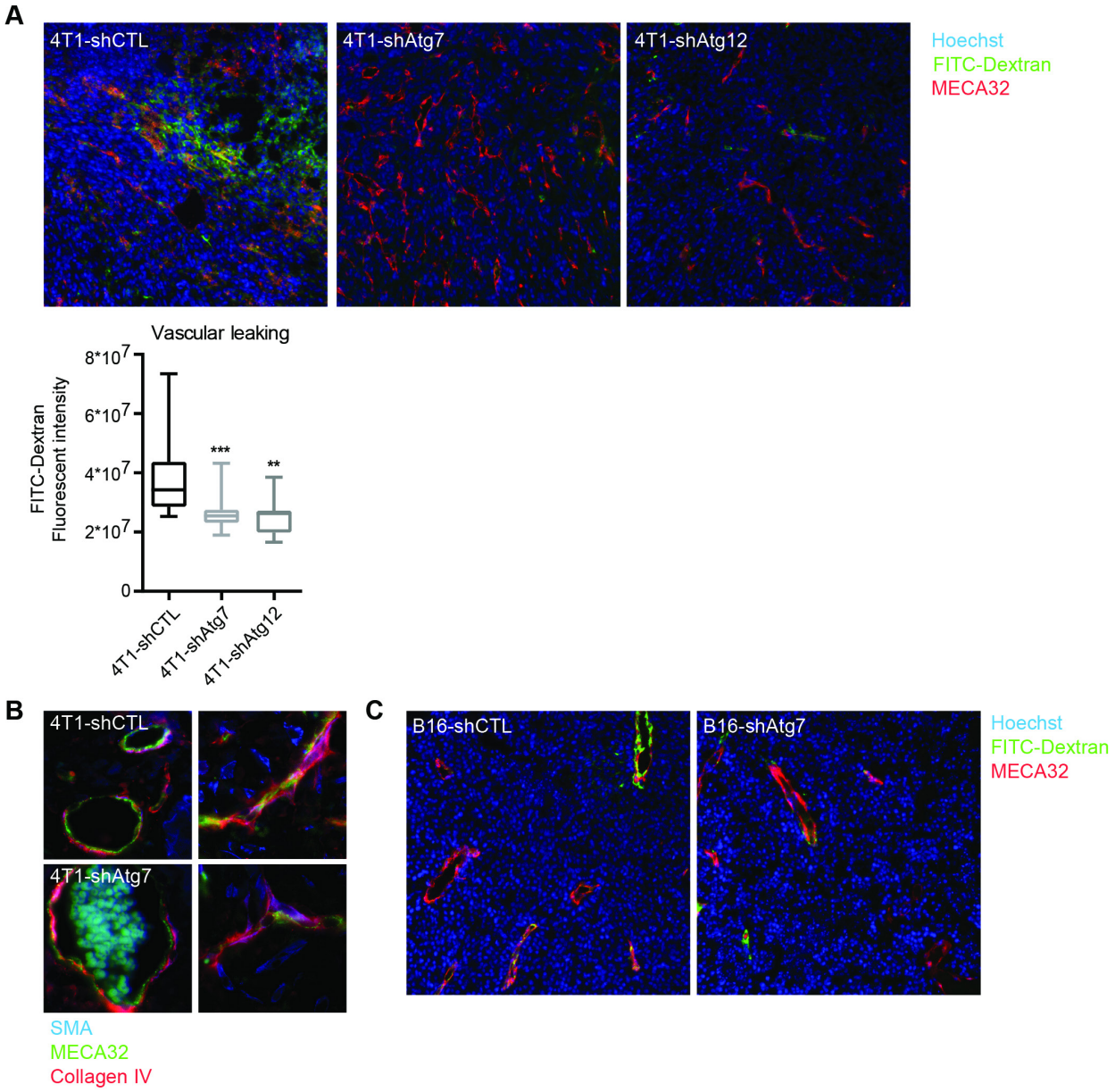

Figure 3. Autophagy deficiency leads to decreased vascular leaking in 4T1 mammary tumors but not B16 melanomas. (A) Mice bearing autophagy-competent and deficient 4T1 mammary tumors were injected with FITC-dextran (green) two hours prior to tumor resection (IV). Resected tumors were fixed and stained by fluorescent immunohistochemistry for the endothelial marker MECA32 (red). Nuclei were counterstained with Hoechst (blue). Extent of vascular leaking was quantified by fluorescent intensity of FITC-dextran. Box and whisker plots indicate minimum, median, and maximum values. Students t-test results are presented as ** ($p < 0.01$) and *** ($p < 0.001$). (B) Vascular structure in 4T1 tumors was evaluated by fluorescent immunochemistry for the pericyte marker SMA, the endothelial marker MECA32, and collagen IV. (C) Mice bearing B16 melanomas were injected with FITC-dextran two hours prior to tumor resection (IV) and stained for the endothelial marker MECA32; nuclei were counterstained with Hoechst.

Figure 4. Autophagy-deficient 4T1 mammary cancer cells exhibit an attenuated angiogenic secretome.

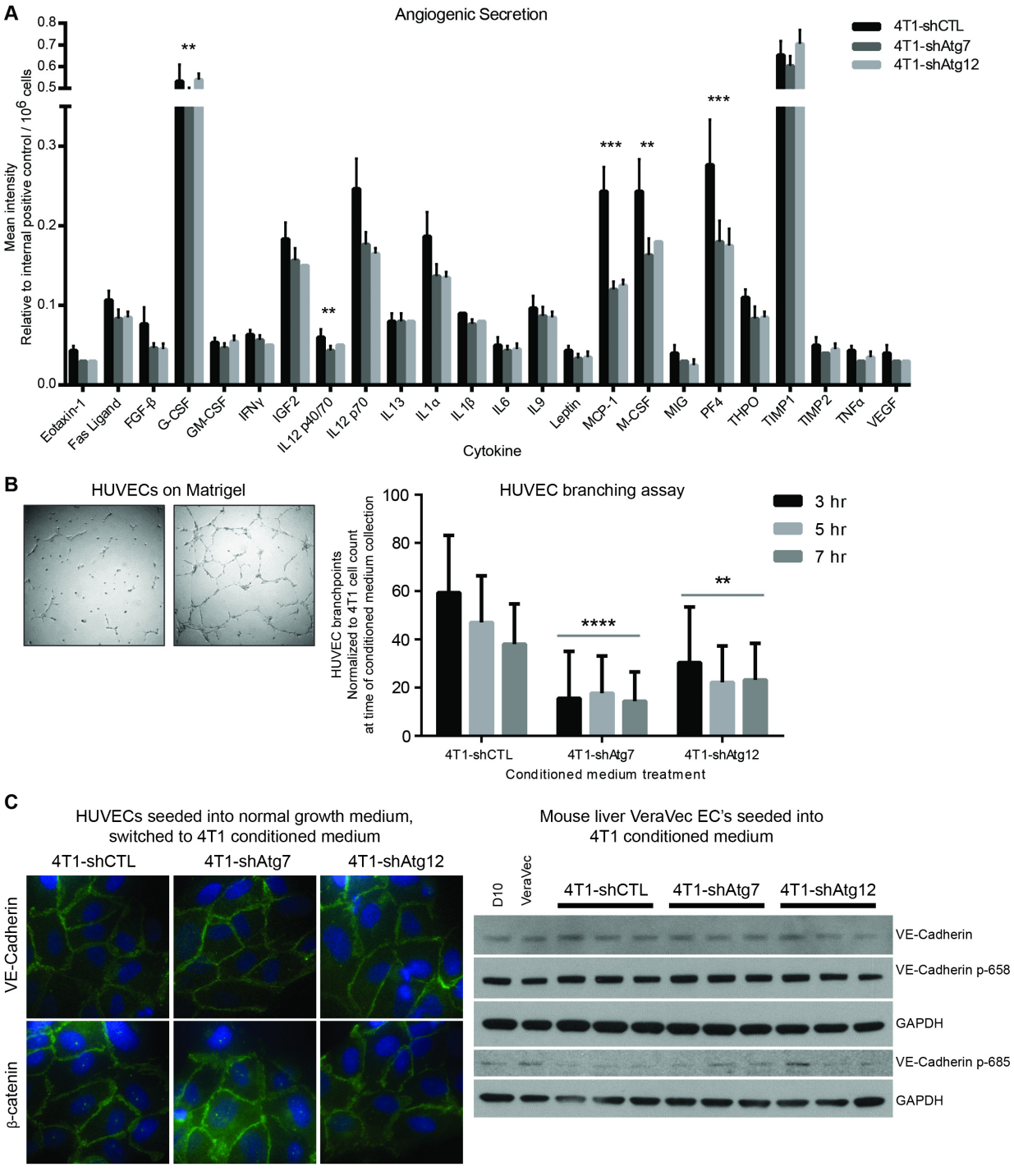

Figure 4. Autophagy-deficient 4T1 mammary cancer cells exhibit an attenuated angiogenic secretome. Autophagy-competent and deficient 4T1 mammary cancer cells were cultured *in vitro*. (A) 4T1 cells were cultured in DMEM with 0.5% serum and conditioned medium was analyzed by commercial antibody array for angiogenic cytokines. Student's t-test results are presented as ** ($p < 0.01$) and *** ($p < 0.001$). (B) 4T1 cells were cultured in DMEM with 10% serum and conditioned medium was collected and transferred to HUVECs on top of Matrigel. Left: representative images of HUVECs cultured on Matrigel show low (left image) and high (right image) amounts of branching. Right: branch points were quantified manually by the intersection of 3 or more branches. Student's t-test results are presented as ** ($p < 0.01$) and **** ($p < 0.0001$). (C) Left: 4T1 cells were cultured in DMEM with 0.5% serum and conditioned medium was collected and transferred to HUVECs cultured on fibronectin-coated coverslips. HUVECs were then stained by immunofluorescence for junction proteins VE-Cadherin (green) and β-catenin (green). Nuclei were counterstained with Hoechst (blue). Right: 4T1 conditioned medium was transferred to VeraVec mouse liver microvascular endothelial cells cultured on tissue culture plastic. After 24 hours, cell lysates were collected and immunoblotted for pan-VE-Cadherin and its phosphorylated forms.

Figure 5. Adaptive immune deficiency leads to decreased vascular leaking in 4T1 mammary tumors.

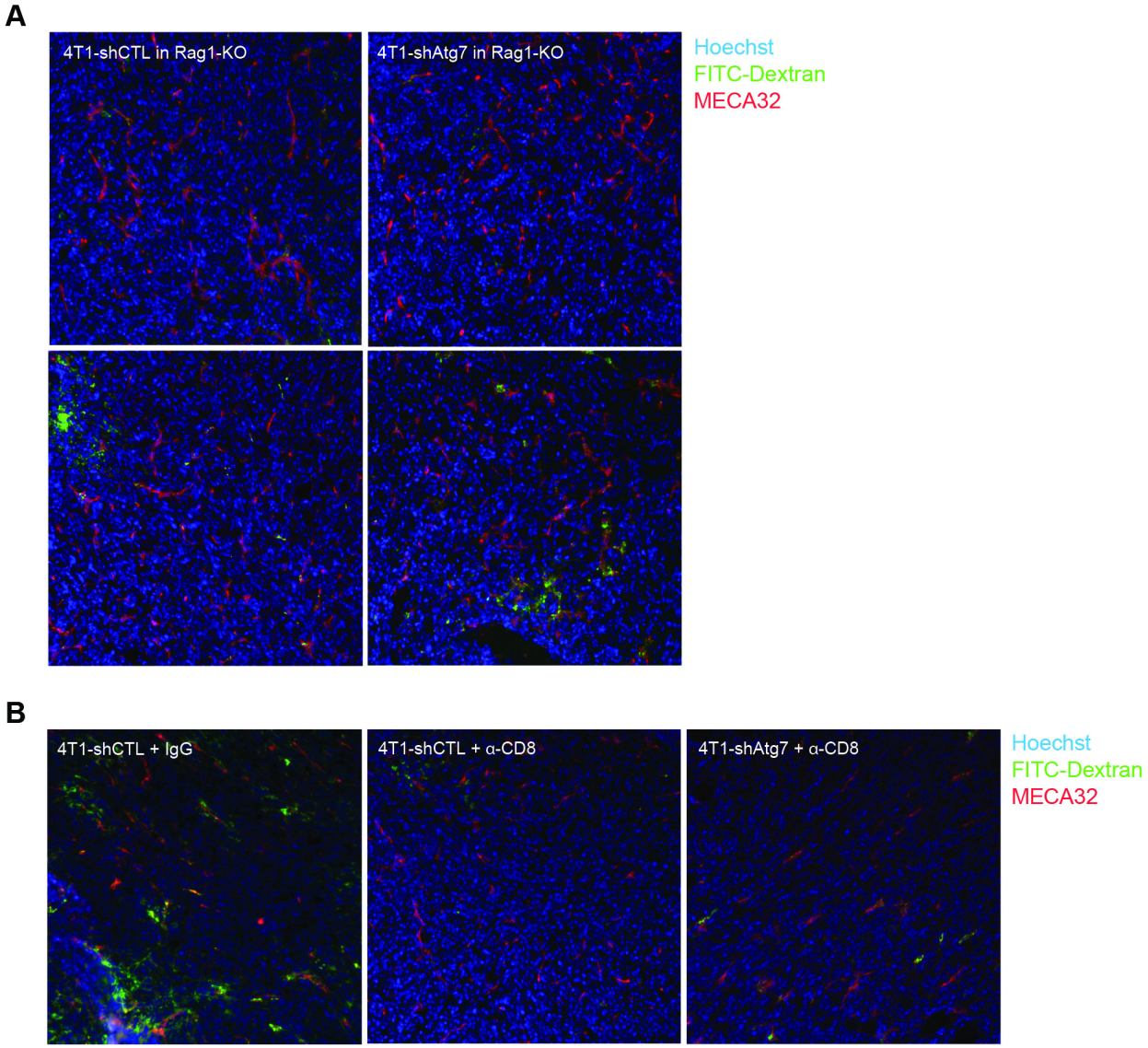

Figure 5. Adaptive immune deficiency leads to decreased vascular leaking in 4T1 mammary tumors. (A) 4T1 mammary cancer cells bearing control (shCTL) or ATG7 (shAtg7) hairpins were injected orthotopically into the mammary fat pads of Rag1 null (Rag1-KO) 6 to 7 week old female FVB mice and allowed to form tumors for 18 days. Tumor-bearing mice were injected with FITC-dextran (green) two hours prior to tumor resection (IV). Resected tumors were fixed with formalin and stained by fluorescent immunohistochemistry for the endothelial marker MECA32 (red) Nuclei were counterstained with Hoechst (blue). (B) Wildtype BALB/c mice bearing 4T1-shCTL or 4T1-shAtg7 tumors were injected weekly with purified rat IgG control antibody or purified anti-CD8 monoclonal antibody (IP) and then with FITC-dextran (green) two hours prior to tumor resection (IV). Resected tumors were stained as in 5A.

Figure 6. P62/SQTSM1 accumulation, but not inhibition of unconventional secretion, decreases vascular leaking in 4T1 mammary tumors.

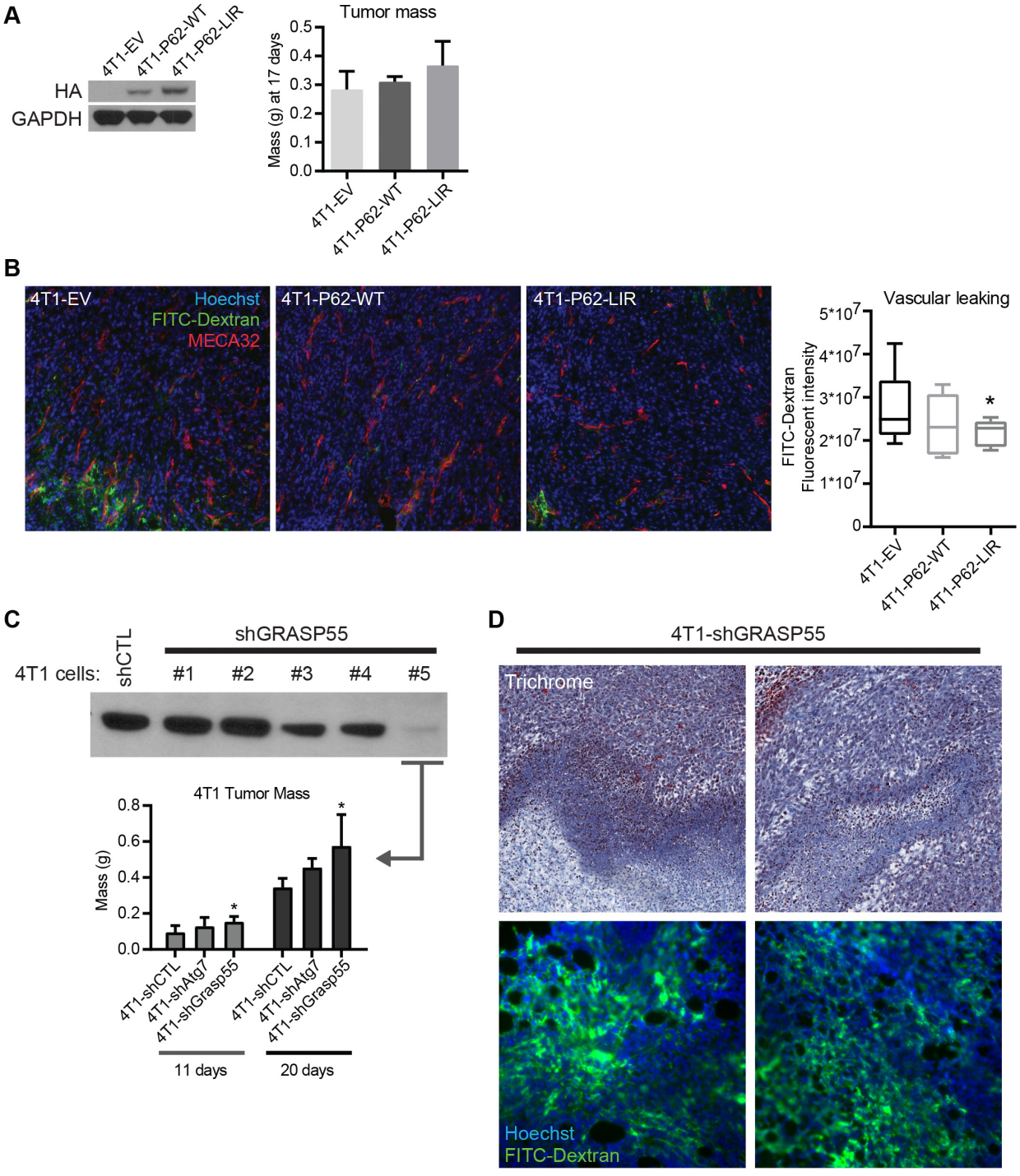

Figure 6. P62/SQTSM1 accumulation, but not inhibition of unconventional secretion, decreases vascular leaking in 4T1 mammary tumors. (A) Left: 4T1 mammary cancer cells stably expressing empty vector (EV), wildtype HA-tagged P62 (P62-WT), or a mutant form of HA-tagged P62 resistant to autophagic degradation (P62-LIR) were lysed and immunoblotted for the HA tag. Right: Cells were injected orthotopically into 6 to 7 week old female wildtype BALB/c mice and allowed to form tumors for 17 days. Tumor mas at resection was not significantly different between cohorts. (B) Tumor-bearing mice were injected with FITC-dextran (green) two hours prior to tumor resection (IV), fixed in formalin, and stained by fluorescent immunohistochemistry for the endothelial marker MECA32 (red). Nuclei were counterstained with Hoechst (blue). Vascular leaking was quantified by FITC-dextran fluorescent intensity. Box and whisker plots indicate minimum, median, and maximum values. Students t-test results are presented as * ($p \leq 0.05$). (C) Top: 4T1 mammary cancer cells stably expressing non-targeting control (shCTL) or a hairpin against GRASP55 were lysed and immunoblotted for the GRASP55 protein to select the highest level of knockdown. 4T1 mammary cancer cells bearing shCTL, shAtg7, or shGRASP55 #5 hairpins were injected orthotopically into mice and allowed to form tumors for 11 and 20 days in two experimental groups. Tumor mass at resection was measured and Student's t-test results are presented as * ($p \leq 0.05$). (D) Top: Masson's Trichrome staining of resected 4T1-shGRASP55 tumors at 20X magnification. Bottom: Mice bearing 4T1-shGRASP55 tumors were injected with FITC-Dextran (green) two hours prior to tumor resection (IV), fixed with formalin and counterstained with Hoechst (blue).

Chapter 4

Discussion

For many years, the study of cancer biology and development of cancer therapy focused on cell-intrinsic properties of cancers and largely overlooked the role of the tumor microenvironment in tumor growth and progression. We now appreciate that the complex network of interactions within the local microenvironment and larger systemic environment strongly influence how tumors behave and how they respond to therapies. Therefore, it is arguably impossible to study any solid tumor without taking into consideration the role of the surrounding normal host cells.

The role of autophagy in tumor biology has been a hot topic for roughly a decade, sparked by the discovery that some tumors – particularly those driven by oncogenic Ras – exhibit a reliance on a highly active autophagy pathway. Autophagy's role as a stress survival pathway makes it an ideal target for cancer therapy, given the numerous mechanical and metabolic stresses experienced by cancer cells in the tumor microenvironment. Pharmacological inhibition of autophagy was facilitated by the existence of a class of FDA-approved antimalarial agents. Despite the strong rationale and accessibility of clinical autophagy inhibition, clinical trials have had variable results. It is therefore imperative that additional pre-clinical and translational studies define the appropriate clinical contexts for inhibiting autophagy.

The cancer cell-intrinsic focus of existing studies of autophagy modulation might explain the mixed results observed in clinical trials. In addition to its role in intracellular degradation, autophagy machinery also overlaps with cellular secretion, and thus can modulate certain paracrine interactions between cancer cells and neighboring host cells. This must be taken into consideration when inhibiting autophagy, because the autophagic

secretion program has not yet been defined, and thus its inhibition can have unpredicted and confounding effects on tumor growth.

In this study, I aimed to define the effects of autophagy inhibition on the development and formation of the immune (Chapter 2) and vascular (Chapter 3) microenvironments of mouse melanomas and mammary tumors, given the success of immune and vascular therapies. I observed no differences between the immune responses to autophagy-competent or deficient tumors, or during acute antimalarial treatment, opening the door for future studies combining autophagy inhibition with cancer immunotherapy in preclinical and clinical studies. Both hydroxychloroquine and anti-PD1 therapy have been successful in clinical trials of melanoma, and therefore should be evaluated in combination in mouse models of melanoma.

The discovery of an autophagy-independent anti-tumor immune response (Chapter 2) directly contradicts existing studies. This speaks to the dynamic and context-dependent nature of autophagy, but also begs the question of which cell biological mechanisms are responsible for these opposing findings. While ICD has been credited with all of autophagy's effects on the immune system, it is possible that other processes, such as translocation or secretion of immune-modulatory factors, are modulated by autophagy. Others observed attenuation of ATP and HMGB1 secretion – two danger-associated molecular patterns associated with immunogenic cell death (ICD) – in autophagy-deficient mouse colon carcinoma cells. I observed this same *in vitro* phenotype in autophagy-deficient melanoma cells, yet unlike mouse colon tumors, autophagy-deficient mouse melanomas incited equivalent T cell responses *in vivo.* Based on this discrepancy, I believe that it will be critically important to define autophagy's non-

canonical functions in different mouse tumor models to develop context-specific prognostic models for immune modulation by autophagy. This will improve our understanding of when it is appropriate to inhibit autophagy, rather than generalizing for all patients based on limited preclinical studies.

I also discovered that in certain tumor types, autophagy inhibition in cancer cells can modulate paracrine interactions in a way that attenuates angiogenesis and normalizes vascular leaking (Chapter 3). This work must be expanded to additional mouse tumor models in order to define the tumor types in which this vascular normalization occurs, and the molecular mechanism by which autophagy leads to this clinically important phenotype. Because there is rising interest in vascular normalization as an alternative to anti-angiogenic therapy, but there is still difficulty in modulating angiogenic factors without challenging tumors to an evolutionary game of “whack-a-mole,” the observation that autophagy can regulate a large set of angiogenic and inflammatory factors may prove advantageous in undermining the overactive vascular program in one fell swoop. To determine if this is the case, it will be necessary to identify which specific secreted factors are modulated by autophagy.

A second precaution during systemic autophagy inhibition, in addition to cell-extrinsic effects, is the effect exerted upon non-cancerous cells. All cells within the tumor microenvironment experience stress, and thus presumably all rely to some extent upon autophagy to survive that stress. Systemic autophagy inhibition almost certainly damages or kills normal host cells in addition to cancer cells, a side effect distinct from other targeted therapies that focus on processes upregulated more specifically in cancer cells. Two prime examples of cells that may be sensitive to systemic autophagy inhibition are

activated T cells, whose high metabolic rates would require extensive protein turnover, and endothelial cells on budding blood vessels, which migrate into hypoxic environments. Assuming that autophagy inhibition would damage these two cells types, this would mean attenuated anti-tumor immunity and attenuated angiogenesis, two phenotypes that would have opposite effects on tumor growth and could therefore greatly confound patient outcomes.

I evaluated the anti-tumor T cell response during acute pharmacological autophagy inhibition using either chloroquine or quinacrine (Chapter 2) and did not observe any impairment to T cell functional activation during short-term treatment. Long-term treatment with antimalarial agents might indeed impair T cell function, as observed in antimalarial treatment of rheumatic disease; this would need to be evaluated in the context of cancer therapy. However, even the short-term ability to treat cancer patients with antimalarial agents without impairing T cell function can be leveraged to improve patient outcomes, for example by combining an antimalarial with another powerful acute treatment such as immune checkpoint blockade.

Finally, to evaluate the effects of autophagy inhibition on endothelial cells, I developed an inducible autophagy knockout mouse model on the pure C57BL/6 mouse background (Appendix B). This model will be used in the future for evaluating the role of autophagy on endothelial cell biology in normal development, normal adult angiogenesis, and in tumor angiogenesis. Such models will be critical for dissecting the role of autophagy in individual cell types of the tumor microenvironment and producing a clearer picture of how an entire tumor will react to systemic autophagy inhibition.

Altogether, this work presents a non-canonical point of view to the study of autophagy in tumor biology. As a homeostatic and stress response program that consists of both degradative and secretory pathways, autophagy is an intriguing choice both for tumors to leverage and for clinicians to disrupt. It will be exciting to follow future studies of secretory autophagy, which will be important for further delineating the effects of autophagy inhibition – or induction – in clinical cancer therapy. It will be equally intriguing to determine whether autophagy inhibition combined with immune checkpoint blockade will prove to be a successful therapeutic approach to eradicating tumors more effectively and across wider types of cancers.

Appendix A

Additional analysis of immune response following autophagy inhibition in tumors

This chapter describes unpublished work.

Contributions: I performed all the experiments and analyzed all the data with the following exceptions. Fanya Rostker was responsible for mouse husbandry and performed caliper measurements of tumors and intraperitoneal injections. Jordan Ye performed cell culture, tissue harvests, and tissue processing for spleen analysis. Miranda Broz performed flow cytometry for mCherry analysis in myeloid populations. Jay Debnath supervised the entire project.

Summary

This Appendix contains additional, unpublished experiments pertaining to the work on the role of autophagy in the anti-tumor immune response described in Chapter 2. In addition to the analysis I performed on tumor-associated T cells, I performed a series of smaller studies that begin to dissect other aspects of the immune response including analysis of tumor-associated myeloid populations, analysis of splenic T cells in tumor-bearing mice, and a study on the combined autophagy and immune inhibition. I observe no differences between autophagy competency and deficiency in any of these additional analyses, further supporting the notion that autophagy deficiency is largely dispensable to the anti-tumor immune response.

Results and Discussion

Quantity and function of myeloid cells are equivalent between autophagy-competent and deficient melanomas.

Autophagic secretion, or the subset of the mechanism of unconventional secretion of cytoplasmic components that utilizes autophagic machinery ([99]), releases cytoplasmic cargo from cells by various mechanisms including secretion of naked proteins as well as those within exosomes. As described in Chapter 3, autophagy deficiency in 4T1 mammary cancer cells attenuated the secretion of several angiogenic and inflammatory cytokines (Chapter 3, Figure 4A). Thus it is possible that the recruitment or function of inflammatory cells in the tumor microenvironment of autophagy-deficient tumors would be different from autophagy-competent controls.

To test this hypothesis, I evaluated quantities myeloid cell populations by flow cytometry in digested B16-shCTL and B16-shAtg7 tumors. Cells expressing CD11b, CD11c, and Ly6G were present in these tumors at equal levels (Figure 1A). Tumor-associated macrophages ($CD45^+$ $CD11b^+$ $F4/80^+$) were also present at equivalent levels. Expression of PD-L1, the ligand for PD-1 that is involved in activation the suppressive T cell checkpoint program, was equivalent between macrophages associated with either autophagy-competent or deficient B16 tumors (Figure 1B).

Phagocytic antigen-presenting cells (APCs) sample their environment by engulfing whole cells, cellular debris, proteins, exosomes, and anything else they encounter, process the components and present antigen peptides on major histocompatibility complex (MHC) proteins to T cells in an effort to recruit the adaptive immune system to

sites of abnormal activity. Autophagy could modulate the availability of antigens presented by APCs by affecting the degradation or secretion of cytoplasmic proteins. Thus, inhibiting autophagy in cancer cells could alter antigen loading into neighboring myeloid cells in the tumor microenvironment (monocytes, neutrophils, dendritic cells, and macrophages) and alter the anti-tumor $CD4^+$ T cell response via an intermediate myeloid cell type.

To test this hypothesis, I generated autophagy-competent (shCTL) and deficient (shAtg12) B78-OVA tumors expressing the fluorescent mCherry protein. These were analyzed by flow cytometry for a panel of myeloid populations as previously defined by M. Broz et al, who is also a collaborator on this study ([100]) and found to be present at equivalent levels (data not shown). These population were then evaluated for tumor-derived mCherry fluorescence, which acted as a surrogate marker for tumor-derived antigen loading into APCs. We detected equivalent levels of mCherry across all tumor-associated myeloid populations (Figure 1C). As expected, T cells showed no mCherry uptake (Figure 1C). We conclude that myeloid cells associated with autophagy-deficient tumors are able to take up tumor antigens just as well as those associated with autophagy-competent tumors, and this is reflected by the unperturbed $CD4^+$ T cell responses in both tumor types described previously (Chapter 2, Figure 4D).

Quantity and function of splenic T cells in autophagy-competent and deficient tumor-bearing mice are unchanged.

To test the possibility that autophagy-competent and deficient tumors affected the systemic anti-tumor immune response to different degrees, I analyzed the quantity and

functional status of splenic T cells to complement my analysis of tumor-associated T cells presented in Chapter 2. $CD4^+$ and $CD8^+$ T cells in the spleens of GREAT reporter mice bearing autophagy-competent or deficient B16 tumors were present at equivalent levels and expressed equivalent levels of activation markers CD44, IFNγ, and the IFNγ-YFP reporter, as well as the immune checkpoint protein PD1 (Figure 2A). These same markers, with the exception of YFP, were also tested in the splenic T cells from wildtype BALB/c mice bearing autophagy-competent or deficient 4T1 tumors, and were also largely equivalent, with the exception of an attenuation of surface CD44 expression (Figure 2B).

Autophagy-competent and deficient tumors form with similar growth kinetics in immune-deficiency.

4T1 and B16 tumors grew at equivalent rates with either control or ATG hairpins, in either wildtype or Rag1 null mice (Figure 3A). Autophagy-competent and deficient 4T1 tumors also grew at equivalent rates in wildtype mice injected with either control IgG or anti-CD8 antibody (Figure 3B). This observation that the combined inhibition of cancer cell autophagy and inhibition of the adaptive immune system does not alter tumor growth kinetics helps to support the idea that these tumors behave similarly in relation to their host immune responses.

Figure 1. Myeloid quantity and function are equivalent between autophagy-competent and deficient melanomas.

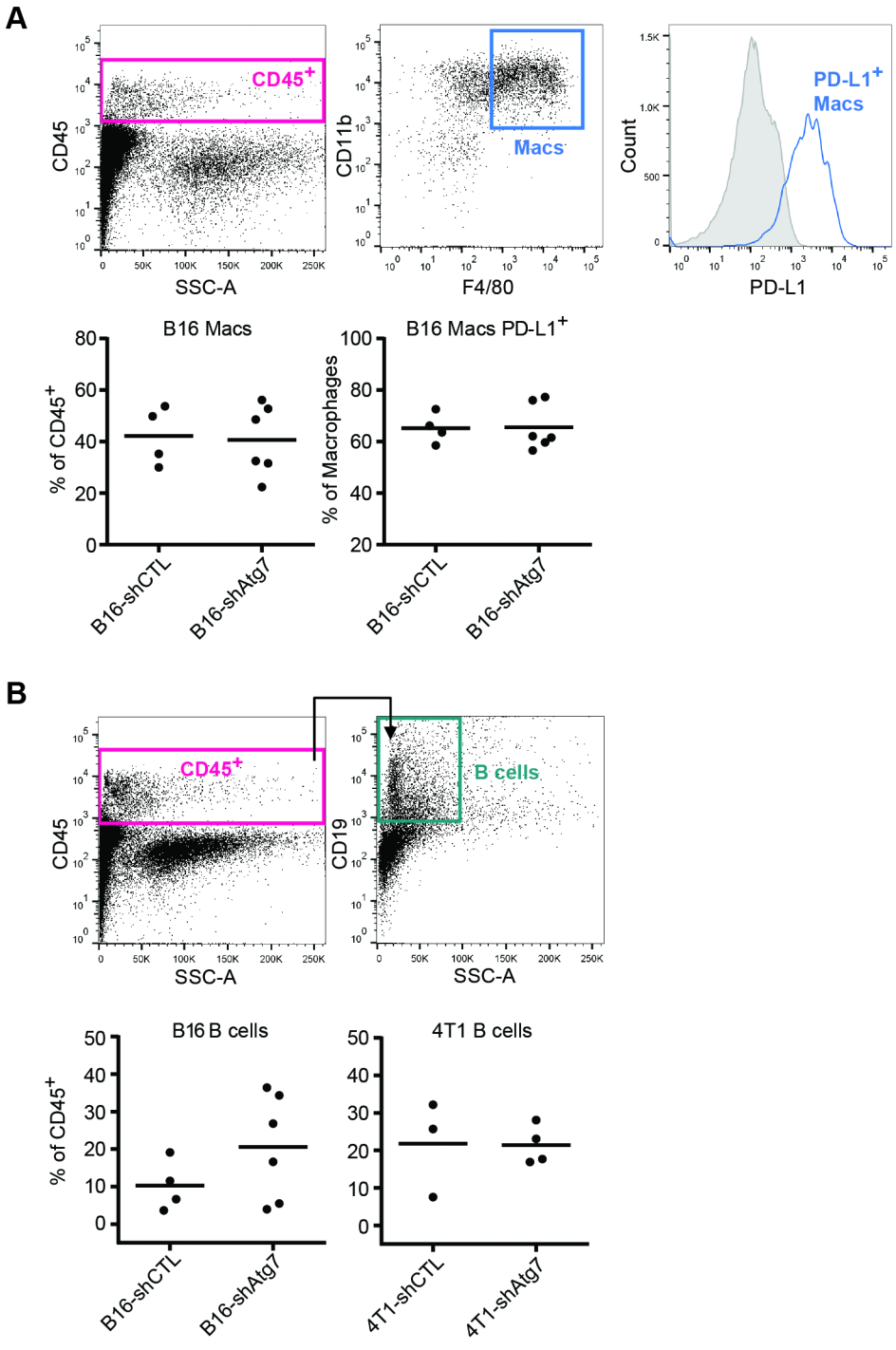

Figure 1. Myeloid quantity and function are equivalent between autophagy-competent and deficient melanomas. B16 tumors stably expressing non-targeting control (shCTL) or ATG7 (shAtg7) hairpins were injected subcutaneously into 6 to 7 week old wildtype C57BL/6 mice and allowed to form tumors for 2 weeks. Myeloid population were evaluated by flow cytometry. (A) Myeloid populations expressing CD11b, CD11c, and Ly6G were presented in equivalent amounts in autophagy-competent and deficient B16 tumors. (B) Macrophages were present in equivalent levels between autophagy-competent and deficient B16 tumors and expressed equivalent levels of the immune checkpoint modulator PD-L1. Histogram: control (gray), stained tumor (blue). (C) Autophagy-competent and deficient B78-OVA melanoma cells expressing the fluorescent mCherry protein were injected subcutaneously into 6 to 7 week old male C57BL/6 mice and allowed to form tumors for 3 weeks. Resected and digested tumors were analyzed for myeloid cell populations by flow cytometry. Tumor-derived mCherry expression in myeloid cells was measured in each population and two-way ANOVA was not significant.

Figure 2. Quantity and function of splenic T cell populations are equivalent between autophagy-competent and deficient tumors.

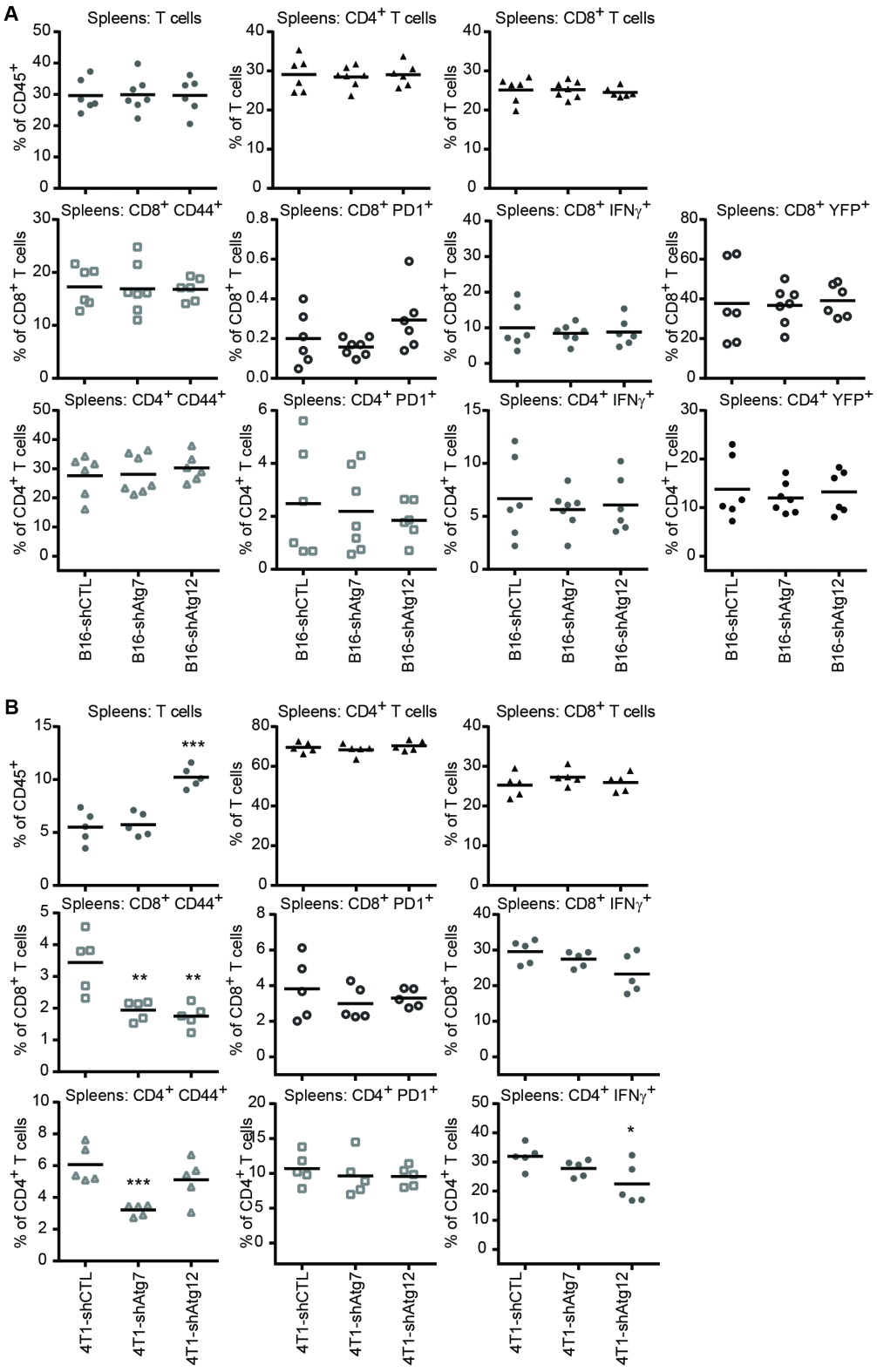

Figure 2. Quantity and function of splenic T cell populations are equivalent between autophagy-competent and deficient tumors. Spleens were isolated from autophagy-competent and deficient B16 (A) and 4T1 (B) tumor-bearing mice and T cell populations were analyzed by flow cytometry as described previously (Chapter 2, Figures 2-3). T-test results are indicated as ** ($p < 0.01$) and *** ($p < 0.001$).

Figure 3. Autophagy-competent and deficient tumors form with similar growth kinetics in immune-deficiency.

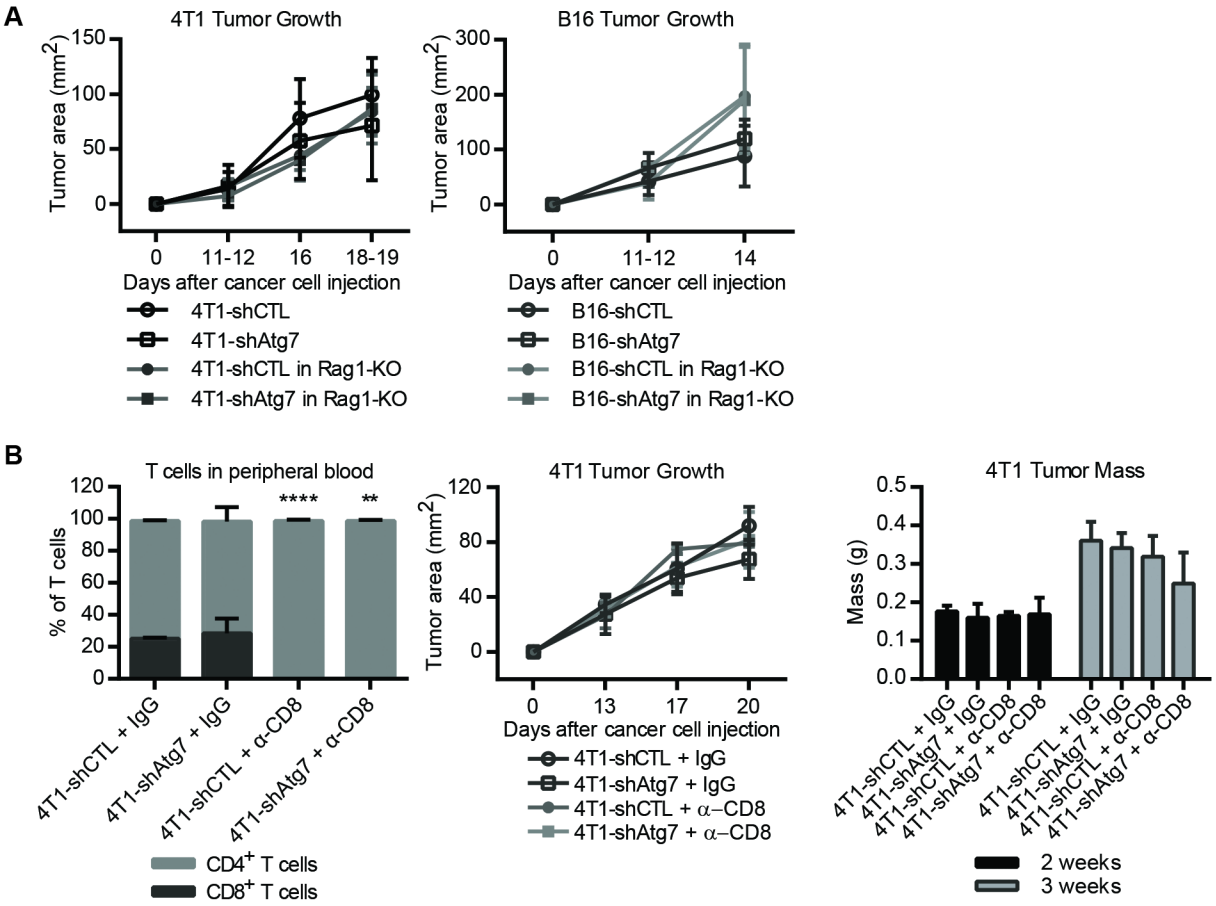

Figure 3. Autophagy-competent and deficient tumors form with similar growth kinetics in immune-deficiency. (A) 4T1 and B16 tumors were generated in parallel in wildtype (BALB/c and C57BL/6, respectively) and immune deficient (Rag1-KO) mice. Tumor growth was measured by caliper and was not significantly different between immune competent and deficient mice or between autophagy competent and deficient tumors. (B) Wildtype BALB/c mice bearing 4T1 tumors were injected weekly with purified Rat IgG control or purified anti-CD8 monoclonal antibody (IP). Left: flow cytometry analysis of a mouse blood sample for $CD4^+$ and $CD8^+$ T cells. $CD8^+$ T cells were ablated by anti-CD8 antibody. Student's t-test results are presented as ** ($p < 0.01$) and **** ($p < 0.0001$). Middle: 4T1 tumor growth by caliper measurements. Right: 4T1 tumor mass at resection at 2 and 3 weeks, in two experimental cohorts.

Appendix B

Generation of transgenic mice for studies of autophagy gene knockout in vascular endothelial cells

This chapter describes unpublished work.

Contributions: I supervised breeding, backcrossing, and genotyping, and developed and tested experimental protocols. Fanya Rostker was responsible for mouse husbandry, genotyping, and intraperitoneal injections.

Summary

Autophagy plays an important role in the function of endothelial cells, the only cell type that must intentionally survive the environmental stress of hypoxia as it helps to build blood vessel ([101]). In cancer therapy, systemic treatment with pharmacological inhibitors inhibits autophagy not only in the cancer cells but also in all normal host cells. Thus, it is important to study autophagy's role in stromal cell populations, particularly in endothelial cells that rely on this stress response, in order to determine the appropriate clinical contexts for using such a systemic treatment.

To this end, I generated two lines of inducible endothelial knockout mice fully back-crossed to the C57BL/6 background:

Cdh5-CreER^{+} Atg5$^{f/f}$ R26-lsl-RFP

Cdh5-CreER^{+} Atg12$^{f/f}$ R26-lsl-RFP

In these mice, Cdh5 (VE-Cadherin) drives conditional expression of the ER-conjugated 4-hydroxy-tamoxifen (4-OHT) inducible Cre recombinase protein in endothelial cells. One of two independent autophagy-dependent genes, *atg5* or *atg12*, are flanked by lox-P sites. Rosa26-lox-stop-lox-RFP acts as a fluorescent reporter of Cre recombinase activity. Thus, mice treated with 4-OHT will induce excision of either *atg5* or *atg12* in endothelial cells, producing an endothelial autophagy knockout in an otherwise autophagy-competent mouse.

Such a model is a powerful genetic tool to dissect the role of autophagy in endothelial cells in both basic and cancer biology. Because our laboratory generated the Atg12$^{f/f}$ mouse, this gene has not been studied in endothelial cells before, and it is now

appreciated to have a role not only in autophagy but also in endosomal trafficking ([102]). Furthermore, with a fully back-crossed model, we can perform tumor transplants to study the behavior of autophagy-null endothelium in a tumor microenvironment and thus ask whether tumor vasculature can still form upon autophagy ablation. I tested *in vivo* angiogenesis by growth factor-loaded Matrigel plug assays in pilot studies in mice treated with 4-OHT or vehicle control. This work will be continued by a postdoctoral fellow.

References

1. Sharma P, Allison JP. Immune checkpoint targeting in cancer therapy: Toward combination strategies with curative potential. *Cell*. 2015;161(2):205-214. doi:10.1016/j.cell.2015.03.030.
2. Rivera LB, Bergers G. Tumor angiogenesis, from foe to friend. *Science (80-)*. 2015;349(6249):694-695. doi:10.1126/science.aad0862.
3. Hanahan D, Weinberg R a. Hallmarks of cancer: the next generation. *Cell*. 2011;144(5):646-674. doi:10.1016/j.cell.2011.02.013.
4. Ludwig J a, Weinstein JN. Biomarkers in cancer staging, prognosis and treatment selection. *Nat Rev Cancer*. 2005;5(11):845-856. doi:10.1038/nrc1739.
5. Shah NP, Tran C, Lee FY, Chen P, Norris D, Sawyers CL. Overriding imatinib resistance with a novel ABL kinase inhibitor. *Science*. 2004;305(5682):399-401. doi:10.1126/science.1099480.
6. Joyce JA, Pollard JW. Microenvironmental regulation of metastasis. 2009;9(ApRII). doi:10.1038/nrc2618.
7. Fidler IJ. The pathogenesis of cancer metastasis: the “seed and soil” hypothesis revisited. *Nat Rev Cancer*. 2003;3(June):453-458. doi:10.1038/nrc1098.
8. Dvorak HF. Tumors: Wounds That Do Not Heal. Similarties between Tumor Stroma Generation and Wound Healing. *New Engl J Med*. 1986;314(3):144-149. doi:10.1056/NEJM198107023050102.
9. Folkman J. Angiogenesis. *Annu Rev Med*. 2006;57:1-18. doi:10.1146/annurev.med.57.121304.131306.
10. Tlsty TD, Coussens LM. Tumor Stroma and Regulation of Cancer Development. *Annu Rev Pathol Mech Dis*. 2006;1(1):119-150. doi:10.1146/annurev.pathol.1.110304.100224.
11. Bissell MJ, Hall HG, Parry G. How does the extracellular matrix direct gene expression? *J Theor Biol*. 1982;99(1):31-68. doi:10.1016/0022-5193(82)90388-5.
12. Schäfer M, Werner S. Cancer as an overhealing wound : an old hypothesis revisited. 2008;9(August):628-638. doi:10.1038/nrm2455.
13. Hanahan D, Folkman J. Patterns and Emerging Mechanisms of the Angiogenic Switch during Tumorigenesis. 1996;86:353-364.
14. Bergers G, Benjamin LE. Tumorigenesis and the angiogenic switch. *Nat Rev Cancer*. 2003;3(6):401-410. doi:10.1038/nrc1093.
15. Littlepage LE, Egeblad M, Werb Z. The Tumor Microenvironment in Cancer Progression. 14.
16. Hanahan D, Coussens LM. Accessories to the Crime : Functions of Cells Recruited to the Tumor Microenvironment. *Cancer Cell*. 2012;21(3):309-322. doi:10.1016/j.ccr.2012.02.022.
17. Pardoll DM. The blockade of immune checkpoints in cancer immunotherapy. *Nat Rev Cancer*. 2012;12(4):252-264. doi:10.1038/nrc3239.
18. Joyce JA. Therapeutic targeting of the tumor microenvironment. *Cancer Cell*. 2005;7(6):513-520. doi:10.1016/j.ccr.2005.05.024.
19. Castaño Z, Tracy K, Mcallister SS. The tumor macroenvironment and systemic

regulation of breast cancer progression. 2011;(November):889-897. doi:10.1387/ijdb.
20. He C, Klionsky DJ. Regulation mechanisms and signaling pathways of autophagy. *Annu Rev Genet*. 2009;43:67-93. doi:10.1146/annurev-genet-102808-114910.
21. Murrow L, Debnath J. Autophagy as a Stress-Response and Quality-Control Mechanism: Implications for Cell Injury and Human Disease. *Annu Rev Pathol Mech Dis*. 2012;8(1):121016121742000. doi:10.1146/annurev-pathol-020712-163918.
22. Harris J. Autophagy and cytokines. *Cytokine*. 2011;56(2):140-144. doi:10.1016/j.cyto.2011.08.022.
23. Stow JL, Manderson AP, Murray RZ. SNAREing immunity: the role of SNAREs in the immune system. *Nat Rev Immunol*. 2006;6(12):919-929. doi:10.1038/nri1980.
24. Denzer K, Kleijmeer MJ, Heijnen HFG, Stoorvogel W, Geuze HJ. Exosome : from internal vesicle of the multivesicular body to intercellular signaling device. 2000;3374:3365-3374.
25. Ponpuak M, Mandell MA, Kimura T, Chauhan S, Cleyrat C, Deretic V. Secretory autophagy. *Curr Opin Cell Biol*. 2015;35(Figure 1):106-116. doi:10.1016/j.ceb.2015.04.016.
26. Nickel W, Rabouille C. Mechanisms of regulated unconventional protein secretion. *Nat Rev Mol cell Biol*. 2009;10.
27. Kinseth MA, Anjard C, Fuller D, Guizzunti G, Loomis WF. The Golgi-Associated Protein GRASP Is Required for Unconventional Protein Secretion during Development. 2007:524-534. doi:10.1016/j.cell.2007.06.029.
28. Deretic V, Jiang S, Dupont N. Autophagy intersections with conventional and unconventional secretion in tissue development, remodeling and inflammation. *Trends Cell Biol*. 2012;22(8):397-406. doi:10.1016/j.tcb.2012.04.008.
29. Duran JM, Anjard C, Stefan C, Loomis WF, Malhotra V. Unconventional secretion of Acb1 is mediated by autophagosomes. *J Cell Biol*. 2010;188(4):527-536. doi:10.1083/jcb.200911154.
30. Dupont N, Jiang S, Pilli M, Ornatowski W, Bhattacharya D, Deretic V. Autophagy-based unconventional secretory pathway for extracellular delivery of IL-1β. *EMBO J*. 2011;30(23):4701-4711. doi:10.1038/emboj.2011.398.
31. Debnath J. The multifaceted roles of autophagy in tumors-implications for breast cancer. *J Mammary Gland Biol Neoplasia*. 2011;16(3):173-187. doi:10.1007/s10911-011-9223-3.
32. Kenific CM, Stehbens SJ, Goldsmith J, et al. NBR 1 enables autophagy-dependent focal adhesion turnover. *J Cell Biol*. 2016;212(5):577-590. doi:10.1083/jcb.201503075.
33. Yang ZJ, Chee CE, Huang S, Sinicrope FA. The role of autophagy in cancer: therapeutic implications. *Mol Cancer Ther*. 2011;10(9):1533-1541. doi:10.1158/1535-7163.MCT-11-0047.
34. Barnard R a, Wittenburg L a, Amaravadi RK, Gustafson DL, Thorburn A, Thamm DH. Phase I clinical trial and pharmacodynamic evaluation of combination hydroxychloroquine and doxorubicin treatment in pet dogs treated for spontaneously occurring lymphoma. *Autophagy*. 2014;10(8):1415-1425. doi:10.4161/auto.29165.

35. Mahalingam D, Mita M, Sarantopoulos J, et al. Combined autophagy and HDAC inhibition: a phase I safety, tolerability, pharmacokinetic, and pharmacodynamic analysis of hydroxychloroquine in combination with the HDAC inhibitor vorinostat in patients with advanced solid tumors. *Autophagy*. 2014;10(8):1403-1414. doi:10.4161/auto.29231.
36. Rangwala R, Chang YC, Hu J, et al. Combined MTOR and autophagy inhibition: phase I trial of hydroxychloroquine and temsirolimus in patients with advanced solid tumors and melanoma. *Autophagy*. 2014;10(8):1391-1402. doi:10.4161/auto.29119.
37. Rangwala R, Leone R, Chang YC, et al. Phase I trial of hydroxychloroquine with dose-intense temozolomide in patients with advanced solid tumors and melanoma. *Autophagy*. 2014;10(8):1369-1379. doi:10.4161/auto.29118.
38. Rosenfeld MR, Ye X, Supko JG, et al. A phase I/II trial of hydroxychloroquine in conjunction with radiation therapy and concurrent and adjuvant temozolomide in patients with newly diagnosed glioblastoma multiforme. *Autophagy*. 2014;10(8):1359-1368. doi:10.4161/auto.28984.
39. Vogl DT, Stadtmauer E a, Tan K-S, et al. Combined autophagy and proteasome inhibition: a phase 1 trial of hydroxychloroquine and bortezomib in patients with relapsed/refractory myeloma. *Autophagy*. 2014;10(8):1380-1390. doi:10.4161/auto.29264.
40. Wolpin BM, Rubinson DA, Wang X, et al. Phase II and Pharmacodynamic Study of Autophagy Inhibition Using Hydroxychloroquine in Patients With Metastatic Pancreatic Adenocarcinoma. *Oncologist*. 2014;19:637-638.
41. Michaud M, Martins I, Sukkurwala AQ, et al. Autophagy-Dependent Anticancer Immune Responses Induced by Chemotherapeutic Agents in Mice. *Science (80-)*. 2011;334:1573-1578.
42. Degenhardt K, Mathew R, Beaudoin B, et al. Autophagy promotes tumor cell survival and restricts necrosis, inflammation, and tumorigenesis. *Cancer Cell*. 2006;10(1):51-64. doi:10.1016/j.ccr.2006.06.001.
43. Grivennikov SI, Greten FR, Karin M. Immunity, Inflammation , and Cancer. *Cell*. 2010;140(6):883-899. doi:10.1016/j.cell.2010.01.025.
44. Schreiber, Robert D; Old, Lloyd J; Smyth MJ. Cancer Immunoediting: Integrating Immunity's Roles in Cancer Suppression and Promotion. *Science (80-)*. 2011;331:1565-1570. doi:10.1126/science.1203486.
45. Krummel MF, Allison JP. CD28 and CTLA-4 Have Opposing Effects on the Response of T ceils to Stimulation. *J Exp Med*. 1995;182:459-465.
46. Nishimura H, Nose M, Hiai H, Minato N, Honjo T. Development of lupus-like autoimmune diseases by disruption of the PD-1 gene encoding an ITIM motif-carrying immunoreceptor. *Immunity*. 1999;11(2):141-151. doi:10.1016/S1074-7613(00)80089-8.
47. Leach DR, Krummel MF, Allison JP. Enhancement of Antitumor Immunity by CTLA-4 Blockade. *Science (80-)*. 1988;28(18):1734-1736.
48. Phan GQ, Yang JC, Sherry RM, et al. Cancer regression and autoimmunity induced by cytotoxic T lymphocyte-associated antigen 4 blockade in patients with metastatic melanoma. *Proc Natl Acad Sci U S A*. 2003;100(14):8372-8377. doi:10.1073/pnas.1533209100.

49. Brahmer JR, Drake CG, Wollner I, et al. Phase I study of single-agent anti-programmed death-1 (MDX-1106) in refractory solid tumors: safety, clinical activity, pharmacodynamics, and immunologic correlates. *J Clin Oncol*. 2010;28(19):3167-3175. doi:10.1200/JCO.2009.26.7609.
50. Schumacher TN, Schreiber RD. Neoantigens in cancer immunotherapy. *Science (80-)*. 2015;348(6230):69-74.
51. Kandel J, Bossy-wetxel E, Radvanyi F, Klagsbrun M, Folkman J, Hanahan D. Neovascularization Is Associated with a Switch to the Export of bFGF in the Multistep Development of Fibrosarcoma. 1991;66.
52. McDonald DM, Choyke PL. Imaging of angiogenesis: from microscope to clinic. *Nat Med*. 2003;9(6):713-725. doi:10.1038/nm0603-713.
53. Hashizume H, Baluk P, Morikawa S, et al. Openings between defective endothelial cells explain tumor vessel leakiness. *Am J Pathol*. 2000;156(4):1363-1380. doi:10.1016/S0002-9440(10)65006-7.
54. Cooke VG, Lebleu VS, Keskin D, et al. Pericyte Depletion Results in Hypoxia-Associated Epithelial-to-Mesenchymal Transition and Metastasis Mediated by Met Signaling Pathway. *Cancer Cell*. 2012;21(1):66-81. doi:10.1016/j.ccr.2011.11.024.
55. Sawada J, Urakami T, Li F, et al. Article Small GTPase R-Ras Regulates Integrity and Functionality of Tumor Blood Vessels. 2012:235-249. doi:10.1016/j.ccr.2012.06.013.
56. Bergers G, Hanahan D. Modes of resistance to anti-angiogenic therapy. *Nat Rev Cancer*. 2008;8(8):592-603. doi:10.1038/nrc2442.
57. Goel S, Wong AH, Jain RK. Vascular Normalization as a Therapeutic Strategy. 2012:1-24.
58. Kaur J, Debnath J. Autophagy at the crossroads of catabolism and anabolism. *Nat Rev Mol cell Biol*. 2015;16(8):461-472. doi:10.1038/nrm4024.
59. Kenific CM, Debnath J. Cellular and metabolic functions for autophagy in cancer cells. *Trends Cell Biol*. 2015;25(1):37-45. doi:10.1016/j.tcb.2014.09.001.
60. White E. The role for autophagy in cancer. *J Clin Invest*. 2015;125(1):42-46. doi:10.1172/JCI73941.Autophagy.
61. Rebecca V, Amaravadi R. Emerging strategies to effectively target autophagy in cancer. *Oncogene*. 2015;(February):1-11. doi:10.1038/onc.2015.99.
62. Zitvogel L, Galluzzi L, Smyth MJ, Kroemer G. Mechanism of action of conventional and targeted anticancer therapies: reinstating immunosurveillance. *Immunity*. 2013;39:74-88. doi:10.1016/j.immuni.2013.06.014.
63. Sistigu A, Yamazaki T, Vacchelli E, et al. Cancer cell-autonomous contribution of type I interferon signaling to the efficacy of chemotherapy. *Nat Med*. 2014;20(11):1301-1309. doi:10.1038/nm.3708.
64. Garg A, Martin S, Golab J, Agostinis P. Danger signalling during cancer cell death: origins, plasticity and regulation. *Cell Death Differ*. 2014;21(1):26-38. doi:10.1038/cdd.2013.48.
65. Michaud M, Xie X, Bravo-San Pedro JM, Zitvogel L, White E, Kroemer G. An autophagy-dependent anticancer immune response determines the efficacy of melanoma chemotherapy. *Oncoimmunology*. 2014;3(7):e944047. doi:10.4161/21624011.2014.944047.
66. Gupta A, Roy S, Lazar AJF, et al. Autophagy inhibition and antimalarials promote

cell death in gastrointestinal stromal tumor (GIST). *Proc Natl Acad Sci*. 2010;107(32):14333-14338. doi:10.1073/pnas.1000248107.
67. Hodi FS, O'Day SJ, McDermott DF, et al. Improved Survival with Ipilimumab in Patients with Metastatic Melanoma. *N Engl J Med*. 2010;363(8):711-723.
68. Topalian SL, Hodi FS, Brahmer JR, et al. Safety, Activity, and Immune Correlates of Anti-PD-1 Antibody in Cancer. *N Engl J Med*. 2012;366(26):2443-2454.
69. Wolchok JD, Kluger H, Callahan MK, et al. Nivolumab plus ipilimumab in advanced melanoma. *N Engl J Med*. 2013;369(2):122-133. doi:10.1056/NEJMoa1302369.
70. Blankenstein T, Coulie PG, Gilboa E, Jaffee EM. The determinants of tumour immunogenicity. *Nat Rev Cancer*. 2012;12(4):307-313. doi:10.1038/nrc3246.
71. Vanneman M, Dranoff G. Combining immunotherapy and targeted therapies in cancer treatment. *Nat Rev Cancer*. 2012;12(4):237-251. doi:10.1038/nrc3237.
72. Baaten BJG, Li C-R, Deiro MF, Lin MM, Linton PJ, Bradley LM. CD44 Regulates Survival and Memory Development in Th1 Cells. *Immunity*. 2010;32(1):104-115. doi:10.1016/j.immuni.2009.10.011.
73. Hogquist KA, Jameson SC, Heath WR, Howard JL, Bevan MJ, Carbone FR. T Cell Receptor Antagonist Peptides Induce Positive Selection. *Cell*. 1994;76:17-27.
74. Reinhardt RL, Liang H-E, Locksley RM. Cytokine-secreting follicular T cells shape the antibody repertoire. *Nat Immunol*. 2009;10(4):385-393. doi:10.1038/ni.1715.
75. Manic G, Obrist F, Kroemer G, Vitale I, Galluzzi L. Chloroquine and hydroxychloroquine for cancer therapy. *Mol Cell Oncol*. 2014;1(e29911):1-11. doi:10.4161/mco.29911.
76. Salas E, Roy S, Marsh T, Rubin B, Debnath J. Oxidative pentose phosphate pathway inhibition is a key determinant of antimalarial induced cancer cell death. *Oncogene*. 2015;(August):1-10. doi:10.1038/onc.2015.348.
77. Overwijk WW, Restifo NP. B16 as a Mouse Model for Human Melanoma. *Curr Protoc Immunol*. 2000;20.1:1-29.
78. Pulaski BA, Ostrand-Rosenberg S. Mouse 4T1 Breast Tumor Model. *Curr Protoc*. 2000;20.2:1-16.
79. Salmeron G, Lipsky P. Immunosuppressive Potential of Antimalarials. *Am J Med*. 1983;(July):19-24.
80. Fox RI. Mechanism of action of hydroxychloroquine as an antirheumatic drug. *Semin Arthritis Rheum*. 1993;23(2):82-91. doi:10.1016/S0049-0172(10)80012-5.
81. Vyas JM, Van der Veen AG, Ploegh HL. The known unknowns of antigen processing and presentation. *Nat Rev Immunol*. 2008;8(8):607-618. doi:10.1038/nri2368.
82. Demachi-Okamura A, Torikai H, Akatsuka Y, Miyoshi H. Autophagy Creates a CTL Epitope That Mimics Tumor- Associated Antigens. *PLoS One*. 2012;7(10):1-13. doi:10.1371/journal.pone.0047126.
83. Fung C, Lock R, Gao S, et al. Induction of Autophagy during Extracellular Matrix Detachment Promotes Cell Survival. *Mol Biol Cell*. 2008;19:797-806. doi:10.1091/mbc.E07.
84. Engelhardt JJ, Boldajipour B, Beemiller P, et al. Marginating dendritic cells of the tumor microenvironment cross-present tumor antigens and stably engage tumor-specific T cells. *Cancer Cell*. 2012;21(3):402-417. doi:10.1016/j.ccr.2012.01.008.

85. Raza A, Franklin MJ, Dudek AZ. Pericytes and vessel maturation during tumor angiogenesis and metastasis. *Am J Hematol*. 2010;85(8):593-598. doi:10.1002/ajh.21745.
86. Maes H, Rubio N, Garg AD, Agostinis P. Autophagy: shaping the tumor microenvironment and therapeutic response. *Trends Mol Med*. 2013;19(7):428-446. doi:10.1016/j.molmed.2013.04.005.
87. Kenific CM, Thorburn A, Debnath J. Autophagy and metastasis: another double-edged sword. *Curr Opin Cell Biol*. 2010;22(2):241-245. doi:10.1016/j.ceb.2009.10.008.
88. Cooke VG, Lebleu VS, Keskin D, et al. Article Pericyte Depletion Results in Hypoxia-Associated Epithelial-to-Mesenchymal Transition and Metastasis Mediated by Met Signaling Pathway. *Cancer Cell*. 2012;21(1):66-81. doi:10.1016/j.ccr.2011.11.024.
89. Baluk P, Morikawa S, Haskell A, Mancuso M, McDonald DM. Abnormalities of basement membrane on blood vessels and endothelial sprouts in tumors. *Am J Pathol*. 2003;163(5):1801-1815. doi:10.1016/S0002-9440(10)63540-7.
90. Shiao SL, Ganesan a P, Rugo HS, Coussens LM. Immune microenvironments in solid tumors: new targets for therapy. *Genes Dev*. 2011;25(24):2559-2572. doi:10.1101/gad.169029.111.
91. Dejana E. Endothelial Cell-Cell Junctions: Happy Together. 2004;5(April):1-10. doi:10.1038/nrm1357.
92. Nolan DJ, Ginsberg M, Israely E, et al. Resource Molecular Signatures of Tissue-Specific Microvascular Endothelial Cell Heterogeneity in Organ Maintenance and Regeneration. *Dev Cell*. 2013;26(2):204-219. doi:10.1016/j.devcel.2013.06.017.
93. Lee H-M, Shin D-M, Yuk J-M, et al. Autophagy Negatively Regulates Keratinocyte Inflammatory Responses via Scaffolding Protein p62/SQSTM1. *J Immunol*. 2011;186(2):1248-1258. doi:10.4049/jimmunol.1001954.
94. White E. Deconvoluting the context-dependent role for autophagy in cancer. *Nat Rev Cancer*. 2012;12(6):401-410. doi:10.1038/nrc3262.
95. Chen N, Eritja N, Lock R, Debnath J. Autophagy restricts proliferation driven by oncogenic phosphatidylinositol 3-kinase in three-dimensional culture. *Oncogene*. 2013;32(20):2543-2554. doi:10.1038/onc.2012.277.
96. Rolland P, Madjd Z, Durrant L, Ellis IO, Layfield R, Spendlove I. The ubiquitin-binding protein p62 is expressed in breast cancers showing features of aggressive disease. *Endocr Relat Cancer*. 2007;14(1):73-80. doi:10.1677/erc.1.01312.
97. Maes H, Kuchnio A, Peric A, et al. Tumor vessel normalization by chloroquine independent of autophagy. *Cancer Cell*. 2014;26(2):190-206. doi:10.1016/j.ccr.2014.06.025.
98. Mombaerts P, Johnson RS, Herrup K, Tonegawa S, Papaioannouo VE. RAG-1-Deficient Mice Have No Mature 8 and T Lymphocytes. *Cell*. 1992;68:869-877.
99. Zhang M, Schkman R. Unconventional secretion, unconventional solutions. *Science (80-)*. 2013;340:559-562. doi:10.1017/CBO9781107415324.004.
100. Broz ML, Binnewies M, Boldajipour B, et al. Dissecting the Tumor Myeloid Compartment Reveals Rare Activating Antigen-Presenting Cells Critical for T Cell Immunity. *Cancer Cell*. 2014;26(5):638-652. doi:10.1016/j.ccell.2014.09.007.

101. Torisu T, Torisu K, Lee IH, et al. Autophagy regulates endothelial cell processing, maturation and secretion of von Willebrand factor. *Nat Med*. 2013;19(10):1281-1287. doi:10.1038/nm.3288.
102. Murrow L, Malhotra R, Debnath J. ATG12-ATG3 interacts with Alix to promote basal autophagic flux and late endosome function. *Nat Cell Biol*. 2015;17(3):300-310. doi:10.1038/ncb3112.

Publishing Agreement

It is the policy of the University to encourage the distribution of all theses, dissertations, and manuscripts. Copies of all UCSF theses, dissertations, and manuscripts will be routed to the library via the Graduate Division. The library will make all theses, dissertations, and manuscripts accessible to the public and will preserve these to the best of their abilities, in perpetuity.

Please sign the following statement:

I hereby grant permission to the Graduate Division of the University of California, San Francisco to release copies of my thesis, dissertation, or manuscript to the Campus Library to provide access and preservation, in whole or in part, in perpetuity.

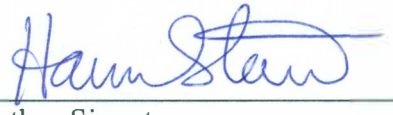

Author Signature

8/24/16

Date